AB INITIO SELF-CONSISTENT FIELD CALCULATIONS

ON Mn-RELATED DEFECTS IN

CALCIUM FLUORIDE

By

ANTHONY CLARK LEWANDOWSKI

Bachelor of Science
in Arts and Sciences
Oklahoma State University
Stillwater, Oklahoma
1986

Master of Science
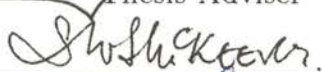Oklahoma State University
Stillwater, Oklahoma
1990

Submitted to the Faculty of the
Graduate College of the
Oklahoma State University
in partial fulfillment of
the requirements for
the Degree of
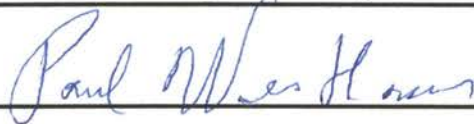DOCTOR OF PHILOSOPHY
December, 1993

AB INITIO SELF-CONSISTENT FIELD CALCULATIONS
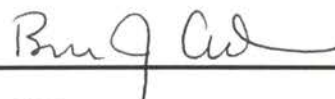
ON Mn-RELATED DEFECTS IN

CALCIUM FLUORIDE

Thesis Approved:

_____
Thesis Adviser

_____

_____

_____

_____

_____
Dean of the Graduate College

ACKNOWLEDGMENTS

Someone who trusts science to explain the everyday must continually make connections between textbook knowledge and real knowledge, the knowledge we receive and the knowledge we truly own. For this, I thank the faculty of the Department of Physics, Oklahoma State University.

In particular, I would like to thank my research advisor Dr. Tim Wilson. His advise and insight has many times helped me overcome what at the time appeared intractable complications. His encouragement kept me focused and his knowledge of the practical aspects of quantum chemical computation kept me from getting lost in the theory. Dr. Wilson has a deep concern for the welfare of his graduate students for which I am most appreciative.

I would like to thank Dr. S.W.S. McKeever for serving on my committee. I also want to thank Dr. McKeever and co-authors for writing *Manganese absorption in CaF_2:Mn; I*. This paper provided the experimental justification for this research project. Besides being a beautiful piece of physics, this paper posed the problem in a way that theoretical studies can begin and they even suggested possible solutions. I've must have read it a hundred times.

I would like to thank Dr. Paul Westhaus, Dr. Bruce Ackerson and Dr. Donald Thompson for serving on my committee. Dr. Ackerson was the first faculty member I met upon coming to OSU as a junior and Dr. Westhaus was the instructor of my first OSU Physics course.

Dr. Westhaus is the hardest working teacher in the business. Over the years, I've personally spent hours in his office struggling with, at first, elementary and then later more advanced concepts. I asked him once to teach a many-body theory course and he did. I thank him for this because I am sure he instructed that course on his own time. Dr. Westhaus really cares about whether a student understands

the material. The time spent with Dr. Westhaus represents for me irreplaceable treads running through the fabric of my knowledge.

Dr. Ackerson first impressed me by actually reading my Masters Thesis. Not only did he read it, he offered insight into the nature of the equations we were trying to solve. His enthusiasm for Physics is contagious. From discussions ranging from the thermodynamics of a box of allen wrenches to the nature of gravity, Dr. Ackerson has demonstrated time and again that Physics is understandable to anybody who is willing to think.

I would like to thank Konrad Brandemuhl and Terry Klarich at the University Computer Center. Without their help and knowledge this work could not have been accomplished.

To my wife Kyong Ran, thank you for sharing with me my vision of the future.

TABLE OF CONTENTS

LIST OF TABLES

LIST OF FIGURES

CHAPTER I

INTRODUCTION

With its introduction as a highly efficient thermoluminescent radiation dosimeter by Ginther and Kirk[1] in 1957, CaF_2:Mn has been the subject of much study because of the wide range linearity of its thermoluminescent response to radiation dose and the location of a major glow peak well above room temperature. Much of the early work centered around the operational importance of CaF_2:Mn and its use in dosimeter applications. For instance, Schulman *et. al.* [2–4] discuss such issues as anomalous fading and Lucas *et. al.* [5] consider the various heating treatments designed to enhance reusability. However, it was not until the last two decades that detailed studies became available as to the role $3d$ ions play in altering the optical properties of CaF_2. In fact the physical properties associated with transition metal ions and rare-earth ions in crystals of the fluorite structure have only been extensively studied since the 1970's. Gehlhoff and Ulrici[6] present an excellent review of this subject.

In general, the purpose of these more recent studies has been to examine the processes of energy storage in this material following irradiation and the subsequent release of this energy in the form of luminescence. With regard to Mn in particular, optical absorption[7–10], photoluminescence[7,11–13] and thermoluminescence (TL)[1,9,14–16] studies have led to a wealth of experimental data from which different models and energy level assignments have been put forward. For instance, CaF_2:Mn irradiated at room temperature is characterized by one main TL glow peak near 550 K. If irradiated at 80 K a second more intense peak becomes present at 200 K[16]. The emission spectra of both peaks indicate a process which involves the relaxation of an excited $*Mn^{2+}$ ion to a ground state Mn^{2+} ion

1

producing an emission peak at 495 nm. A peak at this same wavelenght from photoluminescence measurements has been assigned to a transition from the $^4T_{1g}(^4G)$ level of the Mn^{2+} ion[11]. X-ray-induced luminescence has also been shown to emit at the same wavelength [7,12]

Of particular interest is the work of McKeever $et.$ $al.$ [10] in which they describe a series of Mn absorption studies in CaF_2 with varying levels of Mn dopant before and after irradiation. Before irradiation they observe optical absorption spectra characteristic of internal Mn^{2+} transitions. After irradiation they observed not only an order of magnitude increase in the spectra but also the creation of new structure which they explain in terms of substitutional Mn^{2+} becoming associated with radiation-induced defects such as F-centers[10]. The model they present is that the adjacent F-center breaks the O_h symmetry of isolated substitutional Mn^{2+} impurities and the additional F-center electron couples with the $3d^5$ electrons in Mn^{2+} thus removing the spin and parity forbiddeness of optical transitions resulting in a greatly enhanced and more complex absorption pattern[10].

This idea is further enhanced by the observed thermal quenching of the absorption bands and the appearance of an intense TL signal at 495 nm during heating following irradiation. This is the same wavelenght that had previously been assigned to a transition from the $^4T_{1g}(^4G)$ excited state to the $^6A_{1g}$ ground state in Mn. This model envisions several types of Mn-defect complex each differing as to the location of the radiation-induced defect with respect to the Mn^{2+} ion, the type of the radiation-induced defect, and the number of Mn^{2+} ions within the complex[10]. However, a remaining question is whether the observed spectra are due to internal Mn^{2+} transitions or whether the transitions actually take place within the F-center.

According to the internal transition model, the association of the Mn^{2+} ion with the F-center gives rise to a spin exchange coupling which in turn increases the oscillator strength of the Mn^{2+} transitions by a factor of 10^3. Since the ground state of the $3d^5$ electrons in Mn^{2+} is a spin sextet the excited state transitions all require a spin reversal and hence are spin forbidden. This and parity considerations

lead to excited state lifetimes greater than 10^{-3} s and oscillator strengths of the order $10^{-6} - 10^{-7}$. Thus this theory relies on the perturbation of the neighboring defect to increase the oscillator strengths so that the internal Mn^{2+} transitions become visible and give measurable absorption peaks.

The alternative model to explain the observed spectra and its annealing behavior does not rely on the enhancement of the oscillator strengths as such. This model stems mainly from the observation that a 564 nm absorption band quenches at the same temperature as the lower wavelength bands leading to the conclusion that the 564 nm band is due to the same defect as the lower wavelength Mn-related absorption bands. Since the quenching of the Mn-related bands is accompanied by a TL emission at 495 nm, and since this emission has already been confirmed as being due to the first excited state to ground state transition in Mn^{2+}[10], it follows that the 564 nm band is not due to Mn^{2+} transitions. Therefore, the lower wavelength absorption bands are also not due to internal Mn^{2+} transitions. A model that could explain this behavior is that the transitions actually occur within an F-center perturbed by one or more Mn^{2+} ions.

The above two models notwithstanding, optical dichroism measurements[17] indicate that the optically active defect possess C_{2v} symmetry with an alignment along the $\langle 100 \rangle$-direction. While several defect structures could posses this symmetry[18] (such as M-centers or Mn/H-centers), this alignment indicates that the center could consist of an F-center perturbed by two Mn^{2+} ions. This model proposed by McKeever $et.$ $al.$ [17] is shown as Fig. 1.

While the available experimental data has gone far in illuminating the processes involved and has even been responsible for a plausible qualitative model, the present state of research has reached a point where quantum chemical calculations can begin to contribute insight. The employment of quantum chemical computational techniques now represent the next logical step in the understanding of these processes. Molecular orbital calculations of defect clusters within the Hartree-Fock formalism and its extensions such as configuration interaction (CI),
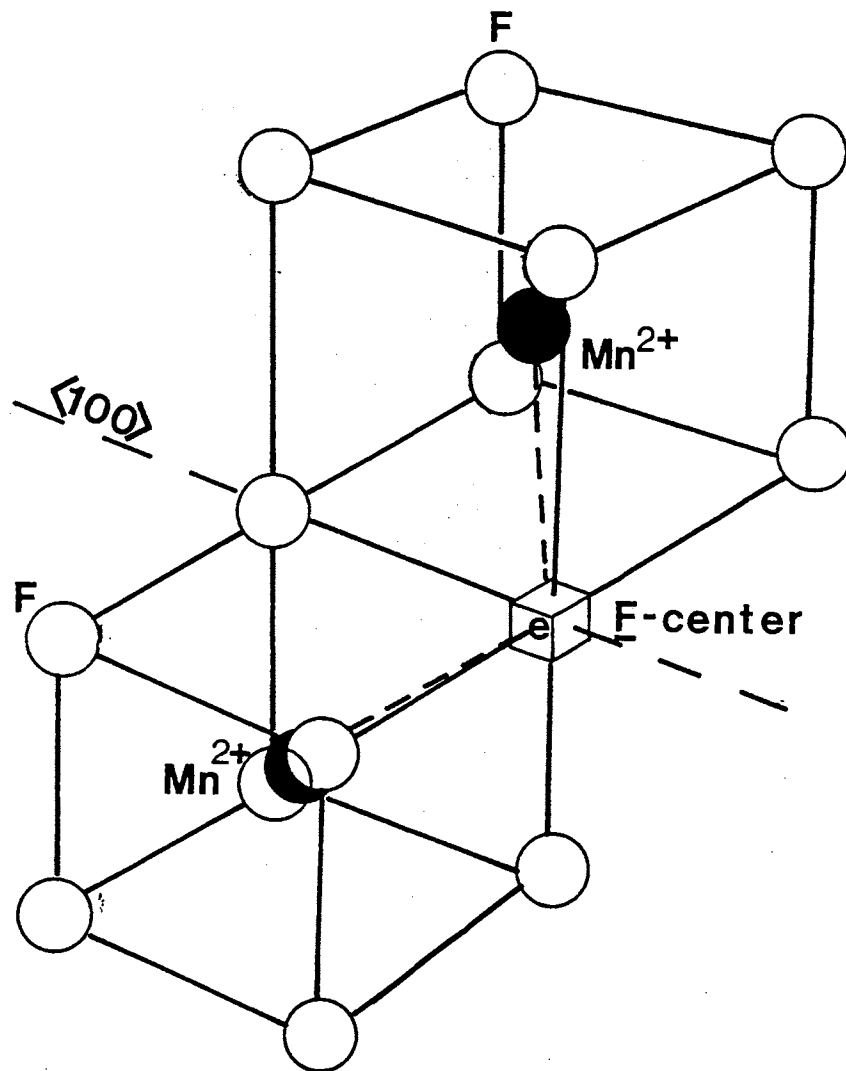
Figure 1. Model for the Mn-perturbed F-center in CaF_2 proposed by McKeever *et. al.* [17].

many-body perturbation theory to second (MP2) and fourth order (MP4) and multiconfigurational self-consistent field (MCSCF) techniques have been incorporated into the *Gaussian 92*[19] general purpose quantum chemical program. With the recent incorporation of external charge distributions and an effective treatment of d electrons, large scale calculations of the electronic structure of both the ground state and excited states of defect clusters in crystals containing $3d$ ions can now be accomplished. This is also facilitated by the recent widespread availability of relatively inexpensive high-speed electronic computers.

The ultimate purpose of this dissertation therefore is to analyze the Mn absorption spectrum in CaF_2 by the calculation of both the ground state and excited states of Mn-related defect structures. To model the absorption spectrum before irradiation we will perform calculations on the $(MnF_8)^{6-}$ cluster. This cluster is chosen to represent the isolated Mn substitutional impurity in an otherwise perfect, undamaged crystal. To model the spectrum after irradiation we will perform calculations on the F-center cluster, $(Ca_4F_6)^{1+}$, and the Mn-perturbed F-center cluster, $(MnCa_3F_6Vac)^{1+}$. These two clusters involve an electron trapped in a vacancy represented by diffuse electronic states and is therefore more sensitive to the external field due to the surrounding crystal lattice. As a consequence, a major part of this research project involved the development of a method to mathematically embed the cluster in a perfect crystal lattice and represent this external electrostatic field by a finite arrangement of charge.

The methods employed include Unrestricted Hartree-Fock (UHF), Restricted Open-Shell Hartree-Fock (ROHF), CI, MP2 and MP4. The main questions center around cluster geometry, electron correlation and the effects of the basis set and the external field due to the surrounding ionic lattice. With this groundwork, the method of MCSCF is used for the calculation of excited state energy levels. The resulting mulitplet levels will then be compared to the experimental optical absorption spectra. To our knowledge, this will be the first time the MCSCF technique has been applied to $3d$ ions in crystals.

In addition to the above calculations, the ligand field Tanabe-Sugano[20] diagrams of the eight-fold coordinated Mn^{2+} impurity with O_h symmetry will be developed. It is to be noted that while ligand field theory has been applied to this system before[10,11], the Tanabe-Sugano diagrams used in the analysis were for six-coordinated O_h Mn^{2+}. From group theory the same terms will arise from both the six- and eight-coordinated systems, however, the spacing of the terms in energy will be effected by the coordination number and we will show that this leads to a larger value for the crystal splitting parameter Dq than has thus far been reported[10,11]. While ligand field methods provide a useful approach for analyzing the multiplet structure of the Mn^{2+} impurity, it must be noted that this approach cannot be accurately extended to more complicated defect structures such as a Mn-F-center complex. For this reason the MCSCF technique (which can be extended to the more complicated defect structures) must first be shown to work for the eight-coordinated O_h Mn^{2+} system.

CHAPTER II

LIGAND FIELD THEORY

Introduction

The lowest lying electronic level in Mn^{2+} is ^6S arising from the configuration $3d^5$. In the free ion this configuration also gives rise to ^4G, ^4P, ^4D, and ^4F terms which lie 25000 to 50000 cm^{-1} above the ground level[21]. In a crystal the quartet levels are split by the influence of the surrounding ions, the most important of which are those immediately adjacent to the central Mn^{+2} ion ("the ligands"). If the ligands are arranged at the corners of a regular tetrahedron, octahedron or cube then the strength of the ligand field may be specified by a single parameter, usually called Dq, from which it is possible to calculate the positions of the energy levels in the crystal arising from this perturbed Mn^{2+} ion. The bulk of the theoretical development surrounding the application of ligand field analysis to transition-metal ions in crystals rests in a series of early papers by Tanabe and Sugano[22] and Orgel[23] in which they discuss the splitting in the free ion terms of $3d$ ions for fields with various symmetries. Several books and review articles have also appeared in the literature most notably by Tanabe and Sugano[20] and Gliemann and Schläfer[24].

Some of the earliest work on Mn^{2+} surrounded by F^{-1} ions was carried out by Stout[21] in his analysis of Manganous Fluoride. Some of the first experimental results and applications of ligand field theory to the substitutional Mn^{2+} impurity in CaF_2, however, was performed by Alcala and Alonso[11] in their analysis of photoluminescence excitation spectra and Bagai and Warrier[25] from ultraviolet optical absorption. However, these results lead to disagreement as to the value of Dq and the assignment of energy levels. One reason for this is that the analysis

of excitation spectra is limited in the sense that these measurements are only able to observe those absorptions that give rise to luminescence. It was not until 1986 when optical absorption in the visible region was measured by McKeever *et. al.* [10] that the Mn^{2+} absorption transitions were observed directly. From the application of ligand field theory, McKeever *et. al.* suggest a value for Dq of 420 cm^{-1}. This was in agreement with Alcala and Alonso[11] but differed significantly with the value of 810 cm^{-1} suggested by Bagai and Warrier[25]. The 420 cm^{-1} value for Dq obtained by Alcala and Alonso, and McKeever *et. al.* is considered to be too low for it is only about 60% of those values for Dq obtained for compounds such as $RbMnF_3$, $NaMnF_3$ and MnF_2[26]. For instance, an analysis of MnF_2 spectra led Stout[21] to assign a value of approximately 800 cm^{-1} for this system. Barriuso and Moreno[26] were the first to point out that the application of the published Tanabe-Sugano diagrams to the Mn impurity in CaF_2 may not be valid while it remains valid for the $RbMnF_3$, $NaMnF_3$ and MnF_2 compounds. The reason for this is that while the symmetry of Mn^{2+} in these compounds and in CaF_2 is O_h, Mn^{2+} is eight-coordinated in CaF_2 instead of six-coordinated as in the other compounds. Furthermore, since the published Tanabe-Sugano diagrams were calculated assuming the six-coordinated O_h ligand field[20], their application to eight-coordinated systems may lead to a sizable error. Since both systems have O_h symmetry, the terms arising from the ligand field will remain the same. However, since group theory can only identify the symmetry and hence the number of the resulting terms, the remaining question as to the ordering of the terms and the magnitude of the splitting as a function of Dq remained unresolved.

In this section we will briefly outline some of the principles behind ligand field theory and describe the calculation of the term splitting diagram for a $3d^5$ ion in the presence of an electrostatic field of O_h symmetry. The field will be produced by eight point ions arranged as on the corners of a cube with the $3d^5$ ion in the center. We will denote this field as $O_h^{(8)}$. It is clearly impossible in this dissertation to provide in the space and time available an exhaustive treatment of ligand field theory; nor would it be desirable to do so. The full theory of

ligand fields is sufficiently rich and complicated so as to fill several dissertations. Instead the approach will be to establish the fundamentals for one and two electron systems*, provide a justification for the Racah parameters, and indicate how one would proceed to get the wave functions for $3d^5$ systems. The energy matrices for the $3d^5$ system will then simply be presented and diagonalized to provide the $O_h^{(8)}$ term splitting diagrams. For the details several texts have been written on the subject, most notably by Tanabe and Sugano[20] and, Gliemann and Schläfer[24]. In addition there are numerous books on molecular group theory and quantum chemistry the reader may refer to. For group theory this should include texts by Cotton[27] and Tinkham[28], for quantum chemistry this may include the classic by Eyring, Walter and Kimball[29]. In addition, the theory of atomic spectra is treated extensively in the classic book by Condon and Shortley[30].

Group Theoretical Preliminaries

In general, the wave functions of a state are the bases of an irreducible representation of the group whose symmetry operations leave the system unchanged. Consider the Schrödinger equation for a given system,

$$\mathbf{H}\phi_k = \epsilon_k \phi_k, \tag{1}$$

where $k = 1, 2 \ldots$. Say the system is invariant to symmetry operations $\mathbf{R}$ of group $\mathcal{G}$. The Hamiltonian operator is invariant when it is transformed by $\mathbf{R}$, thus,

$$\mathbf{R}\mathbf{H}\mathbf{R}^{-1} = \mathbf{H}. \tag{2}$$

Operating on Eq. (1) from the left with $\mathbf{R}$ we obtain,

$$\mathbf{R}\mathbf{H}\phi_k = \mathbf{R}\mathbf{H}\mathbf{R}^{-1}\mathbf{R}\phi_k = \mathbf{H}\mathbf{R}\phi_k = \epsilon_k \mathbf{R}\phi_k. \tag{3}$$

So if ϕ_k is an eigenfunction of $\mathbf{H}$ with eigenvalue ϵ_k then so is $\mathbf{R}\phi_k$ an eigenfunction with the same eigenvalue. Therefore in order to satisfy Eq. (1), $\mathbf{R}\phi_k$ must at most

---

*by this we will mean $3d^1$ and $3d^2$ electron systems outside closed shells.

simply be equal to a constant times the same function back again. This is the case of non-degeneracy, that is, one eigenfunction ϕ_k for one eigenvalue ϵ_k.

For the case of degeneracies, the Schrödinger equation is written,

$$\mathbf{H}\phi_{ki} = \epsilon_k \phi_{ki}, \tag{4}$$

where, $k = 1, 2 \ldots$ and $i = 1, 2, \ldots g_k$ with g_k denoting the number of eigenfunctions that produce the same eigenvalue ϵ_k. Operating with $\mathbf{R}$ in the group $\mathcal{G}$ we get,

$$\mathbf{H}\mathbf{R}\phi_{ki} = \epsilon_k \mathbf{R}\phi_{ki}. \tag{5}$$

Here we have g_k eigenfunctions per eigenvalue ϵ_k. The functions are said to span the kth degenerate subspace*. To satisfy Eq. (5), any operation $\mathbf{R}$ in the group $\mathcal{G}$ on ϕ_{ki} will transform it into another function which must lie in the kth degenerate subspace. That is,

$$\mathbf{R}\phi_{kj} = \sum_{i=1}^{g_k} \phi_{ki} \Gamma_{ij}^{(k)}(\mathbf{R}), \tag{6}$$

where $\Gamma_{ij}^{(k)}(\mathbf{R})$ are the numerical coefficients. This means that the new function $\mathbf{R}\phi_{kj}$ must at most be a linear combination of the set of functions within the kth degenerate subspace corresponding to the eigenvalue ϵ_k. The matrix $\mathbf{\Gamma}^{(k)}(\mathbf{R})$ is the representation for the operator $\mathbf{R}$ for the bases $\{\phi_{ki}; i = 1, 2, \ldots g_k\}$.

The connection between group theory and quantum mechanics can be now be stated. Given a group $\mathcal{G}$ which is the symmetry group of the system (i. e. $\mathbf{R}\mathbf{H}\mathbf{R}^{-1} = \mathbf{H}$) the solutions to the Schrödinger equation, ϕ_{ki}, form the basis of the kth irreducible representation of this group. Every energy level (i. e. eigenvalue ϵ_k) corresponds to an irreducible representation. Therefore, every energy level may be labeled by an irreducible representation of the symmetry group. Furthermore, the dimension of an irreducible representation is the degeneracy of its corresponding energy level. Since spectra measures energy levels we can denote spectra peaks by the irreducible representations of the symmetry group of the complex.

---

*also called the kth manifold.

Representations that are irreducible for one symmetry group frequently become reducible as the environment reduces symmetry. For example, an isolated atom has the symmetry of the full rotation group, R_∞. The solutions to the Schrödinger equation are therefore basis of the irreducible representations of the full rotation group denoted $\{\mathbf{\Gamma}_s, \mathbf{\Gamma}_p, \mathbf{\Gamma}_d, \cdots\}$ having dimensions $\{1, 3, 5, \cdots\}$ respectively. If the atom is placed in an environment of O_h symmetry the representations, $\{\mathbf{\Gamma}_s, \mathbf{\Gamma}_p, \mathbf{\Gamma}_d, \cdots\}$ become reducible. Given a reducible representation, group theory provides a method by which one may always reduce it to its constituent irreducible representations[27]. Specifically, $\Gamma_s \to a_{1g}$, $\Gamma_p \to t_{1u}$ and $\Gamma_d \to e_g \oplus t_{2g}$. The results of group theory are exact. From symmetry arguments alone we can say that for the case of a single d electron outside closed shells, if the isolated atom is placed in an environment of O_h symmetry the 5-fold degenerate d orbitals break up into a 3-fold degenerate and a 2-fold degenerate level. As far as the magnitude of the splitting is concerned group theory cannot answer this. This is because group theory does not allow one to actually solve the Schrödinger equation. It simply gives us information concerning the symmetry of the solutions once the symmetry of the Hamiltonian is known. In order to get the magnitude of the splitting one must at least approximately solve the Schrödinger equation. In this dissertation we will discuss two approaches, (1) ligand field perturbation theory and, (2) the method of Hartree-Fock. The method of ligand field perturbation theory will now be discussed.

One electron in a cubic field

Following the development of Tanabe and Sugano[20] we will first consider the case of a single d electron outside otherwise closed shells in a cubic six-coordinated $(O_h^{(6)})$ field. While we wish to consider the eight-coordinated ligand field, it turns out that the formalism is simplified if one works through the development for the six-coordinated system and then introduce the necessary corrections to convert to the eight-coordinated field at the end. For our purposes we will denote the six- and eight-coordinated O_h fields by $O_h^{(6)}$ and $O_h^{(8)}$ respectively.

Figure 2 defines the coordinate system. The $3d$ ion is located at the origin with six point charges arrayed along the axis as shown a distance a from the center. Each point ion has charge Z. The Schrödinger equation for this system is,

$$\left[-\frac{\hbar^2}{2m}\nabla^2 + U(\mathbf{r}) + V_c(\mathbf{r})\right]\phi(\mathbf{r}) = \epsilon\phi(\mathbf{r}), \tag{7}$$

where $U(\mathbf{r})$ is the potential energy due to the electrostatic field of the nucleus. $V_c(\mathbf{r})$ is the potential energy of an electron in the ligand (or crystal) field and is written,

$$V_c(\mathbf{r}) = \sum_{i=1}^{6} \frac{Ze^2}{|\mathbf{R}_i - \mathbf{r}|}, \tag{8}$$

where $\mathbf{r}$ is the electron coordinate and $\mathbf{R}_i$ is the position of the ith point ion. The potential energy is usually expanded in terms of Legendre polynomials, thus,

$$V_c(\mathbf{r}) = Ze^2 \sum_{i=1}^{6} \sum_{k=0}^{\infty} a^{-1}(r/a)^k P_k(\cos w_i), \tag{9}$$

where w_i is the angle between $\mathbf{R}_i$ and $\mathbf{r}$. Using the addition theorem for spherical harmonics, $V_c(\mathbf{r})$ can be written[20],

$$V_c(\mathbf{r}) = \sum_{k=0}^{\infty} \sum_{m=-k}^{k} r^k q_{km} C_m^{(k)}(\theta\phi), \tag{10}$$

where,

$$q_{km} = \left(\frac{4\pi}{2k+1}\right)^{1/2} \frac{Ze^2}{a^{k+1}} \sum_{i=1}^{6} Y_{km}^*(\theta_i\phi_i), \tag{11}$$

and,

$$C_m^{(k)}(\theta\phi) = \left(\frac{4\pi}{2k+1}\right)^{1/2} Y_{km}(\theta\phi). \tag{12}$$

The coordinates (r, θ, ϕ) locate the electron and the coordinates (a, θ_i, ϕ_i) locate the ligand point ions. Since $\{(\theta_1, \phi_1), (\theta_2, \phi_2), \cdots\} = \{(\frac{\pi}{2}, 0), (\frac{\pi}{2}, \frac{\pi}{2}), \cdots\}$, we know the q_{km}'s. These are given by,

$$q_{k0} = \left(\frac{2}{2k+1}\right)^{1/2} \frac{Ze^2}{a^{k+1}} \left[\Theta_{k0}(0) + 4\Theta_{k0}\left(\frac{\pi}{2}\right) + \Theta_{k0}(\pi)\right]$$

$$q_{km} = \left(\frac{2}{2k+1}\right)^{1/2} \frac{Ze^2}{a^{k+1}} \Theta_{km}\left(\frac{\pi}{2}\right) \left[1 + e^{i\frac{m\pi}{2}} + e^{im\pi} + e^{i\frac{3m\pi}{2}}\right] \quad (m : \text{ even} \neq 0)$$

$$q_{km} = 0 \quad (m : \text{ odd})$$
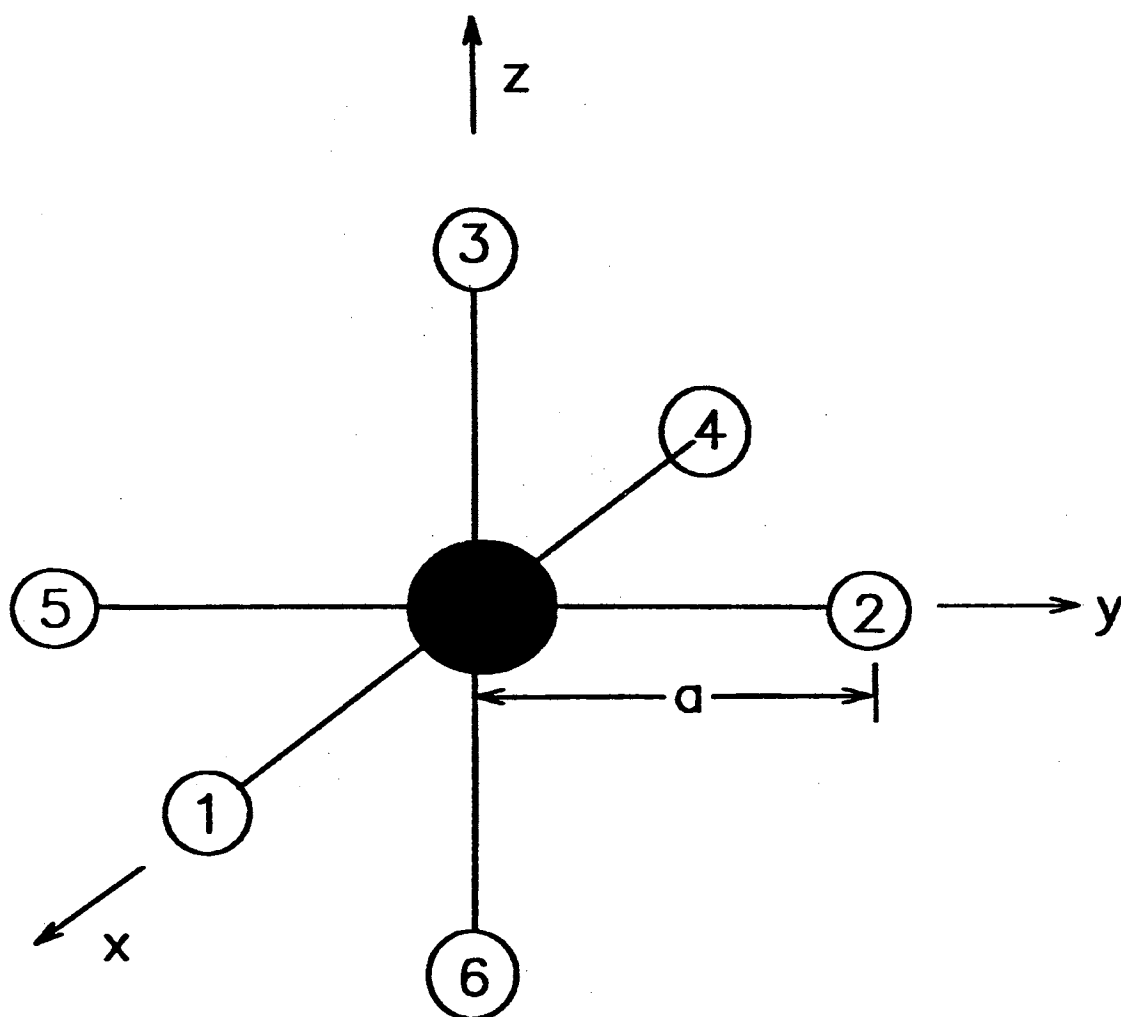
Figure 2. A 3*d* atom surrounded by six point charges, $-Ze$; O_h symmetry. Here $Z > 0$ for the negative charge and $Z < 0$ for the positive charge. The distance between the 3*d* atom and each point charge is a, so that the system has cubic symmetry.

here $\Theta_{km}(\theta)$ is defined by, $Y_{km}(\theta\phi) = (2\pi)^{-1/2}\Theta_{km}(\theta)e^{im\phi}$. We are thus able to expand the potential energy due to the ligand field in terms of the spherical harmonics, thus,

$$V_c(\mathbf{r}) = \frac{6Ze^2}{a} + \frac{7Ze^2}{2a^5}r^4\left\{ C_0^{(4)}(\theta\phi) + \left(\frac{5}{14}\right)^{1/2}[C_4^{(4)}(\theta\phi) + C_{-4}^{(4)}(\theta\phi)] \right\}$$

$$+ \frac{3Ze^2}{4a^7}r^6\left\{ C_0^{(6)}(\theta\phi) - \left(\frac{7}{2}\right)^{1/2}[C_4^{(6)}(\theta\phi) + C_{-4}^{(6)}(\theta\phi)] \right\}$$

$$+ \cdots \tag{13}$$

This field giving rise to the potential energy whose angular dependence is given by this equation is called a cubic field. The first term is a constant and represents the potential energy of the electron at the origin and elevates all the energy levels by the same amount, $6Ze^2/a$. As we will see the other terms split some of the degenerate levels. Since the first term in Eq. (13) is independent of the electron coordinate and since we will only be interested in the relative energy differences we will shift the energy origin by $6Ze^2/a$. In what follows we shall work with the potential energy function $V_c^0(\mathbf{r})$ given by,

$$V_c^0(\mathbf{r}) = V_c(\mathbf{r}) - \frac{6Ze^2}{a}. \tag{14}$$

$V_c^0(\mathbf{r})$ will act as the perturbation on the isolated atom.

The unperturbed wave function may be written,

$$\phi_{nlm}(\mathbf{r}) = R_{nl}(r)Y_{lm}(\theta\phi). \tag{15}$$

From perturbation theory[29], the first order correction to the energies is given by diagonalizing the matrix consisting of elements formed from the perturbing operator, $V_c^0(\mathbf{r})$, and the unperturbed states. These matrix elements are,

$$\langle \phi_{nlm}|V_c^0|\phi_{n'l'm'}\rangle = \int d\mathbf{r}\,\phi_{nlm}^*(\mathbf{r})V_c^0(\mathbf{r})\phi_{n'l'm'}(\mathbf{r}). \tag{16}$$

It may be demonstrated [20] that Eq. (16) is nonvanishing only when,

$$k + l + l' = \text{even} \qquad \text{and} \qquad |l - l'| \leq k \leq l + l'. \tag{17}$$

The matrix elements of V_c^0 between the $s(l = l' = 0)$ and $p(l = l' = 1)$ vanish. For the s states $k = 0$ and the expansion of V_c^0 does not include a $k = 0$ term. For the p states $k = 0, 1, 2$ and again V_c^0 does not include $k = 0, 1$ or 2 term. Therefore the s and p states do not split in a cubic field. This result agrees with that predicted from group theory. Between the d states ($l = l' = 2$), $k = 0, 1, 2, 3, 4$ so we see that terms for $k > 4$ vanish. So setting $n = n'$ and $l = l' = 2$ we get the following matrix elements,

$$\langle \phi_{nd\pm2}|V_c^0|\phi_{nd\pm2}\rangle = Dq$$

$$\langle \phi_{nd\pm1}|V_c^0|\phi_{nd\pm1}\rangle = -4Dq$$

$$\langle \phi_{nd0}|V_c^0|\phi_{nd0}\rangle = 6Dq$$

$$\langle \phi_{nd\pm2}|V_c^0|\phi_{nd\mp2}\rangle = 5Dq \tag{18}$$

where $D = 35Ze^2/4a^5$ and $q = (2/105)\langle r^4\rangle_{nd}$ *.

From degenerate perturbation theory, the perturbed energies, ϵ, of the $3d$ level due to the presence of the point charges is given by solving the secular equation,

$$\begin{vmatrix} \epsilon_d^0 + Dq - \epsilon & 0 & 0 & 0 & 5Dq \\ 0 & \epsilon_d^0 - 4Dq - \epsilon & 0 & 0 & 0 \\ 0 & 0 & \epsilon_d^0 + 6Dq - \epsilon & 0 & 0 \\ 0 & 0 & 0 & \epsilon_d^0 - 4Dq - \epsilon & 0 \\ 5Dq & 0 & 0 & 0 & \epsilon_d^0 + Dq - \epsilon \end{vmatrix} = 0 \tag{19}$$

where $\epsilon_d^0 = \epsilon_d + (6Ze^2/a)$. From this secular equation we get the following five roots; three are the same and two are the same.

$$\epsilon^{(1)}, \epsilon^{(2)}, \epsilon^{(3)} = \epsilon_d^0 - 4Dq = \epsilon(t_{2g}) \tag{20}$$

$$\epsilon^{(4)}, \epsilon^{(5)} = \epsilon_d^0 + 6Dq = \epsilon(e_g) \tag{21}$$

Figure 3 shows that for the six-coordinated O_h field, the energies of the $3d$ levels, ϵ_d, is first raised by a constant factor $6Ze^2/a$ to ϵ_d^0 and then split into $\epsilon(e_g)$ and

---

*$\langle r^m\rangle_{nd} = \int r^{2+m}|R_{nd}(r)|^2 dr$

$\epsilon(t_{2g})$ as the angular perturbation of the O_h field is accounted for. We find that the magnitude of the splitting is $10Dq$.

Also from degenerate perturbation theory we find that diagonalizing the perturbation matrix (that is, solving the secular equation), leads to the wave functions of the split levels. For the t_{2g} state:

$$
\begin{aligned}
\phi_\xi &= (i/\sqrt{2})(\phi_{3d1} + \phi_{3d-1}), \\
\phi_\eta &= -(1/\sqrt{2})(\phi_{3d1} - \phi_{3d-1}), \\
\phi_\zeta &= -(i/\sqrt{2})(\phi_{3d2} - \phi_{3d-2}).
\end{aligned}
\tag{22}
$$

For the e_g state:

$$
\begin{aligned}
\phi_\mu &= \phi_{3d0}, \\
\phi_\nu &= (1/\sqrt{2})(\phi_{3d2} + \phi_{3d-2}).
\end{aligned}
\tag{23}
$$

The functions $\{\phi_\xi, \phi_\eta, \phi_\zeta\}$ form the basis for the t_{2g} irreducible representation and the functions $\{\phi_\mu, \phi_\nu\}$ form the basis of the e_g irreducible representation of the O_h group.

<center>Two electrons in a cubic field</center>

The two-electron wave functions

For the case of the one d electron in a cubic field* we treated the interaction with the ligand field as the perturbation. Also for the one electron case we did not include spin explicitly nor did we have to consider antisymmetry. In this section will introduce the methods required to treat two or more $3d$ electrons in the ligand field. We will work out much of the detail for two electrons and then argue that by using the same methods one may successfully treat the $3d^5$ case.

The general plan of attack in constructing the two-electron wave function will involve the following five elements.

- Explicitly include spin.

---

*again, by this we actually mean one d electron outside otherwise closed shells
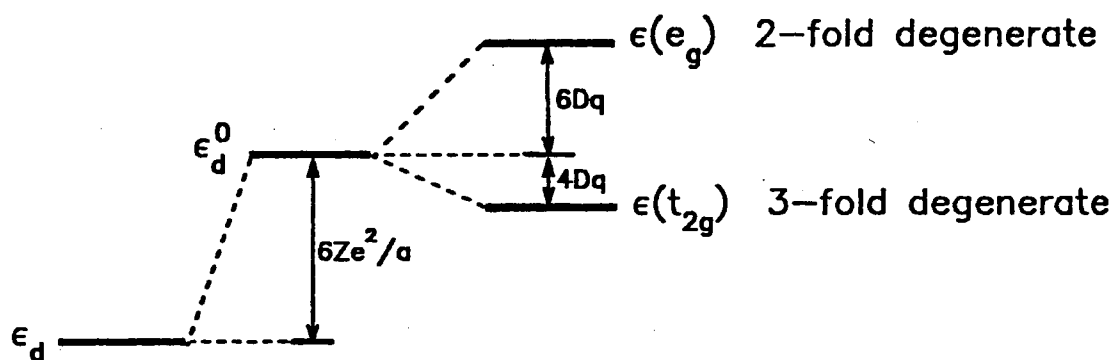
Figure 3. The splitting of one-electron energy levels for the six-coordinated O_h field. ϵ_d is first raised by a constant factor $6Ze^2/a$ to ϵ_d^0 and then split into $\epsilon(e_g)$ and $\epsilon(t_{2g})$ as the angular perturbation of the O_h field is accounted for.

- Include the principle of antisymmetry.

- Construct the two-electron wave functions out of the perturbed one-electron wave functions from the previous section. In this way we build in the ligand field effects.

- Construct the two-electron wave functions in such a way that they maintain symmetry. That is, the two-electron wave functions must form the basis for the irreducible representations of the symmetry group; in this case O_h.

- Treat the inter-electron coulombic interaction as a perturbation.

Notice that we will assume here that the ligand field is much stronger than the inter-electron interaction. This is the so-called *strong field* approach[20].

For a stationary nucleus and two electrons, the Schrödinger equation is,

$$\mathbf{H}\Psi(\mathbf{r}_1,\sigma_1,\mathbf{r}_2,\sigma_2) = E\Psi(\mathbf{r}_1,\sigma_1,\mathbf{r}_2,\sigma_2), \tag{24}$$

where σ_i $(i = 1,2)$ is the spin coordinate of electron i and takes on two values $1/2$ and $-1/2$. In accordance with perturbation theory, we split the Hamiltonian as,

$$\mathbf{H} = \mathbf{H}_0 + \mathbf{H}_1. \tag{25}$$

$\mathbf{H}_0$ is the unperturbed (or "core") Hamiltonian and is, written $\mathbf{H}_0 = \mathbf{f}_1 + \mathbf{f}_2$ where $\mathbf{f}_i = -\frac{1}{2}\nabla_i^2 + V_c(\mathbf{r}_i)$. The perturbation is produced by $\mathbf{H}_1 = g_{12} = 1/r_{12}$ where $r_{12} = |\mathbf{r}_1 - \mathbf{r}_2|$ and represents the inter-electron coulombic interaction in atomic units.

The standard way to proceed is to first solve the unperturbed problem. The unperturbed Schrödinger equation is,

$$\mathbf{H}_0\Psi_0(\mathbf{r}_1,\sigma_1,\mathbf{r}_2,\sigma_2) = E_0\Psi_0(\mathbf{r}_1,\sigma_1,\mathbf{r}_2,\sigma_2). \tag{26}$$

Since $\mathbf{H}_0 = \mathbf{f}_1 + \mathbf{f}_2$, the solution to this equation can be obtained if the solution to the single electron problem is known. This equation is,

$$\mathbf{f}\phi_k(\mathbf{r},\sigma) = \epsilon_k\phi_k(\mathbf{r},\sigma). \tag{27}$$

Since the operator $\mathbf{f}$ does not include the spin-coordinate, $\phi_k(\mathbf{r}, \sigma)$ is given by a simple product of a spatial orbital function, $\phi_k(\mathbf{r})$ obtained from solving Eq. (27), and a spin function $\alpha(\sigma)$ or $\beta(\sigma)$. Thus $\phi_k(\mathbf{r}, \sigma)$ is called a *spin-orbital*. The spin functions are defined as,

$$\alpha(\sigma = 1/2) = 1 \qquad \alpha(\sigma = -1/2) = 0$$

$$\beta(\sigma = 1/2) = 0 \qquad \beta(\sigma = -1/2) = 1. \qquad (28)$$

One could construct the unperturbed two-electron wave function as a simple product of the spin-orbital solutions to the one-electron problem. However a simple product is not antisymmetric. Another choice is to construct the unperturbed two-electron solution, $\Psi_{0kl}(\mathbf{r}_1, \sigma_1, \mathbf{r}_2, \sigma_2)$, as an antisymmetrized product of the spin orbitals. The simplest antisymmetrized product is a single Slater determinant, thus,

$$\Psi_{0kl}(\mathbf{r}_1, \sigma_1, \mathbf{r}_2, \sigma_2) = \frac{1}{\sqrt{2!}} \begin{vmatrix} \phi_k(\mathbf{r}_1\sigma_1) & \phi_l(\mathbf{r}_1\sigma_1) \\ \phi_k(\mathbf{r}_2\sigma_2) & \phi_l(\mathbf{r}_2\sigma_2) \end{vmatrix} \equiv |\phi_k\phi_l|. \qquad (29)$$

It can be shown that the Slater determinant is an eigenfunction of $\mathbf{H}_0$ with eigenvalue $E_0 = \epsilon_k + \epsilon_l$.

For the one electron case only two configurations are possible, t_{2g} and e_g. If we add one electron but do not let the two electrons interact, the possible configurations become, t_{2g}^2, e_g^2 and $t_{2g}e_g$. Since,

$$E_{t_{2g}} = \langle \phi_\xi |\mathbf{f}| \phi_\xi \rangle = \langle \phi_\eta |\mathbf{f}| \phi_\eta \rangle = \langle \phi_\zeta |\mathbf{f}| \phi_\zeta \rangle = \epsilon_d^0 - 4Dq,$$

$$E_{e_g} = \langle \phi_\mu |\mathbf{f}| \phi_\mu \rangle = \langle \phi_\nu |\mathbf{f}| \phi_\nu \rangle = \epsilon_d^0 + 6Dq,$$

the unperturbed two-electron energies then are,

$$E_{t_{2g}^2} = 2\langle \phi_\xi |\mathbf{f}| \phi_\xi \rangle = 2\epsilon_d^0 - 8Dq,$$

$$E_{e_g^2} = 2\langle \phi_\mu |\mathbf{f}| \phi_\mu \rangle = 2\epsilon_d^0 + 12Dq, \qquad (30)$$

$$E_{t_{2g}e_g} = \langle \phi_\xi |\mathbf{f}| \phi_\xi \rangle + \langle \phi_\mu |\mathbf{f}| \phi_\mu \rangle = E_{t_{2g}} + E_{e_g} = 2\epsilon_d^0 + 2Dq.$$

The next step is to determine the degeneracy of the three unperturbed two-electron states t_{2g}^2, e_g^2 and $t_{2g}e_g$. Consider for example the t_{2g}^2 state. We know that the orbital functions associated with t_{2g} are $\phi_\xi(\mathbf{r})$, $\phi_\eta(\mathbf{r})$ and $\phi_\zeta(\mathbf{r})$ which we will simply

write as $\xi(\mathbf{r})$, $\eta(\mathbf{r})$ and $\zeta(\mathbf{r})$. Since we have two spin functions $\alpha(\sigma)$ and $\beta(\sigma)$ we have six spin orbitals $\xi(\mathbf{r})\alpha(\sigma), \xi(\mathbf{r})\beta(\sigma), \eta(\mathbf{r})\alpha(\sigma), \cdots$. So there are six ways of placing the first electron in the first t_{2g} single-electron state. However, because of the exclusion principle the second electron cannot be placed in the spin orbital where the first one is already accommodated, so the number of ways of accommodating two electrons is given by the binomial coefficient $_6C_2 = \frac{6!}{2!4!} = 15^*$. Abbreviating the spin orbitals for example $\xi\alpha$ and $\xi\beta$ as ξ and $\bar{\xi}$, we get the following 15 unperturbed two-electron states for the t_{2g}^2 configuration:

$$
\begin{array}{cccccc}
|\xi\eta| & |\bar{\xi}\bar{\eta}| & |\eta\zeta| & |\bar{\eta}\bar{\zeta}| & |\zeta\xi| & |\bar{\zeta}\bar{\xi}| \\
|\xi\bar{\eta}| & |\bar{\xi}\eta| & |\eta\bar{\zeta}| & |\bar{\eta}\zeta| & |\zeta\bar{\xi}| & |\bar{\zeta}\xi| \\
|\xi\bar{\xi}| & |\eta\bar{\eta}| & |\zeta\bar{\zeta}| & & &
\end{array}
\tag{31}
$$

In the same way we get $_4C_2 = 6$ for the e_g^2 configuration and for $t_{2g}e_g$ we need not worry about the exclusion principle so we get $6 \times 4 = 24$ different valid arrangements. When the inter-electron interaction is neglected all the states arising from the different configurations are degenerate. This degeneracy will be partially removed when the inter-electron interaction is taken into account. We could proceed according to degenerate perturbation theory and diagonalize the $\mathbf{H}_1$ matrix formed from the unperturbed two-electron wave functions. These matrices would be 15×15 for t_{2g}^2, 6×6 for e_g^2 and 24×24 for $t_{2g}e_g$. However, just as for the single electron case we can determine the splitting by group theory.

We note that the total Hamiltonian $\mathbf{H}_0 + \mathbf{H}_1$ is invariant under an operation $\mathbf{R}$ of the O_h group. Therefore, according to group theory the eigenfunctions associated with a certain energy level of this system are the basis of an irreducible representation, say Γ, of the O_h group. Therefore every energy level may be labeled by Γ. Also, the full Hamiltonian commutes with the spin operator $\mathbf{S}$. Therefore $\mathbf{S}^2$ is a constant of the motion and has a definite value $S(S+1)$ in the eigenstate.

As a whole, the energy levels are characterized by $S\Gamma$ and have $(2S+1) \times (\Gamma)$-fold degeneracy. Here (Γ) is the dimension of the irreducible representation Γ. The

---

$^*{}_nC_k = \frac{n!}{k!(n-k)!}$

$2S + 1$ occurs because the eigenvalues M_S of $\mathbf{S}_z$ in the eigenstate take on values $S, S - 1, \ldots - S + 1, -S$ and the energy eigenvalues are independent of these values of M_S. The energy levels characterized by $S\Gamma$ are called *terms* and are denoted by $^{2S+1}\Gamma$. The $(2S + 1) \times (\Gamma)$ wave functions of the $^{2S+1}\Gamma$ term are expressed as $\Psi(\alpha S\Gamma M\gamma)$ where,

α: denotes the parent configuration, t_{2g}^2, e_g^2, $t_{2g}e_g$ in this case,

S: is the spin angular momentum quantum number,

Γ: is the irreducible representation of the symmetry group for which $\Psi(\alpha S\Gamma M\gamma)$ transforms,

M: is an abbreviation of M_S,

γ: denotes the different functions which form the bases of Γ, that is, if Γ is three-dimensional γ indexes the three different functions.

From the Slater determinants for each configuration t_{2g}^2, e_g^2 and $t_{2g}e_g$ we must find linear combinations to construct the $\Psi(\alpha S\Gamma M\gamma)$ functions such that they satisfy the following requirements,

$$\mathbf{R}\Psi(\alpha S\Gamma M\gamma) \;=\; \sum_{\gamma'} \Psi(\alpha S\Gamma M\gamma')\Gamma_{\gamma\gamma'}(\mathbf{R}), \tag{32}$$

$$\mathbf{S}^2\Psi(\alpha S\Gamma M\gamma) \;=\; S(S + 1)\Psi(\alpha S\Gamma M\gamma), \tag{33}$$

$$\mathbf{S}_z\Psi(\alpha S\Gamma M\gamma) \;=\; M\Psi(\alpha S\Gamma M\gamma). \tag{34}$$

We note that since the $\Psi(\alpha S\Gamma M\gamma)$ functions are the unperturbed two-electron wave functions so they of course must be eigenfunctions of $\mathbf{H}_0$, but because they are being constructed out of linear combinations of the Slater determinants given above they already are.

From group theory, the functions $\Psi(\alpha S\Gamma M\gamma)$ will transform as basis of their respective product representations. That is,

$\Psi(t_{2g}^2 S\Gamma M\gamma)$	will transform as	$T_{2g} \otimes T_{2g},$
$\Psi(e_g^2 S\Gamma M\gamma)$	will transform as	$E_g \otimes E_g,$
$\Psi(t_{2g}e_g S\Gamma M\gamma)$	will transform as	$T_{2g} \otimes E_g.$

We will adopt a notation using capital letters to denote the irreducible representations of the symmetry group under which the many-electron wave functions transform.

We will not develop the theory of product representations here except to say that each of these product representations are reducible in the O_h group. That is, it can be shown[20,27,29] that,

$$T_{2g} \otimes T_{2g} = A_{1g} \oplus E_g \oplus T_{1g} \oplus T_{2g}, \tag{35}$$

$$E_g \otimes E_g = A_{1g} \oplus A_{2g} \oplus E_g, \tag{36}$$

$$T_{2g} \otimes E_g = T_{1g} \oplus T_{2g}. \tag{37}$$

From group theory alone we have determined that the t_{2g}^2 level splits into 4 levels, the e_g^2 level into 3, and the $t_{2g}e_g$ splits into 2 levels.

Now to deal with spin multiplicity. For a two electron system $S = 0, 1$, this means for example that the t_{2g}^2 configuration the following terms are possible,

$$t_{2g}^2 : \quad \left\{ \begin{array}{cccc} {}^1A_{1g} & {}^1E_g & {}^1T_{1g} & {}^1T_{2g} \\ {}^3A_{1g} & {}^3E_g & {}^3T_{1g} & {}^3T_{2g} \end{array} \right\}. \tag{38}$$

For the e_g^2 and $t_{2g}e_g$ configurations the following terms are possible,

$$e_g^2 : \quad \left\{ \begin{array}{ccc} {}^1A_{1g} & {}^1A_{2g} & {}^1E_g \\ {}^3A_{1g} & {}^3A_{2g} & {}^3E_g \end{array} \right\} \tag{39}$$

$$t_{2g}e_g : \quad \left\{ \begin{array}{cc} {}^1T_{1g} & {}^1T_{2g} \\ {}^3T_{1g} & {}^3T_{2g} \end{array} \right\}. \tag{40}$$

From group theory alone we cannot ascertain the spin multiplicity of each term. One must actually construct the wave functions.

Without presenting the details, the formula for constructing the two-electron unperturbed wave function from the Slater determinants which is base γ of irreducible representation Γ of the O_h group and at the same time an eigenfunction of the $\mathbf{S}^2$ and $\mathbf{S}_z$ operators with eigenvalues $S(S+1)$ and M respectively is[20],

$$\Psi(\alpha S \Gamma M \gamma) = \sum_{m_1, m_2 = \pm 1/2} \sum_{\gamma_1, \gamma_2} |\phi(\Gamma_1 m_1 \gamma_1) \phi(\Gamma_2 m_2 \gamma_2)|$$

$$\times \quad \left\langle \frac{1}{2}m_1 \frac{1}{2}m_2 \Big| SM \right\rangle \langle \Gamma_1 \gamma_1 \Gamma_2 \gamma_2 | \Gamma \gamma \rangle, \tag{41}$$

where $\langle \frac{1}{2}m_1 \frac{1}{2}m_2 | SM \rangle$ are the *Wigner spin-coupling coefficients* and $\langle \Gamma_1 \gamma_1 \Gamma_2 \gamma_2 | \Gamma \gamma \rangle$ are the *Clebsch-Gordan vector coupling coefficients*. They are tabulated in texts dealing with the subject of multiplet structure such as Condon and Shortly[30] or Tanabe and Sugano[20]. As one example we consider the specific case where $\alpha = t_{2g}^2$. Equation (41) becomes,

$$\begin{aligned}
\Psi(t_{2g}^2 S \Gamma M \gamma) &= \sum_{m_1, m_2 = \pm 1/2} \sum_{\gamma_1, \gamma_2 = \xi, \eta, \zeta} |\phi(t_{2g} m_1 \gamma_1) \phi(t_{2g} m_2 \gamma_2)| \\
&\times \left\langle \frac{1}{2}m_1 \frac{1}{2}m_2 \Big| SM \right\rangle \langle t_{2g} \gamma_1 t_{2g} \gamma_2 | \Gamma \gamma \rangle,
\end{aligned} \tag{42}$$

where, $S = 0, 1$, $M = -S, -S+1, \dots S$, $\Gamma = A_{1g}, E_g, T_{1g}, T_{2g}$, and γ denotes the different functions which are the basis of the irreducible representation Γ (for example, γ takes on three values if $\Gamma = T_{1g}$, say, α, β, γ). By using this formula we find that of the eight possible sets of $^{2S+1}\Gamma$ for t_{2g}^2, the wave functions of $^3A_{1g}$, ^3E_g, $^1T_{1g}$, and $^3T_{2g}$ are identically zero. This leaves only the four terms $^1A_{1g}$, ^1E_g, $^3T_{1g}$ and $^1T_{2g}$. So we find that the wave functions for the t_{2g}^2 configuration are,

$^1A_{1g}$:
$$\Psi(t_{2g}^2{}^1A_{1g}) = [|\xi\bar\xi| + |\eta\bar\eta| + |\zeta\bar\zeta|](1/\sqrt{3}) \tag{43}$$

^1E_g : 2-fold degen.
$$\begin{cases} \Psi(t_{2g}^2{}^1E_g u) = [-|\xi\bar\xi| - |\eta\bar\eta| + 2|\zeta\bar\zeta|](1/\sqrt{6}) \\ \Psi(t_{2g}^2{}^1E_g v) = [|\xi\bar\xi| - |\eta\bar\eta|](1/\sqrt{2}) \end{cases} \tag{44}$$

$^3T_{1g}$: 9-fold degen.
$$\begin{cases} \Psi(t_{2g}^2{}^3T_{1g}M = 1\gamma) = |\xi\eta| \\ \Psi(t_{2g}^2{}^3T_{1g}M = 0\gamma) = [|\xi\bar\eta| - |\eta\bar\xi|](1/\sqrt{2}) \\ \Psi(t_{2g}^2{}^3T_{1g}M = -1\gamma) = |\bar\xi\bar\eta| \\ \vdots \end{cases} \tag{45}$$

$^1T_{2g}$: 3-fold degen.
$$\begin{cases} \Psi(t_{2g}^2{}^1T_{2g}\zeta) = [|\xi\bar\eta| + |\eta\bar\xi|](1/\sqrt{2}) \\ \vdots \end{cases} \tag{46}$$

In the same way the remaining terms from the e_g^2 configuration are $^1A_{1g}$, $^3A_{2g}$, ^1E_g. The remaining terms for the $t_{2g}e_g$ are $^3T_{1g}$, $^3T_{2g}$, $^1T_{1g}$ and $^1T_{2g}$. Figure 4 shows the splitting of the two-electron configurations.
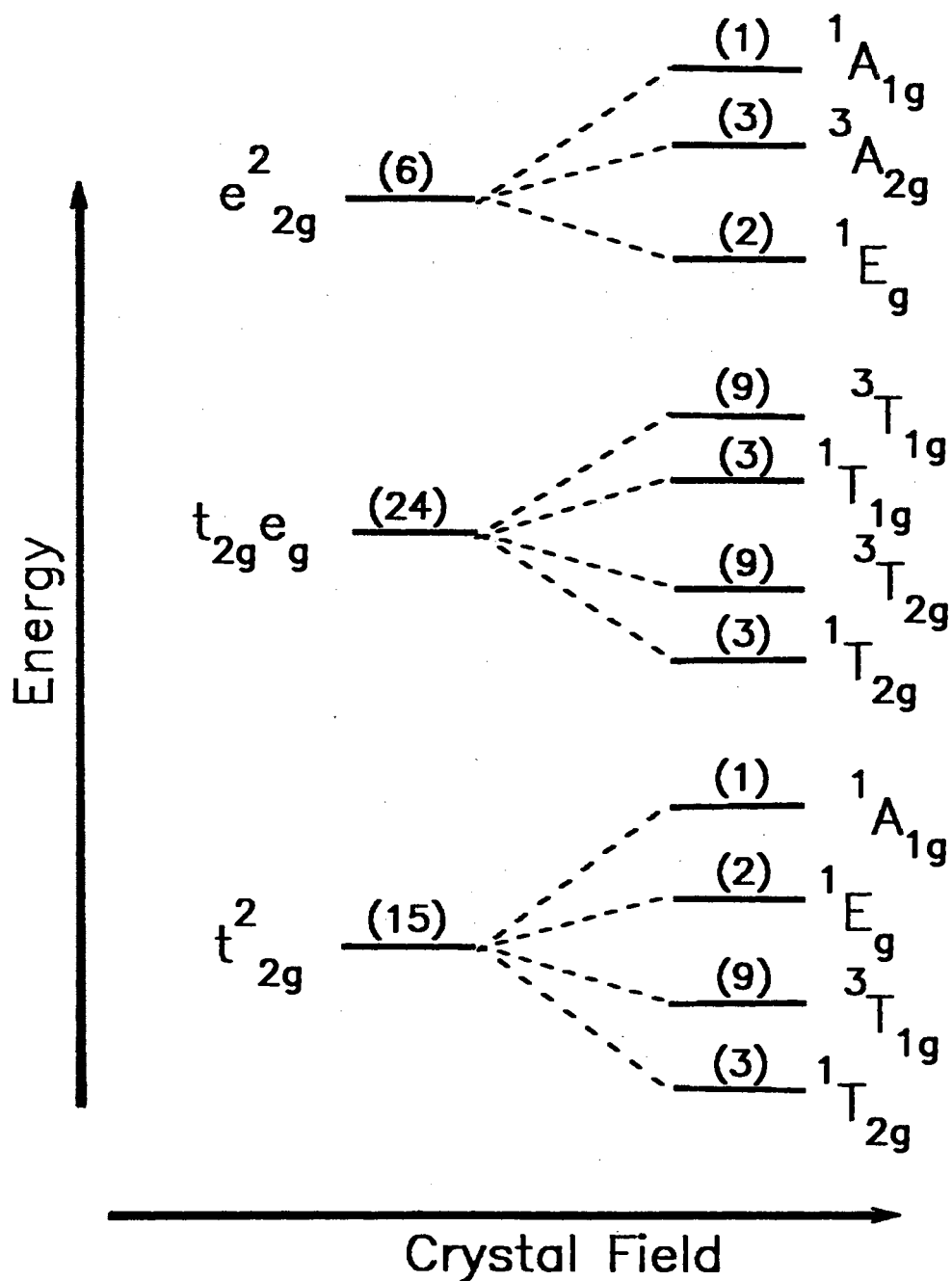
Figure 4. The surviving terms arising from the two-electron configurations, t_{2g}^2, e_g^2 and $t_{2g}e_g$. Note that all the states possible from group theory are not manifested in the final term splitting. Also the total number of states must be conserved.

Term energies

In this section we will develop some of the ideas behind the calculation of term energies and the definition of the Racah parameters. As a means of illustration we will continue with the two electron case.

From first order perturbation theory, we get the first order correction to the energy by calculating the matrix elements of the perturbation operator $\mathbf{H}_1$ between the unperturbed wave functions found in the previous section. We get the final energies by diagonalizing the total Hamiltonian matrix, $\mathbf{H}_0 + \mathbf{H}_1$. For instance, the first order correction to the energy of the state $^1A_{1g}$ of the configuration t_{2g}^2 is given by solving,

$$\langle t_{2g}^2\,^1A_{1g}|\mathbf{H}_1|t_{2g}^2\,^1A_{1g}\rangle. \tag{47}$$

Since $\Psi(t_{2g}^2\,^1A_{1g}) = [|\xi\bar{\xi}| + |\eta\bar{\eta}| + |\zeta\bar{\zeta}|](1/\sqrt{3})$, we must evaluate integrals of the type,

$$I = \sum_{\sigma_1,\sigma_2=\uparrow\downarrow} \int d\tau_1 d\tau_2 \ |\phi_{\lambda_1 m_1 \gamma_1}(\mathbf{r}_1\sigma_1)\phi_{\lambda_2 m_2 \gamma_2}(\mathbf{r}_2\sigma_2)|^*\,(1/r_{12})$$
$$\times |\phi_{\lambda_1' m_1' \gamma_1'}(\mathbf{r}_1\sigma_1)\phi_{\lambda_2' m_2' \gamma_2'}(\mathbf{r}_2\sigma_2)| \tag{48}$$

where λ_1, λ_2 represent t_{2g} and/or e_g. The spin orbitals $\phi_{\lambda m \gamma}(\mathbf{r}\sigma)$ can be written,

$$\phi_{\lambda m \gamma}(\mathbf{r}\sigma) = \Phi_{\lambda\gamma}(\mathbf{r})\theta_{\frac{1}{2}m}(\sigma), \tag{49}$$

where the spin functions are defined in the usual sense,

$$\theta_{\frac{1}{2}\frac{1}{2}}(\uparrow) = 1 \qquad \theta_{\frac{1}{2}-\frac{1}{2}}(\uparrow) = 0$$
$$\theta_{\frac{1}{2}\frac{1}{2}}(\downarrow) = 0 \qquad \theta_{\frac{1}{2}-\frac{1}{2}}(\downarrow) = 1$$

Since $1/r_{12}$ does not depend on spin coordinates, the spin part of each spin orbital can be summed over. It can be shown that an integral of this type may be written, for $\lambda_1 = \lambda_1'$, $\gamma_1 = \gamma_1'$ and $\lambda_2 = \lambda_2'$, $\gamma_2 = \gamma_2'$, as[20],

$$I = J(\lambda_1\gamma_1\lambda_2\gamma_2) - \delta_{m_1 m_2}K(\lambda_1\gamma_1\lambda_2\gamma_2), \tag{50}$$

where,

$$J(\lambda_1\gamma_1\lambda_2\gamma_2) = \int d\tau_1 d\tau_2 \phi^*_{\lambda_1\gamma_1}(\mathbf{r}_1)\phi^*_{\lambda_2\gamma_2}(\mathbf{r}_2)$$

$$\times \left(\frac{1}{r_{12}}\right) \phi_{\lambda_1\gamma_1}(\mathbf{r}_1)\phi_{\lambda_2\gamma_2}(\mathbf{r}_2) \equiv \langle\lambda_1\gamma_1\lambda_2\gamma_2||\lambda_1\gamma_1\lambda_2\gamma_2\rangle, \quad (51)$$

is called the *Coulomb Integral*, and where,

$$K(\lambda_1\gamma_1\lambda_2\gamma_2) = \int d\tau_1 d\tau_2 \phi^*_{\lambda_1\gamma_1}(\mathbf{r}_1)\phi^*_{\lambda_2\gamma_2}(\mathbf{r}_2)$$

$$\times \left(\frac{1}{r_{12}}\right) \phi_{\lambda_2\gamma_2}(\mathbf{r}_1)\phi_{\lambda_1\gamma_1}(\mathbf{r}_2) \equiv \langle\lambda_1\gamma_1\lambda_2\gamma_2||\lambda_2\gamma_2\lambda_1\gamma_1\rangle, \quad (52)$$

is called the *Exchange Integral*. We note that $J(\lambda_1\gamma_1\lambda_2\gamma_2) \geq K(\lambda_1\gamma_1\lambda_2\gamma_2) \geq 0$[20].

Using the two-electron wave functions obtained for the various terms we may now express the first order correction to the energy in terms of the Coulomb and Exchange Integrals. Recall that λ_1, λ_2 represent t_{2g} and/or e_g and γ_1, γ_2 index the functions associated with either λ_1 or λ_2. For instance, if $\lambda_1 = t_{2g}$ then $\gamma_1 = \xi, \eta, \zeta$. If $\lambda_1 = e_g$ then $\gamma_1 = \mu, \nu$. Lets consider the t_{2g}^2 configuration. In this case $\lambda_1 = \lambda_2 = t_{2g}$ and $\gamma_1, \gamma_2 = \xi, \eta, \zeta$. If we only consider the t_{2g}^2 configuration we can simplify the notation by writing $J(t_{2g}\gamma_1 t_{2g}\gamma_2)$ as $J(\gamma_1\gamma_2)$ and $K(t_{2g}\gamma_1 t_{2g}\gamma_2)$ as $K(\gamma_1\gamma_2)$. With this notational convention we find for t_{2g}^2[20],

$$\langle t_{2g}^2\,^1A_{1g}|\mathbf{H}_1|t_{2g}^2\,^1A_{1g}\rangle = J(\zeta\zeta) + 2K(\xi\eta), \quad (53)$$

$$\langle t_{2g}^2\,^1E_g u|\mathbf{H}_1|t_{2g}^2\,^1E_g u\rangle = J(\zeta\zeta) - K(\xi\eta), \quad (54)$$

$$\langle t_{2g}^2\,^3T_{1g}M = 0\gamma|\mathbf{H}_1|t_{2g}^2\,^3T_{1g}M = 0\gamma\rangle = J(\xi\eta) - K(\xi\eta), \quad (55)$$

$$\langle t_{2g}^2\,^1T_{2g}\zeta|\mathbf{H}_1|t_{2g}^2\,^1T_{2g}\zeta\rangle = J(\xi\eta) + K(\xi\eta). \quad (56)$$

It turns out that if the t_{2g} functions are d-functions, the ^1E_g and $^1T_{2g}$ terms are degenerate. Figure 5 shows a diagram of the splitting of the two-electron terms arising from the t_{2g}^2 configuration.
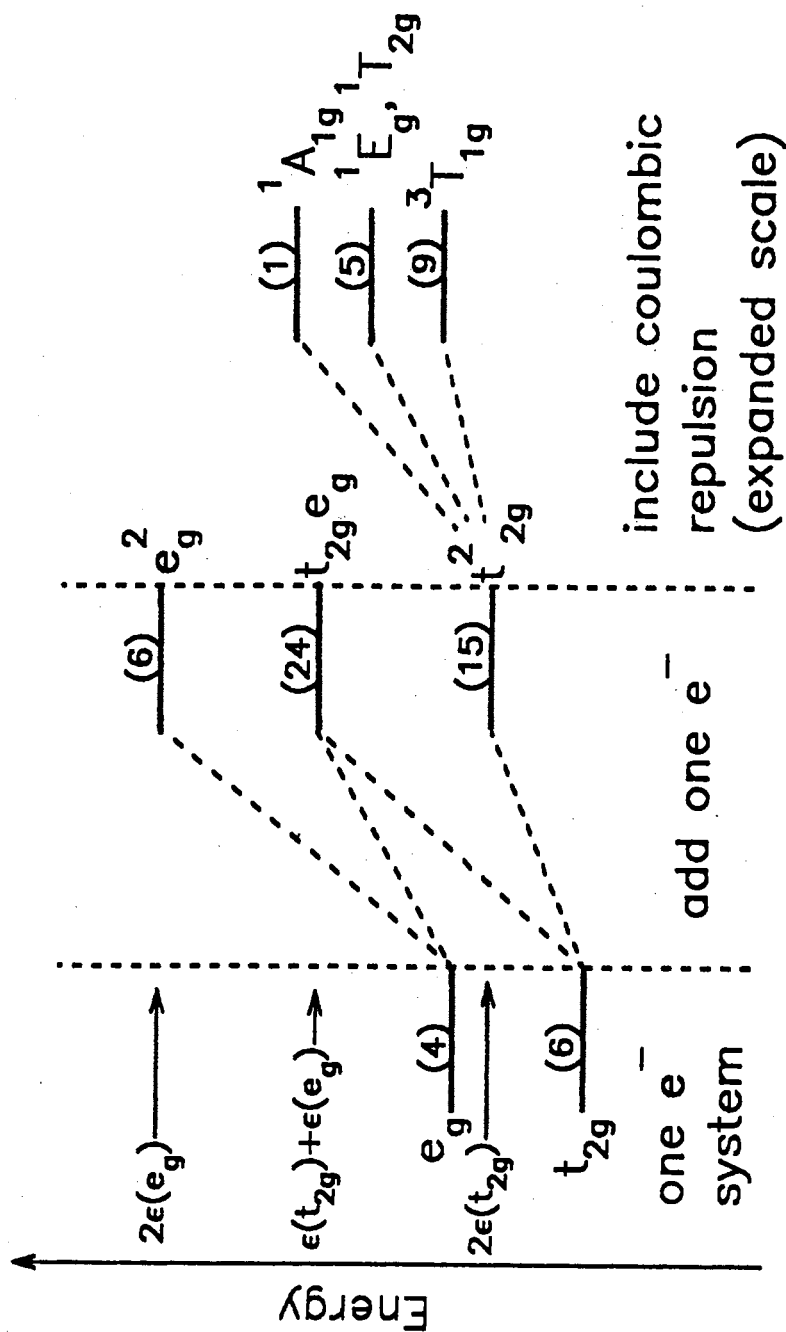
Figure 5. Splitting diagram for the one- and two-electron states. Starting with the one-electron configurations, t_{2g} and e_g, as one more electron is added but not allowed to interact with the previous one we form the two-electron configurations, t_{2g}^2, $t_{2g}e_g$ and e_g^2. As shown is the splitting of the t_{2g}^2 configuration under the inter-electron repulsion perturbation into the $^3T_{1g}$, $(^1E_g\,^1T_{2g})$ and $^1A_{1g}$ terms.

Slater Integrals and Racah Parameters

We will assume that the t_{2g} and e_g wave functions have a pure d character. However, this approximation does not necessarily mean that the radial part $R_{3d}(\mathbf{r})$ be that of a free atom or ion. In this sense we will write $R_d(\mathbf{r})$ for $R_{3d}(\mathbf{r})$. Since the t_{2g} and e_g wave functions are now assumed to be linear combinations of $\phi_{dm}(\mathbf{r}) = R_d(\mathbf{r})Y_{2m}(\theta\phi)$ $(m = 2, 1, 0, -1, -2)$, for instance, $\phi_\zeta = (-i/\sqrt{2})(\phi_{3d2} - \phi_{3d-2})$, etc. . For example, for $J(\zeta\zeta)$ in the previous section one has,

$$
\begin{aligned}
J(\zeta\zeta) &= \langle t_{2g}\zeta t_{2g}\zeta || t_{2g}\zeta t_{2g}\zeta \rangle = \int d\tau_1 d\tau_2 \left(\frac{i}{\sqrt{2}}\right) [\phi_{d2}^*(\mathbf{r}_1) - \phi_{d-2}^*(\mathbf{r}_1)] \left(\frac{i}{\sqrt{2}}\right) \\
&\times [\phi_{d2}^*(\mathbf{r}_2) - \phi_{d-2}^*(\mathbf{r}_2)] \left(\frac{1}{r_{12}}\right) \left(\frac{-i}{\sqrt{2}}\right) [\phi_{d2}(\mathbf{r}_1) - \phi_{d-2}(\mathbf{r}_1)] \left(\frac{-i}{\sqrt{2}}\right) \\
&\times [\phi_{d2}(\mathbf{r}_2) - \phi_{d-2}(\mathbf{r}_2)] \\
&= \frac{1}{4} [\langle 22||22 \rangle + \langle -2-2||-2-2 \rangle + \langle 2-2||2-2 \rangle \\
&\quad + \langle -22||-22 \rangle + \langle 2-2||-22 \rangle + \langle -22||2-2 \rangle],
\end{aligned}
\tag{57}
$$

where,

$$
\langle m_1 m_2 || m_1' m_2' \rangle = \int d\tau_1 d\tau_2 \phi_{dm_1}^*(\mathbf{r}_1)\phi_{dm_2}^*(\mathbf{r}_2)\frac{1}{r_{12}}\phi_{dm_1'}(\mathbf{r}_1)\phi_{dm_2'}(\mathbf{r}_2).
\tag{58}
$$

One may expand $1/r_{12}$ in terms of Legendre polynomials, thus,

$$
\frac{1}{r_{12}} = \sum_k \frac{r_<^k}{r_>^{k+1}} \sum_q (-1)^q C_q^{(k)}(\theta_1\phi_1) C_{-q}^{(k)}(\theta_2\phi_2),
\tag{59}
$$

where $r_<$ is the lessor and $r_>$ is the greater of r_1 and r_2. One then finds[20],

$$
\begin{aligned}
\langle 22||22 \rangle &= \langle -2-2||-2-2 \rangle = \langle 2-2||2-2 \rangle = \langle -22||-22 \rangle \\
&= F^{(0)} + \frac{4}{49}F^{(2)} + \frac{1}{441}F^{(4)} \\
\langle 2-2||-22 \rangle &= \langle -22||2-2 \rangle = \frac{70}{441}F^{(4)},
\end{aligned}
\tag{60}
$$

where,

$$
F^{(k)} = \int_0^\infty r_1^2 dr_1 \int_0^\infty r_2^2 dr_2 R_d^2(r_1) R_d^2(r_2) \frac{r_<^k}{r_>^{k+1}},
\tag{61}
$$

are called *Slater Integrals* or *Slater-Condon Parameters*. To simplify the results, F_k's are often used in place of the $F^{(k)}$'s where,

$$F_0 = F^{(0)}, \qquad F_2 = \frac{1}{49}F^{(2)}, \qquad F_4 = \frac{1}{441}F^{(4)}. \tag{62}$$

We then find, $J(\zeta\zeta) = F_0 + 4F_2 + 36F_4$. We could also define the *Racah Parameters* A, B, C by,

$$A = F_0 - 49F_4$$

$$B = F_2 - 5F_4 \tag{63}$$

$$C = 35F_4$$

then $J(\zeta\zeta) = A + 4B + 3C$. Table I shows ten two-electron integrals in terms of Racah parameters[20]. With the definitions of the Racah parameters given in Eq. (63), it is possible to express all the matrix elements of $\mathbf{H}_1$ in terms of the A, B, or C parameters. For instance Eqs. (53) -(56), now may be written,

$$\langle t_{2g}^2\,{}^1A_{1g}|\mathbf{H}_1|t_{2g}^2\,{}^1A_{1g}\rangle = A + 10B + 5C, \tag{64}$$

$$\langle t_{2g}^2\,{}^1E_g u|\mathbf{H}_1|t_{2g}^2\,{}^1E_g u\rangle = A + B + 2C, \tag{65}$$

$$\langle t_{2g}^2\,{}^3T_{1g}M = 0\gamma|\mathbf{H}_1|t_{2g}^2\,{}^3T_{1g}M = 0\gamma\rangle = A - 5B, \tag{66}$$

$$\langle t_{2g}^2\,{}^1T_{2g}\zeta|\mathbf{H}_1|t_{2g}^2\,{}^1T_{2g}\zeta\rangle = A + B + 2C. \tag{67}$$

TABLE I.

TEN TWO-ELECTRON INTEGRALS IN TERMS OF THE RACAH PARAMETERS

$J(\zeta\zeta) = A + 4B + 3C$	$J(\mu\nu) = A - 4B + C$
$J(\xi\eta) = A - 2B + C$	$K(\mu\nu) = 4B + C$
$K(\xi\eta) = 3B + C$	
$J(\zeta\mu) = A - 4B + C$	$J(\zeta\nu) = A + 4B + C$
$K(\zeta\mu) = 4B + C$	$K(\zeta\nu) = C$
$\langle\xi\eta||\zeta\mu\rangle = \sqrt{3}B$	

Equations (64)-(67) are the diagonal elements of the $\mathbf{H}_1$ operator in the t_{2g}^2 manifold. However, the entire $\mathbf{H}_1$ matrix is not diagonal. For cases where two different configurations give terms with the same symmetry and spin multiplicity, their matrix element will, in general, be nonzero. For instance, the t_{2g}^2 and e_g^2 configurations both give rise to a $^1A_{1g}$ term. The matrix element between these terms, expressed in Racah parameters is,

$$\langle t_{2g}^2\,^1A_{1g}|\mathbf{H}_1|e_g^2\,^1A_{1g}\rangle = \sqrt{6}(2B + C). \tag{68}$$

In this way terms with the same symmetry and spin multiplicity arising from different configurations interact. The act of diagonalizing the full $\mathbf{H}_1$ matrix including these off-diagonal matrix elements is called *configuration interaction*. Table II shows the complete set of Coulomb interaction matrices of the $3d^2$ system expressed in terms of Racah parameters. A common factor of A exists along the diagonal of each matrix and has been subtracted out since in the final analysis we are only interested in relative energy differences.

Diagonalization of the two-electron energy matrices

The final step in constructing the term splitting diagrams is to form the total energy matrix $\mathbf{H}_0 + \mathbf{H}_1$ and solve for the energy eigenvalues by diagonalizing it. It should be noted that the construction of the Coulomb interaction matrix $\mathbf{H}_1$ *has nothing to do with the ligand field.* It should be recalled that $\mathbf{H}_1$ was constructed using first-order perturbation theory for the inter-electron interaction only. To take into account both the ligand field and the inter-electron interaction we must now add $\mathbf{H}_0$ and $\mathbf{H}_1$ and thereby construct the total energy matrix. From Eq. (30) we see that $\mathbf{H}_0$ consists of only diagonal elements in the electronic configuration. Therefore to construct the total energy matrix we need only add $2\epsilon_d^0 + (-4n + 6m)Dq$ for configuration $t_{2g}^n e_g^m$ along the diagonal of the Coulomb interaction matrices in Table II. As an example, the total energy matrix for the

TABLE II.

MATRIX ELEMENTS OF COULOMB INTERACTION FOR THE $3d^2$ SYSTEM

$^1A_{1g}(^1G,{}^1S)$	
t_{2g}^2	e_g^2
$10B + 5C$	$\sqrt{6}(2B + C)$
	$8B + 4C$

$^1E_g(^1D,{}^1G)$	
t_{2g}^2	e_g^2
$B + 2C$	$-2\sqrt{3}B$
	$2C$

$^1T_{2g}(^1D,{}^1G)$	
t_{2g}^2	$t_{2g}e_g$
$B + 2C$	$2\sqrt{3}B$
	$2C$

$^3T_{1g}(^3F,{}^3P)$	
t_{2g}^2	$t_{2g}e_g$
$-5B$	$6B$
	$4B$

$t_{2g}e_g\ {}^1T_{1g}(^1G)$	$4B + 2C$
$t_{2g}e_g\ {}^3T_{2g}(^3F)$	$-8B$
$e_g^2\ {}^3A_{2g}(^3F)$	$-8B$

$^1A_{1g}$ terms is,

$$\begin{pmatrix} 10B + 5C - 8Dq & \sqrt{6}(2B + C) \\ \sqrt{6}(2B + C) & 8B + 4C + 12Dq \end{pmatrix}$$
$$= B \begin{pmatrix} 10 + 5g - 8(Dq/B) & \sqrt{6}(2 + g) \\ \sqrt{6}(2 + g) & 8 + 4g + 12(Dq/B) \end{pmatrix}, \qquad (69)$$

where we have dropped the term $2\epsilon_d^0$ common along the diagonal since our concern is only with relative energies. To apply the theory to the analysis of experimental data it is convenient to plot the energies of the states as a function of the parameters involved in the energy matrices. For this purpose it has been found that the ratio $C/B = g$ is almost independent of both the atomic number and the number of electrons in the iron-group ions[20]. It is therefore possible to reduce the number of parameters.

This fact can be understood by the following discussion. If the radial part of the wave function $R_d(\mathbf{r})$ is assumed to be that of a hydrogen-like or Slater-type wave function with an effective nuclear charge, then,

$$R_d(\mathbf{r}) = Nr^2 e^{-\kappa r}, \qquad (70)$$

where,

$$N = \sqrt{(2\kappa)^7/6!}, \qquad (71)$$

then the Slater integral $F^{(k)}$ given in Eq. (61) is calculated as[20],

$$\begin{aligned} F^{(k)} &= \int_0^\infty dr_1 r_1^2 \int_0^\infty dr_2 r_2^2 R_d^2(r_1) R_d^2(r_2) \frac{r_<^k}{r_>^{k+1}} \\ &= 2N^4 \int_0^\infty dr_1 r_1^{-(k-1)} R_d^2(r_1) \int_0^{r_1} dr_2 r_2^{k+2} R_d^2(r_2) \\ &= \frac{4\kappa(6+k)!}{(6!)^2} \left[(5-k)! - \sum_{n=1}^{7+k} \frac{(12-n)!}{2^{13-n}(7+k-n)!} \right], \qquad (72) \end{aligned}$$

which is always proportional to κ. Therefore from Eqs. (62) and (63) we see that the ratio of B to C is independent of κ. Since κ is a measure of the ionic size both isolated and when placed in a crystal field, and since the ratio B/C is independent

of κ, it should show little variation from ion to ion and from crystal environment to crystal environment. From spectroscopic data for the Mn^{2+} free ion, g has been found to have a value of 4.48 by Stout[21], however, Tanabe and Sugano[20] report a value of 4.42.

It is now a simple task to diagonalize the matrix of Eq. (69). Using $g = 4.42$ the eigenvalues of Eq. (69) are,

$$^1A_{1g} : \quad \frac{E(Dq/B)}{B} = \frac{57.78 + 4(Dq/B) \pm \sqrt{5\left[206.08 - 51.36(Dq/B) + 80(Dq/B)^2\right]}}{2}.$$

$$(73)$$

In this fashion we are able to calculate E/B as a function of Dq/B for each term arising from the two-electron system in the $O_h^{(6)}$ ligand field. Figure 6 shows E/B versus Dq/B for all the two-electron terms. The diagram is constructed so that the energies of the higher terms are measured with respect to the ground state term, $^3T_{1g}$.

The d^5 System in $O_h^{(8)}$ Symmetry

With the theoretical background reviewed in the previous sections, the problem at hand is to calculate the crystal splitting diagram for the d^5 system in $O_h^{(8)}$ symmetry. As far as the change in the ligand field symmetry is concerned, this only enters the formalism by a change in the unperturbed Hamiltonian matrix $\mathbf{H_0}$. For the $O_h^{(6)}$ system the $\mathbf{H_0}$ matrix consists of diagonal elements that depend only on the configuration, namely, $(6m - 4n)Dq$ for $t_{2g}^n e_g^m$. As discussed by Gliemann and Schläfer[24], for the $O_h^{(8)}$ system the matrix elements are given by $(4n - 6m)\frac{8}{9}Dq$. We see will see this leads to an inversion of the configurations in energy and produces a smaller magnitude in the splitting for a given value of Dq. This will then lead to larger Dq values for the Mn-impurity in CaF_2 than has hitherto been reported in the literature. The matrices for the inter-electron interaction, $\mathbf{H_1}$ remain unchanged in going from $O_h^{(6)}$ to $O_h^{(8)}$ symmetry since they only reflect the Coulomb interaction between the electrons around the central nucleus.
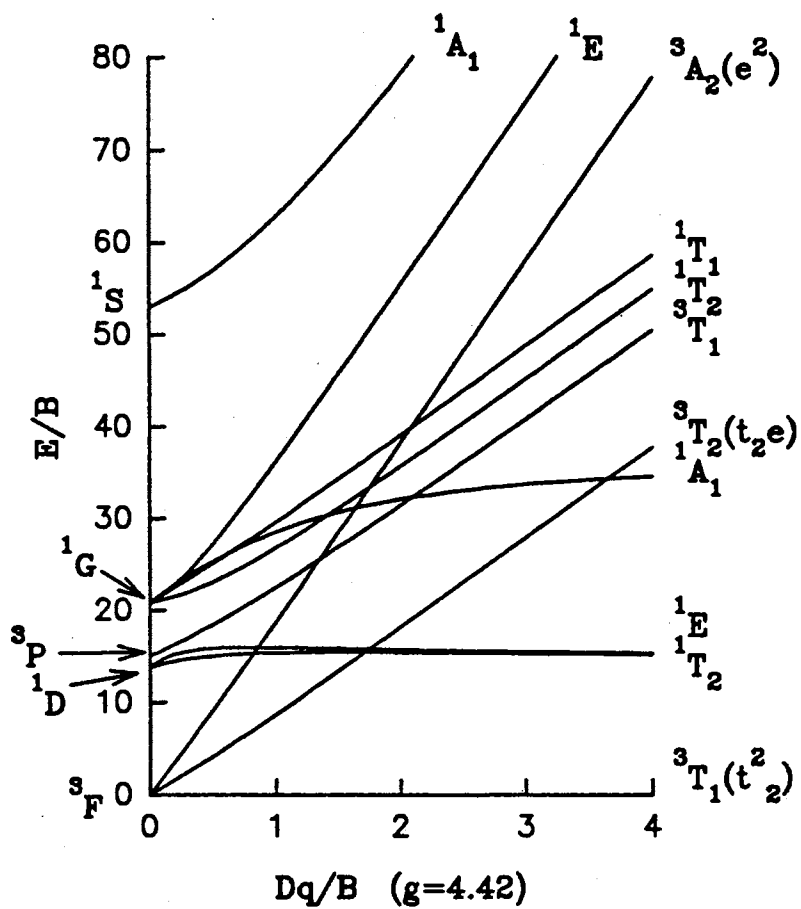
Figure 6.   Crystal field splitting diagram for the d^2, $O_h^{(6)}$ system obtained from diagonalizing the total energy matrices. The diagram is constructed such that the energies of the higher term energies are measured with respect to the ground state term, $^3T_{1g}$.

In this discussion we will be interested in the sextet ground state and the quartet excited states. While the d^5 system will lead to many doublet states, experimentally transitions into them cannot be measured due to the highly forbidden nature of these transitions. It is true that transitions from the ground state sextet to excited state quartets are dipole forbidden, with proper experimental techniques these have been measured[10]. For the d^5 system the free ion terms in order of increasing energy are: ^6S, ^4G, ^4P, ^4D and ^4F. By the application of group theory and the spin and vector coupling methods discussed in the previous sections, we find that these free-ion terms break into multiplet terms that are the irreducible representations of the O_h group. However, not all the terms allowed by group theory actually manifest themselves. Table III shows the free-ion terms and the surviving O_h terms. Also shown are the configurations that give rise to those terms[20]. Note that the t_{2g}^5 and $t_{2g}e_g^4$ configurations are not present since these will only lead to doublet terms.

Considering just the sextet and quartet terms, the Coulomb interaction matrices for the d^5 system under O_h symmetry are given in Table IV. Again the common factor of A along the diagonal of each matrix is subtracted out. For a listing of the doublet Coulomb matrices, the reader is referred to Appendix A.

TABLE III.

THE SURVIVING O_h TERMS ARISING FROM THE
SEXTET AND QUARTET FREE-ION TERMS

Free-ion terms	O_h terms
^6S	$^6A_{1g}(t_{2g}^3 e_g^2)$
^4G	$^4T_{1g}(t_{2g}^2 e_g^3)$, $^4T_{2g}(t_{2g}^2 e_g^3)$, $^4E_g(t_{2g}^3 e_g^2)$, $^4A_{1g}(t_{2g}^3 e_g^2)$
^4P	$^4T_{1g}(t_{2g}^3 e_g^2)$
^4D	$^4T_{2g}(t_{2g}^3 e_g^2)$, $^4E_g(t_{2g}^3 e_g^2)$
^4F	$^4A_{2g}(t_{2g}^3 e_g^2)$, $^4T_{1g}(t_{2g}^4 e_g)$, $^4T_{2g}(t_{2g}^4 e_g)$

Next the contribution due to the unperturbed Hamiltonian matrix, $\mathbf{H_0}$ is included by adding a factor of $(4n - 6m)\frac{8}{9}Dq$ along the diagonals of the Coulomb matrices in Table IV. This done, the full energy matrices are diagonalized to find the energy eigenvalues as a function of Dq/B. Figure 7 shows the full crystal field splitting diagram for the d^5 system with $O_h^{(8)}$ symmetry. This diagram includes the ground state sextet and all the quartet and doublet terms. The matrices for the doublet terms where quite large and had to be diagonalized numerically. This was easily accomplished using the $Mathematica^{TM}$[31] computer mathematics system.

To complete the analysis this diagram must be compared to experimental data so that the crystal field splitting parameter Dq can be determined. Figure 8 shows the optical absorption spectrum for CaF_2:Mn (3%) obtained by McKeever et. al. [10]. The figure shows the spectra peaks and their term assignments. From the Mn spectra for several hosts it has been found that the sharp peak at 395 nm is relatively independent of the crystal lattice. Therefore this peak has been assigned to a transition from $^6A_{1g}(^6S)$ to $^4A_{1g}(^4G)$. From Table IV we see that the $^4A_{1g}(^4G)$ term is independent of Dq and the $^4A_{1g}(^4G) - {}^6A_{1g}(^6S)$ separation is $10B + 5C$. Then assuming a C/B ratio of 4.48, McKeever et. al. calculate $B = 781\text{cm}^{-1}$ and $C = 3.498 \times 10^3\text{cm}^{-1}$. With these values of B and C, the diagram of Fig. 7 is recalculated with Dq as the only independent parameter. Figure 9 shows the crystal field splitting diagram for these values of B and C. As in the other diagrams, the energies are presented with respect to the ground state $^6A_{1g}(^6S)$. For clarity, only the quartet excited states are represented in the diagram and since only spin 5/2 to 3/2 transitions can be observed. The dashed line shows the value of Dq that gives the best fit to the experimental data of McKeever et. al. [10]. With the proper crystal field splitting diagram for $O_h^{(8)}$ symmetry the observed Dq value is now 570 cm^{-1} instead of the much lower value of 420 cm^{-1} which brings it more in line with expectations.

TABLE IV.

THE SEXTET AND QUARTET COULOMB INTERACTION MATRICES FOR THE d^5 SYSTEM

$^4T_{2g}(^4F, {}^4D, {}^4G)$		
$t_{2g}^4 e_g$	$t_{2g}^3 e_g^2$	$t_{2g}^2 e_g^3$
$-17B + 6C$	$-\sqrt{6}B$	$-4B - C$
	$-22B + 5C$	$-\sqrt{6}B$
		$-17B + 6C$

$^4T_{1g}(^4F, {}^4P, {}^4G)$		
$t_{2g}^4 e_g$	$t_{2g}^3 e_g^2$	$t_{2g}^2 e_g^3$
$-25B + 6C$	$3\sqrt{2}B$	$-C$
	$-16B + 7C$	$-3\sqrt{2}B$
		$-25B + 6C$

$^4E_g(^4G, {}^4D)$	
$t_{2g}^3 e_g^2 a$	$t_{2g}^3 e_g^2 b$
$-22B + 5C$	$-2\sqrt{3}B$
	$-21B + 5C$

$t_{2g}^3 e_g^2 \, {}^4A_{2g}(^4F)$	$-13B + 7C$
$t_{2g}^3 e_g^2 \, {}^4A_{1g}(^4G)$	$-25B + 5C$
$t_{2g}^3 e_g^2 \, {}^6A_{1g}(^6S)$	$-35B$
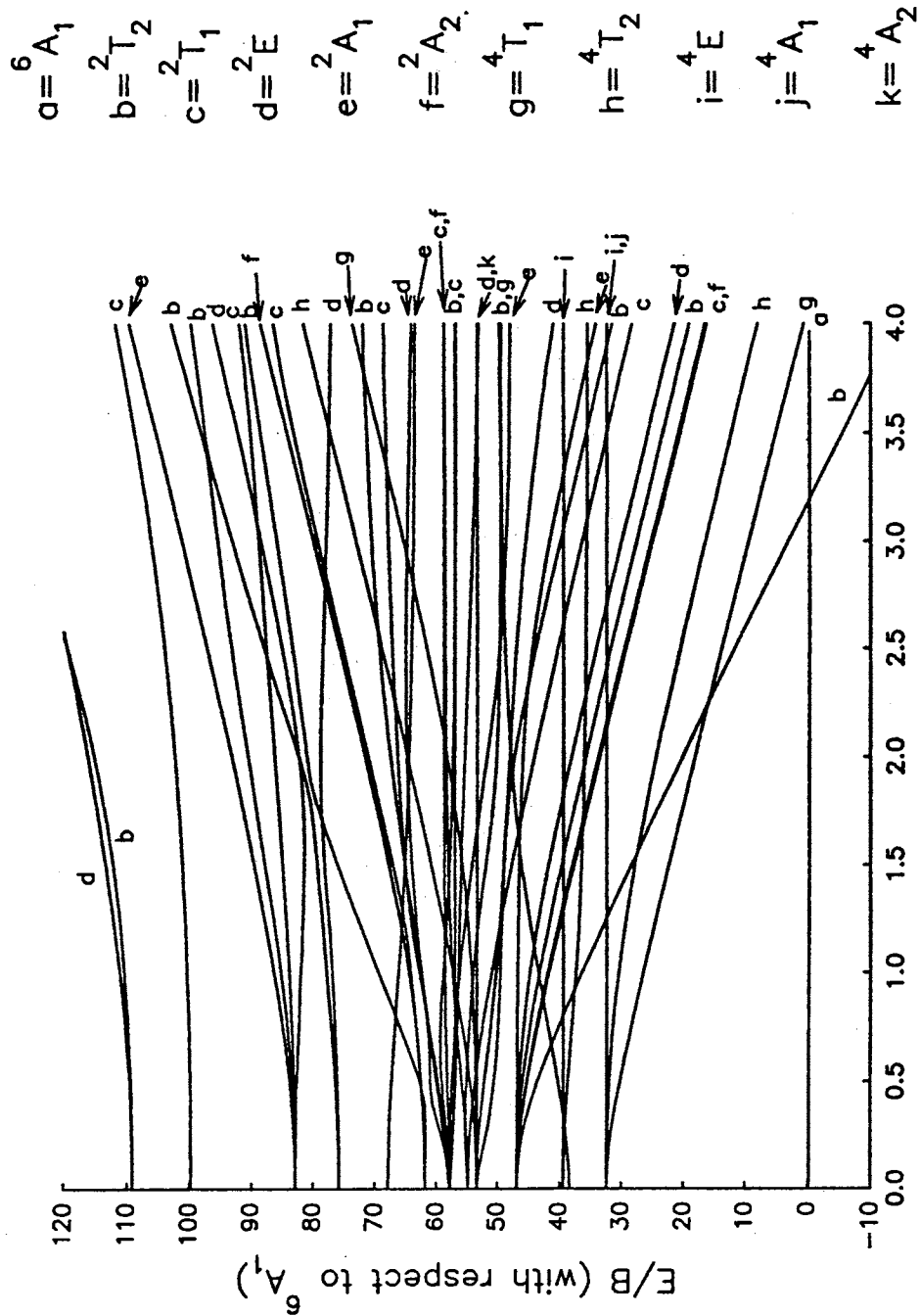
Figure 7. Full crystal field splitting diagram for a d^5 system with $O_h^{(8)}$ symmetry. This diagram includes the ground state sextet and all the quartet and doublet terms. The energies are with respect to the ground state term $^6A_{1g}$.
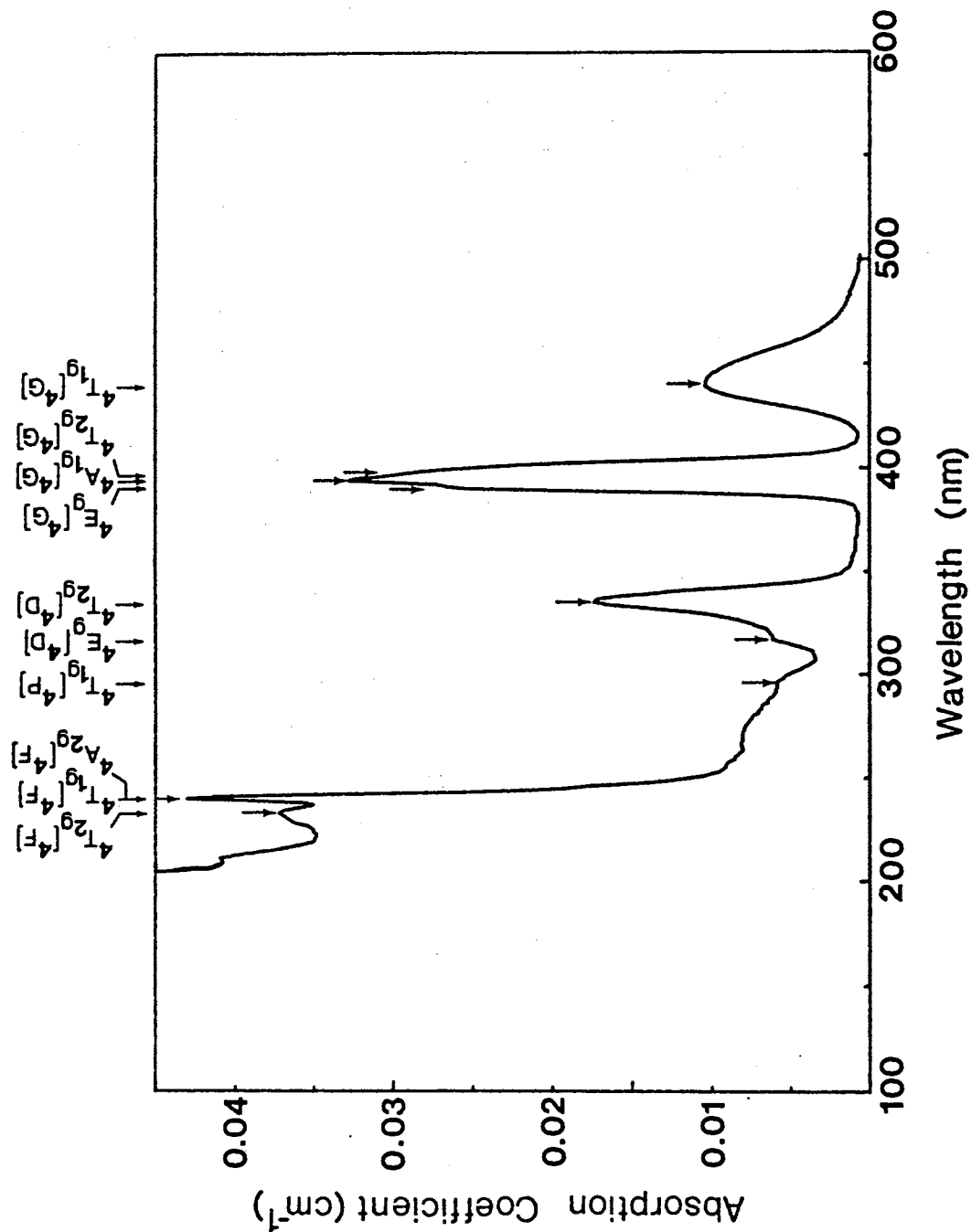
Figure 8. Optical absorption of an unirradiated specimen of CaF$_2$:Mn (3%). The absorption peaks have been assigned to the multiplet terms arising from the free-ion energy levels ^4G, ^4D, ^4P and ^4F as described in the text. (McKeever *et. al.* [10])
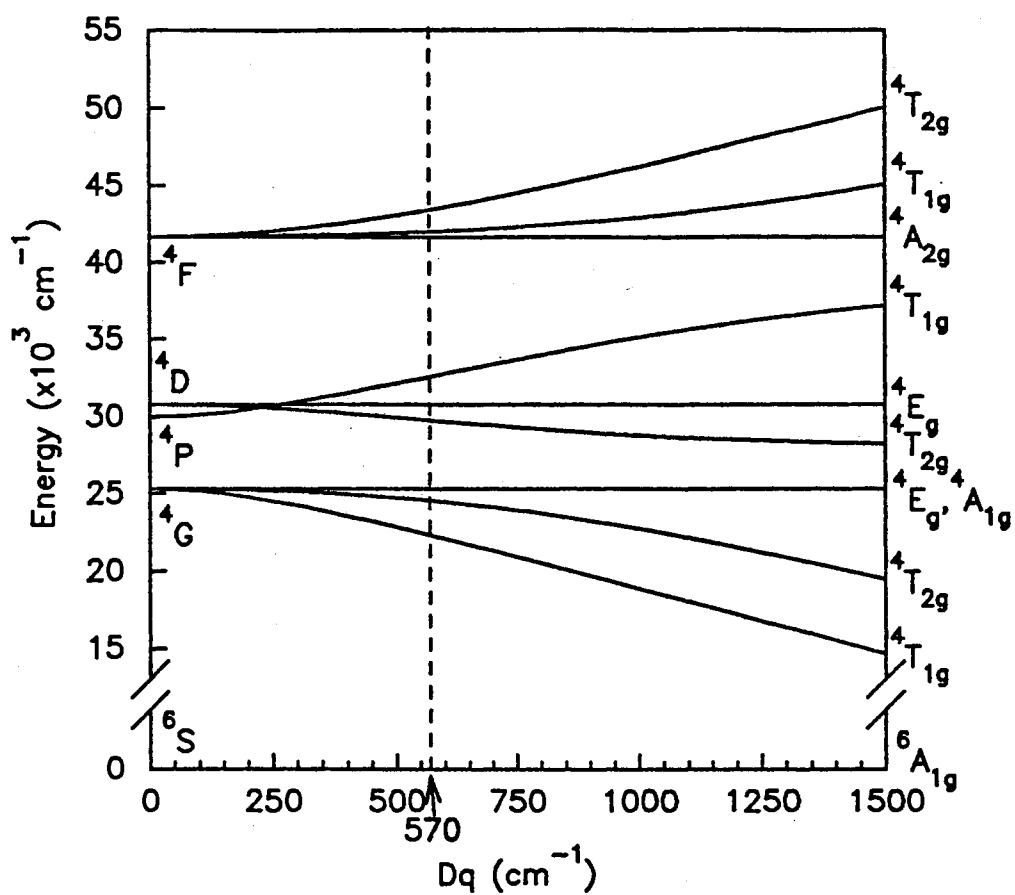
Figure 9. Crystal field splitting diagram for the d^5 system in $O_h^{(8)}$ symmetry for $B = 781\text{cm}^{-1}$ and $C = 3.498 \times 10^3\text{cm}^{-1}$. The energies are presented with respect to the ground state $^6A_{1g}$. The dashed line shows the value of Dq that gives the best fit to the experimental data of McKeever et. al. [10]

CHAPTER III

THE METHOD OF HARTREE-FOCK

The Hartree-Fock Wave function

The literature on the method of Hartree-Fock is extensive with numerous articles published on various aspects of the theory including several review articles and books[32–34]. While a full and detailed discussion of the underlying theory of the Hartree-Fock method and its extensions is outside the scope of this thesis, it will be worthwhile to briefly describe some of the essential features.

The goal of *ab initio* electronic structure theory is the solution of the quantum electronic problem. That is, given a collection of nuclei and electrons, we would like to find accurate approximate solutions to the non-relativistic time-independent Schrödinger equation,

$$\mathbf{H}|\Phi\rangle = E|\Phi\rangle, \tag{74}$$

where, $\mathbf{H}$ is the electronic Hamiltonian operator. In the Born-Oppenheimer approximation the electronic Hamiltonian describing the motion of N electrons in the field of M nuclear charges, in atomic units is,

$$\mathbf{H} = -\sum_{i=1}^{N} \frac{1}{2}\nabla_i^2 - \sum_{i=1}^{N}\sum_{A=1}^{M} \frac{Z_A}{r_{iA}} + \sum_{i=1}^{N}\sum_{i>j}^{N} \frac{1}{r_{ij}}. \tag{75}$$

If it were not for the last term involving $(1/r_{ij})$ in the Hamiltonian then Eq. (74) could be solved exactly. As a consequence we must look for approximate solutions. In this section we will be concerned with the nomenclature, the conventions and the procedure for writing down the wave functions that we use to describe many-electron systems. However, before considering wave functions for many-electron systems, it is necessary to discuss wave functions for a single electron.

For our present purposes, we will define the *molecular orbital* as the solution to the Schrödinger equation using the Hamiltonian of Eq. (75) without the $(1/r_{ij})$ term and only for a single electron where the single electron is under the influence of some averaged electrostatic potential due the presence of all the other electrons. This idea will be made more clear shortly. As we will see, in Hartree-Fock theory these molecular orbitals are combined together in the form of a Slater determinant and the molecular orbitals are then adjusted according to the variational principle such that this single Slater determinant is an approximate eigenfunction of the full Hamiltonian in Eq. (75). A *spatial molecular orbital* (simply referred to here as a *spatial orbital*) $\psi_i(\mathbf{r})$ is a function of the position vector $\mathbf{r}$ and describes the spatial distribution of an electron in the averaged field of the other electrons such that $|\psi_i(\mathbf{r})|^2 d\mathbf{r}$ is the probability of finding the electron in a small volume element $d\mathbf{r}$ surrounding $\mathbf{r}$. Spatial orbitals are usually assumed to form an orthonormal set so that,

$$\int \psi_i^*(\mathbf{r})\psi_j(\mathbf{r})d\mathbf{r} = \delta_{ij}. \tag{76}$$

To completely describe an electron it is necessary to specify its spin. This is done by the way of a complete set of spin functions $\alpha(\omega)$ and $\beta(\omega)$, where ω is the spin coordinate and take on the values $1/2$ ($\uparrow$ or "spin up") or $-1/2$ ($\downarrow$ or "spin down"). The spin functions themselves have the values: $\alpha(\uparrow) = 1$, $\alpha(\downarrow) = 0$, $\beta(\uparrow) = 0$, and $\beta(\downarrow) = 1$. Since the electronic Hamiltonian of Eq. (75) does not include the spin coordinate we may write a wave function for an electron which describes both its spatial distribution and its spin as a simple product of the spatial orbital and a spin function, known as a *spin orbital*, $\chi(\mathbf{x})$. Therefore, from each spatial orbital one may form two spin orbitals*, namely,

$$\chi(\mathbf{x}) = \begin{cases} \psi(\mathbf{r})\alpha(\omega) \\ \quad\text{or} \quad , \\ \psi(\mathbf{r})\beta(\omega) \end{cases} \tag{77}$$

---

*for the unrestricted Hartree-Fock method (UHF) this restriction is relaxed and the spatial parts of spin up and spin down electrons are allowed to differ

where $\mathbf{x} = \{\mathbf{r}, \omega\}$ indicates both spin and space coordinates.

The wave function for an N electron system is then a function of $\mathbf{x}_1, \mathbf{x}_2, \ldots, \mathbf{x}_N$. That is, we write $\Phi(\mathbf{x}_1, \mathbf{x}_2, \ldots, \mathbf{x}_N)$. A satisfactory theory of electronic structure can only be obtained if we impose the following additional requirement on a wave function: *A many-electron wave function must be antisymmetric with respect to the interchange of the coordinate* $\mathbf{x}$ *(both space and spin) of any two electrons*, thus,

$$\Phi(\mathbf{x}_1, \ldots, \mathbf{x}_i, \ldots, \mathbf{x}_j, \ldots, \mathbf{x}_N) = -\Phi(\mathbf{x}_1, \ldots, \mathbf{x}_j, \ldots, \mathbf{x}_i, \ldots, \mathbf{x}_N). \qquad (78)$$

This is a very general statement of the Pauli exclusion principle and is an independent postulate of quantum mechanics. Thus the exact wave function must not only satisfy the Schrödinger equation, it also must be antisymmetric in the sense of Eq. (78). We shall see that the requirement of antisymmetry is easily enforced by using Slater determinants.

For our purposes, we will equate Hartree-Fock theory to a single determinant theory*. Within a molecular orbital picture, the Hartree-Fock approximation assumes an antisymmetric wave function in the form of a single Slater determinant,

$$\Psi(\mathbf{x}_1, \mathbf{x}_2, \ldots, \mathbf{x}_N) = (N!)^{-\frac{1}{2}} \begin{vmatrix} \chi_i(\mathbf{x}_1) & \chi_j(\mathbf{x}_1) & \cdots & \chi_k(\mathbf{x}_1) \\ \chi_i(\mathbf{x}_2) & \chi_j(\mathbf{x}_2) & \cdots & \chi_k(\mathbf{x}_2) \\ \vdots & \vdots & & \vdots \\ \chi_i(\mathbf{x}_N) & \chi_j(\mathbf{x}_N) & \cdots & \chi_k(\mathbf{x}_N) \end{vmatrix}, \qquad (79)$$

which is the simplest form of the wave function that satisfies the antisymmetry requirement. The factor $(N!)^{-1/2}$ is a normalization factor. This Slater determinant represents in the Hartree-Fock approximation N electrons occupying N spin orbitals $(\chi_i, \chi_j, \ldots, \chi_k)$. The coordinates, $(\mathbf{x}_1, \mathbf{x}_2, \ldots, \mathbf{x}_N)$ identify both the spin and spatial coordinates. It is convenient to introduce a short-hand notation for a normalized Slater determinant, which includes the normalization constant and

---

*Hartree-Fock theory in special cases, such as for restricted open-shell wave functions involves a multideterminantal wave function. Also extensions of Hartree-Fock theory such as Configuration Interaction use linear combinations of Slater determinants

only shows the diagonal elements of the determinant,

$$\Psi(\mathbf{x}_1, \mathbf{x}_2, \ldots, \mathbf{x}_N) = |\chi_i(\mathbf{x}_1)\chi_j(\mathbf{x}_2)\cdots\chi_k(\mathbf{x}_N)\rangle. \tag{80}$$

If we choose the electron labels to be in the order $\mathbf{x}_1, \mathbf{x}_2, \ldots, \mathbf{x}_N$ then Eq. (80) can be further shortened to,

$$\Psi(\mathbf{x}_1, \mathbf{x}_2, \ldots, \mathbf{x}_N) = |\chi_i\chi_j\cdots\chi_k\rangle. \tag{81}$$

Antisymmetrizing the Hartree product as in the above Slater determinant introduces so-called exchange effects meaning that the motion of two electrons with parallel spins are correlated. However, this single determinant form leaves the motion of electrons with opposite spins uncorrelated.[33] As we will see, it is the purpose then of the various extensions to Hartree-Fock theory such as CI, MP2, MP4 and MCSCF to build in correlation effects.[32] So, since the motion of electrons with opposite spins remains uncorrelated, it is customary to refer to a single determinantal wave function as an uncorrelated wave function.

To see how exchange correlation arises, consider a two-electron Slater determinant in which spin orbitals χ_1 and χ_2 are occupied,

$$\Psi(\mathbf{x}_1, \mathbf{x}_2) = |\chi_1(\mathbf{x}_1)\chi_2(\mathbf{x}_2)\rangle. \tag{82}$$

Say that the two electrons have opposite spins and occupy different spatial orbitals,

$$\chi_1(\mathbf{x}_1) = \psi_1(\mathbf{r}_1)\alpha(\omega_1), \tag{83}$$

$$\chi_2(\mathbf{x}_2) = \psi_2(\mathbf{r}_2)\beta(\omega_2). \tag{84}$$

Expanding the determinant, we have,

$$|\Psi|^2 d\mathbf{x}_1 d\mathbf{x}_2 = \frac{1}{2}|\psi_1(\mathbf{r}_1)\alpha(\omega_1)\psi_2(\mathbf{r}_2)\beta(\omega_2) - \psi_1(\mathbf{r}_2)\alpha(\omega_2)\psi_2(\mathbf{r}_1)\beta(\omega_1)|^2 d\mathbf{x}_1 d\mathbf{x}_2, \tag{85}$$

as the simultaneous probability of electron 1 being in $d\mathbf{x}_1$ and electron 2 being in $d\mathbf{x}_2$. Let $P(\mathbf{r}_1\mathbf{r}_2)d\mathbf{r}_1 d\mathbf{r}_2$ be the probability of finding electron 1 in $d\mathbf{r}_1$ at $\mathbf{r}_1$ and

simultaneously electron 2 in dr_2 at $\mathbf{r}_2$. We get this probability by integrating over the spin coordinates ω_1 and ω_2 for the two electrons,

$$
\begin{aligned}
P(\mathbf{r}_1, \mathbf{r}_2) dr_1 dr_2 &= \int d\omega_1 d\omega_2 |\Psi|^2 dr_1 dr_2 \\
&= \frac{1}{2}[|\psi_1(\mathbf{r}_1)|^2 |\psi_2(\mathbf{r}_2)|^2 + |\psi_1(\mathbf{r}_2)|^2 |\psi_2(\mathbf{r}_1)|^2] dr_1 dr_2. \quad (86)
\end{aligned}
$$

The first term in this equation is the product of the probability of finding electron 1 in dr_1 at $\mathbf{r}_1$ times the probability of finding electron 2 in dr_2 at $\mathbf{r}_2$, *if* electron 1 occupies ψ_1 and electron 2 occupies ψ_2. The second term shows the same product except that now electron 1 occupies ψ_2 and electron 2 occupies ψ_1. The correct probability is the average of the two as shown since electrons are indistinguishable. The motion of the two electrons is therefore uncorrelated. For instance if $\psi_1 = \psi_2$ then,

$$
P(\mathbf{r}_1, \mathbf{r}_2) = |\psi_1(\mathbf{r}_1)|^2 |\psi_1(\mathbf{r}_2)|^2. \quad (87)
$$

Note that $P(\mathbf{r}_1, \mathbf{r}_1) \neq 0$ so it turns out that there is a finite probability of finding two electrons with opposite spins at the same point in space. If the electrons have the same spin, say β, then,

$$
\chi_1(\mathbf{x}_1) = \psi_1(\mathbf{r}_1)\beta(\omega_1), \quad (88)
$$

$$
\chi_2(\mathbf{x}_2) = \psi_2(\mathbf{r}_2)\beta(\omega_2). \quad (89)
$$

By the same steps as before, we find,

$$
\begin{aligned}
P(\mathbf{r}_1, \mathbf{r}_2) = \frac{1}{2} \big\{ &|\psi_1(\mathbf{r}_1)|^2 |\psi_2(\mathbf{r}_2)|^2 + |\psi_1(\mathbf{r}_2)|^2 |\psi_2(\mathbf{r}_1)|^2 \\
&- [\psi_1^*(\mathbf{r}_1)\psi_2(\mathbf{r}_1)\psi_2^*(\mathbf{r}_2)\psi_1(\mathbf{r}_2) + \psi_1(\mathbf{r}_1)\psi_2^*(\mathbf{r}_1)\psi_2(\mathbf{r}_2)\psi_1^*(\mathbf{r}_2)] \big\}. \quad (90)
\end{aligned}
$$

We see that there is now a cross term making the probabilities correlated. This is exchange correlation between electrons of parallel spin. Note that $P(\mathbf{r}_1, \mathbf{r}_1) = 0$, and thus the probability of having two electrons with parallel spin at the same point in space is zero. A *Fermi hole* is said to exist around an electron. To summarize, within the single Slater determinantal description the motion of electrons with parallel spins is correlated but the motion of electrons with opposite spins is not.

One method to incorporate the missing correlation of electrons with opposite spins is to adopt a multideterminantal description. This method known as configuration interaction will be discussed in a latter section.

Operators and Matrix Elements

In this section we briefly review the problem of evaluating matrix elements between Slater determinants formed from orthonormal orbitals. Say we are given two N-electron determinants, $|K\rangle$ and $|L\rangle$ and some operator say, $\mathcal{O}$. We would like to evaluate $\langle K|\mathcal{O}|L\rangle$. By "evaluation" we mean reducing them to integrals involving the individual spin orbitals, χ_i in $|K\rangle$ and $|L\rangle$, and then ultimately to the spatial orbitals ψ_i. In what follows, the operator of chief importance will be the full electronic Hamiltonian, $\mathbf{H}$.

If $|\Psi_0\rangle = |\chi_1\chi_2\cdots\chi_N\rangle$ is an antisymmetric trial wave function in a single Slater determinant form for an N-electron system in the ground state, then the variational principle states that the best wave function of this form is the one which gives the lowest possible energy,[33]

$$E_0 = \langle\Psi_0|\mathbf{H}|\Psi_0\rangle, \tag{91}$$

where $\mathbf{H}$ is the full electronic Hamiltonian which we will write as the sum of one-electron and two-electron operators,

$$\mathbf{H} = \sum_{i=1}^{N} \mathbf{h}(i) + \sum_{i=1}^{N}\sum_{j>i}^{N} \frac{1}{r_{12}}, \tag{92}$$

where,

$$\mathbf{h}(i) = -\frac{1}{2}\nabla_i^2 - \sum_A \frac{Z_A}{r_{1A}}, \tag{93}$$

is the *core-Hamiltonian* and describes the kinetic and potential energy of the ith electron in the field of the nuclei (the "core").

Before proceeding, it is important at this time to define the notation we will use for one- and two-electron integrals. In this thesis we will represent two-electron

integrals over spin orbitals by $[ij|kl]$ which is given by,

$$[ij|kl] = \int d\mathbf{x}_1 d\mathbf{x}_2 \chi_i^*(\mathbf{x}_1)\chi_j(\mathbf{x}_1)r_{12}^{-1}\chi_k^*(\mathbf{x}_2)\chi_l(\mathbf{x}_2).\tag{94}$$

This is typically referred to as the "chemists' notation"[33]. You will note that the spin orbitals, which are functions of electron 1 appear side by side on the left and the complex conjugated spin orbital appears first. By interchanging the dummy variables of integration one has,

$$[ij|kl] = [kl|ij].\tag{95}$$

In addition, if the spin orbitals are real*, then one has[33],

$$[ij|kl] = [ji|kl] = [ij|lk] = [ji|lk].\tag{96}$$

For one electron integrals the chemists' notation is,

$$[i|h|j] = \int d\mathbf{x}_1 \chi_i^*(\mathbf{x}_1)h(\mathbf{r}_1)\chi_j(\mathbf{x}_1).\tag{97}$$

Matrix elements between two-electron Slater determinants are fairly easy to evaluate. The N-electron case is more complicated, and here we will simply present a set of rules that can be used to evaluate matrix elements. For the derivation of these rules the reader is referred to Szabo and Ostlund[33]. In quantum chemistry there are two types of operators. The first type is a sum of one-electron operators,

$$\mathcal{O}_1 = \sum_{i=1}^{N} h(i),\tag{98}$$

where $h(i)$ is any operator involving only the ith electron. One-electron operators involve dynamic variables that depend only on the position and/or momentum of the electron in question, independent of the position or momentum of other electrons. A second type of operator is a sum of two-electron operators,

$$\mathcal{O}_2 = \sum_{i=1}^{N}\sum_{j>i}^{N} v(i,j),\tag{99}$$

---

*which is almost always the case in molecular Hartree-Fock calculations

where, $v(i,j)$ is an operator that depends on the position or momentum of both the ith and j^{th} electron. The sum is over all unique pairs of electrons. The coulomb interaction between two electrons, $v(i,j) = r_{ij}^{-1}$, is a two-electron operator.

The rules for matrix elements such as $\langle K|\mathcal{O}|L\rangle$ between determinants $|K\rangle$ and $|L\rangle$ depends on whether $\mathcal{O}$ is a one-electron or two-electron operator and, in addition, it depends on the degree to which the two determinants, $|K\rangle$ and $|L\rangle$ differ. It is possible to distinguish three cases. The first case is when the two determinants are identical, i.e., $\langle K|\mathcal{O}|K\rangle$. For this case we choose the determinant to be,

$$|K\rangle = |\cdots \chi_m \chi_n \cdots\rangle. \tag{100}$$

The second case is when the two determinants differ by one spin orbital, say, χ_m in $|K\rangle$ replaced by χ_p in $|L\rangle$,

$$|L\rangle = |\cdots \chi_p \chi_n \cdots\rangle. \tag{101}$$

The third case is when the determinants differ by two spin orbitals, say, χ_m and χ_n in $|K\rangle$ replaced by χ_p and χ_q in $|L\rangle$,

$$|L\rangle = |\cdots \chi_p \chi_q \cdots\rangle. \tag{102}$$

When the determinants differ by three or more spin orbitals the matrix element is always zero. Tables V and VI summarize the rules for the three cases for the one- and two-electron operators. To use the rules in Tables V and VI require that the two determinants be in *maximum coincidence*. To understand this, consider a matrix element between two determinants, $|K\rangle$ and $|L\rangle$ where,

$$|K\rangle = |abcd\rangle$$
$$|L\rangle = |crds\rangle.$$

It may appear that the two determinants differ in all four columns. However if we interchange the columns, keeping track of the sign, $|L\rangle = |crds\rangle = -|crsd\rangle =$

$|srcd\rangle$, we see that after being placed in maximum coincidence that differ by two columns. We can then use Tables V and VI for case 3 to obtain,

$$\langle K|\mathcal{O}_1|L\rangle = 0$$

$$\langle K|\mathcal{O}_2|L\rangle = [as|br] - [ar|bs].$$

Using the Tables V and VI we can now evaluate the matrix element $\langle \Psi_0|\mathbf{H}|\Psi_0\rangle$ in Eq. (91). Using Case 1 in both tables we find,

$$E_0 = \langle \Psi_0|\mathbf{H}|\Psi_0\rangle = \sum_a^N [a|h|a] + \frac{1}{2}\sum_a^N \sum_b^N [aa|bb] - [ab|ba], \qquad (103)$$

where, N is the number of electrons and $|\Psi_0\rangle = |\chi_1\chi_2\cdots\chi_a\chi_b\cdots\chi_N\rangle$.

The Hartree-Fock Equations

With the ground state energy expressed as in Eq. (103) we will now summarize the main results obtained in a derivation of the Hartree-Fock equation. The derivation itself, however, will not be presented. For the interested reader, the details of the derivation are presented in Szabo and Ostlund[33].

We are interested in finding the set of spin orbitals such that the single determinant $|\Psi_0\rangle$ formed from them gives the best approximation to the ground state of

TABLE V.

MATRIX ELEMENTS BETWEEN DETERMINANTS FOR
ONE-ELECTRON OPERATORS IN TERMS
OF SPIN ORBITALS

$\mathcal{O}_1 = \sum_{i=1}^N h(i)$		
Case 1:	$|K\rangle = |\cdots mn\cdots\rangle$	$\langle K|\mathcal{O}_1|K\rangle = \sum_m^N [m|h|m]$
Case 2:	$|K\rangle = |\cdots mn\cdots\rangle$	$\langle K|\mathcal{O}_1|L\rangle = [m|h|p]$
	$|L\rangle = |\cdots pn\cdots\rangle$	
Case 3:	$|K\rangle = |\cdots mn\cdots\rangle$	$\langle K|\mathcal{O}_1|L\rangle = 0$
	$|L\rangle = |\cdots pq\cdots\rangle$	

the N-electron system described by an electronic Hamiltonian $\mathbf{H}$. According the variational principle, the best spin orbitals are those that minimizes the electronic energy given in Eq. (103)[33]. The only constraint is that the spin orbitals remain orthonormal,

$$\langle \chi_a | \chi_b \rangle = \delta_{ab}. \tag{104}$$

When this is done formally [29,33], one obtains an equation that when solved produces the best set of spin orbitals. The best spin orbitals are those which minimize E_0 within the single determinantal approximation. That equation is known as the Hartree-Fock integro-differential equation,

$$h(1)\chi_a(1) \; + \; \sum_{b \neq a} \left[\int d\mathbf{x}_2 |\chi_b(2)|^2 r_{12}^{-1} \right] \chi_a(1) - \sum_{b \neq a} \left[\int d\mathbf{x}_2 \chi_b^*(2)\chi_a(2) r_{12}^{-1} \right] \chi_b(1)$$
$$= \; \epsilon_a \chi_a(1), \tag{105}$$

where,

$$h(1) = -\frac{1}{2}\nabla_1^2 - \sum_A \frac{Z_A}{r_{1A}} \tag{106}$$

is the kinetic energy and potential energy of a single electron chosen to be electron 1 in the field of the nuclei.

The two terms involving sums over b in Eq. (105) represent electron-electron interactions in the Hartree-Fock single determinant approximation. Without these

TABLE VI.

MATRIX ELEMENTS BETWEEN DETERMINANTS FOR
TWO-ELECTRON OPERATORS IN TERMS
OF SPIN ORBITALS

$\mathcal{O}_2 = \sum_{i=1}^{N} \sum_{j>i}^{N} r_{ij}^{-1}$		
Case 1:	$|K\rangle = |\cdots mn \cdots\rangle$	$\langle K|\mathcal{O}_2|K\rangle = \frac{1}{2}\sum_m^N \sum_n^N [mm|nn] - [mn|nm]$
Case 2:	$|K\rangle = |\cdots mn \cdots\rangle$	$\langle K|\mathcal{O}_2|L\rangle = \sum_n^N [mp|nn] - [mn|np]$
	$|L\rangle = |\cdots pn \cdots\rangle$	
Case 3:	$|K\rangle = |\cdots mn \cdots\rangle$	$\langle K|\mathcal{O}_2|L\rangle = [mp|nq] - [mq|np]$
	$|L\rangle = |\cdots pq \cdots\rangle$	

terms we have,

$$h(1)\chi_a(1) = \epsilon_a\chi_a(1), \tag{107}$$

which is just the one-electron Schrödinger equation and ϵ_a is the one-electron orbital energy of the spin orbital $\chi_a(1)$. The first of the two-electron terms is the *coulomb* term and has a simple interpretation. In an exact theory the coulomb interaction is represented by the two-electron operator r_{ij}^{-1}. In the Hartree-Fock theory Eq. (105) shows that electron 1 in χ_a experiences the one-electron coulomb potential,

$$v_a^{coul}(1) = \sum_{b\neq a} \int d\mathbf{x}_2|\chi_b(2)|^2 r_{12}^{-1}. \tag{108}$$

Suppose that electron 2 occupies χ_b. We see from Eq. (108) that the two-electron potential r_{12}^{-1} felt by electron 1 and associated with the instantaneous position of electron 2 has been replaced by a one-electron potential obtained by averaging the interaction r_{12}^{-1} of electron 1 and electron 2 over the spin and space coordinates $\mathbf{x}_2$ of electron 2, weighted by the probability $d\mathbf{x}_2|\chi_b(2)|^2$ that electron 2 occupies the volume element $d\mathbf{x}_2$ at $\mathbf{x}_2$. When we sum over all b such that $b \neq a$ we obtain the total averaged potential acting on the electron in χ_a arising from the $N-1$ electrons in the other spin orbitals. In this regard, it is convenient to define the *coulomb operator* as,

$$\mathcal{J}_b(1) = \int d\mathbf{x}_2|\chi_b(2)|^2 r_{12}^{-1}. \tag{109}$$

$\mathcal{J}_b(1)$ represents the averaged local potential at $\mathbf{x}_1$ arising from an electron in χ_b.

The second term involving a summation over b in Eq. (105) is the exchange term and arises from the antisymmetric nature of the wave function. Unlike the coulomb term, it does not have a classical interpretation. Nevertheless we may define an *exchange operator*, $\mathcal{K}_b(1)$, by its effect when operating on a spin orbital $\chi_a(1)$,

$$\mathcal{K}_b(1)\chi_a(1) = \left[\int d\mathbf{x}_2\chi_b^*(2)r_{12}^{-1}\chi_a(2)\right]\chi_b(1). \tag{110}$$

Operating with $\mathcal{K}_b(1)$ on $\chi_a(1)$ involves an "exchange" of electron 1 and electron 2 to the right of r_{12}^{-1} Unlike the local coulomb operator, the exchange operator is

nonlocal since there does not exist a simple potential, say $v_b^{ex}(\mathbf{x}_1)$, uniquely defined at a local point in space $\mathbf{x}_1$. Operating with $\mathcal{K}_b(\mathbf{x}_1)$ on $\chi_a(\mathbf{x}_1)$ depends on the value of χ_a throughout all space not just at $\mathbf{x}_1$. One could not, for instance, draw contour plots of the exchange potential as one can for the coulomb potential.

The Hartree-Fock equation written with the coulomb and exchange operators is now,

$$\left[h(1) + \sum_b \mathcal{J}_b - \sum_b \mathcal{K}_b \right] \chi_a(1) = \epsilon_a \chi_a(1), \tag{111}$$

where we have eliminated the restriction $b \neq a$ in the summations by adding the term $[\mathcal{J}_a(1) - \mathcal{K}_a(1)]\chi_a(1) = 0$ to both sides of Eq. (105). We then define the *Fock operator*, f, by,

$$f(1) = h(1) + \sum_b \mathcal{J}_b(1) - \mathcal{K}_b(1). \tag{112}$$

We see that $f(1)$ is the sum of a core-Hamiltonian operator $h(1)$ and an effective one-electron potential operator called the Hartree-Fock potential, $v^{HF}(1)$, where,

$$v^{HF}(1) = \sum_b \mathcal{J}_b(1) - \mathcal{K}_b(1). \tag{113}$$

It is sometimes convenient to express the exchange potential in terms of the permutation operator, $\mathcal{P}_{12}$ which operates to the right and interchanges electron 1 and 2. Thus,

$$
\begin{aligned}
\mathcal{K}_b(1)\chi_a(1) &= \left[\int d\mathbf{x}_2 \chi_b^*(2) r_{12}^{-1} \chi_a(2) \right] \chi_b(1) \\
&= \left[\int d\mathbf{x}_2 \chi_b^*(2) r_{12}^{-1} \mathcal{P}_{12} \chi_b(2) \right] \chi_a(1)
\end{aligned}
\tag{114}
$$

The Fock operator is then,

$$
\begin{aligned}
f(1) &= h(1) + v^{HF}(1) \\
&= h(1) + \sum_b \int d\mathbf{x}_2 \chi_b^*(2) r_{12}^{-1} (1 - \mathcal{P}_{12}) \chi_b(2),
\end{aligned}
\tag{115}
$$

and the Hartree-Fock equation becomes,

$$f|\chi_a\rangle = \epsilon_a |\chi_a\rangle. \tag{116}$$

The exact solution of Eq. (116) will produce the exact Hartree-Fock spin orbitals. However, in practice, it is only possible to solve Eq. (116) exactly for atoms[33]. For molecular systems one normally introduces a set of basis functions for expansion of the spin orbitals and solves a set of matrix equations. Only as the basis set approaches completeness will the spin orbitals obtained approach the exact Hartree-Fock spin orbitals. This is said to approach the Hartree-Fock limit.

Equation (116) is written in the form of a linear eigenvalue equation. In fact it is really a pseudo-eigenvalue equation since the Fock operator itself has a functional dependence through the coulomb and exchange operators on the solutions $\{\chi_a\}$ of the pseudo-eigenvalue equation. The Hartree-Fock equations are thus non-linear and must be solved by iterative procedures.

Restricted Closed-Shell Hartree-Fock: The Roothaan Equations

In the previous sections we developed the Hartree-Fock equations from a formal point of view with a general set of spin orbitals $\{\chi_i\}$. For actual calculations the spin must be integrated out so that only spatial Hartree-Fock equations are solved. To do this we must be more specific about the type of system we are considering (either open-shell or closed-shell) and the degree of flexibility in the spatial wave functions. There are essentially three cases:

- Restricted closed-shell Hartree-Fock (RHF). For this case the all the electrons are spin-paired, so that all the spatial orbitals are doubly occupied. In addition this case restricts the spatial parts of spin up and spin down orbitals to be the same.

- Restricted open-shell Hartree-Fock (ROHF). In this case the spatial orbitals are also restricted to be the same for doubly occupied orbitals. By use of a multideterminantal wave function one may also treat systems that contain an odd number of electrons[34].

- Unrestricted Hartree-Fock (UHF). This method is also known as the "different orbtials for different spins" or "spin polarized" method. The essential

feature is that the spatial orbitals for spin up and spin down electrons are solved independently yet simultaneously so that in general the spatial orbitals may differ whereas in the RHF or ROHF case they would be restricted to be identical. The UHF method uses two single determinantial wave functions, one for the spin up and one for the spin down orbitals.

In this review, we will only consider in detail the RHF case and refer the reader to the literature for the UHF and ROHF cases[33,34].

For closed shell calculations our molecular states are thus allowed to have only an even number N of electrons, with all the electrons paired such that $n = N/2$ spatial orbitals are doubly occupied. In essence this restricts our discussion to closed-shell ground states.

A restricted set of spin orbitals has the form,

$$\chi_i(\mathbf{x}) = \begin{cases} \psi_j(\mathbf{r})\alpha(\omega) \\ \psi_j(\mathbf{r})\beta(\omega) \end{cases} \tag{117}$$

and the closed-shell restricted ground state is,

$$|\Psi_0\rangle = |\chi_1\chi_2\cdots\chi_{N-1}\chi_N\rangle = |\psi_1\bar{\psi}_1\cdots\psi_a\bar{\psi}_a\cdots\psi_{N/2}\bar{\psi}_{N/2}\rangle. \tag{118}$$

We want to convert the general spin orbital Hartree-Fock equation, $f(1)\chi_i(1) = \epsilon_i\chi_i(1)$ to a spatial eigenvalue equation where each of the occupied spatial molecular orbitals $\{\psi_a | a = 1, 2, \ldots N/2\}$ is doubly occupied. To convert from spin orbitals to spatial orbital requires an integrating out of the spin functions. The details are quite straightforward[33] and the result is the closed-shell spatial Hartree-Fock equation,

$$f(1)\psi_j(1) = \epsilon_j\psi_j(1), \tag{119}$$

where the closed-shell restricted Fock operator is,

$$f(1) = h(1) + \sum_a^{N/2} 2J_a(1) - K_a(1), \tag{120}$$

and the closed-shell restricted coulomb and exchange operators are defined,

$$J_a(1) = \int d\mathbf{r}_2 \psi_a^*(2) r_{12}^{-1} \psi_a(2), \qquad (121)$$

$$K_a(1)\psi_i(1) = \left[\int d\mathbf{r}_2 \psi_a^*(2) r_{12}^{-1} \psi_i(2)\right] \psi_a(1). \qquad (122)$$

Introduction of a basis

With the elimination of spin the calculation of the molecular orbitals becomes equivalent to the problem of solving the spatial integro-differential equation $f(\mathbf{r}_1)\psi_i(\mathbf{r}_1) = \epsilon_i\psi_i(\mathbf{r}_1)$. While one might attempt to solve this equation numerically–and this is indeed common in atomic calculations–at present no practical procedures are available for obtaining numerical solutions for molecules. The only practical method available for molecules was first introduced by C. C. J. Roothaan[35] who showed how by the introduction of a set of known spatial basis functions one may convert the Hartree-Fock integro-differential equations to a set of algebraic equations that may then be solved by standard matrix techniques.

We therefore introduce a set of K known basis functions $\{\phi_\mu(\mathbf{r})|\mu = 1, 2, \ldots, K\}$ and expand the unknown molecular orbitals in a linear expansion,

$$\psi_i = \sum_{\mu=1}^{K} C_{\mu i}\phi_\mu, \qquad (123)$$

where $i = 1, 2, \ldots, K$. If $\{\phi_\mu\}$ were complete then Eq. (123) would be an exact expansion. In fact any complete set of functions $\{\phi_\mu\}$ could be used. However, for practical computational reasons one is always restricted as to the number and indeed type of basis functions used. As such, it is important to choose a basis set that will provide, as far as possible, a reasonably accurate expansion for the exact molecular orbitals $\{\psi_i\}$. Also since during the course of obtaining a solution one must evaluate many times multicenter integrals involving the basis functions, those types of basis functions that permit closed form expressions for these integrals have enjoyed the most widespread use. For example, Slater type basis functions have the radial form, $\exp(-kr)$, but Gaussian type basis functions have a radial form

$\exp(-kr^2)$. While Slater type basis functions have the same radial dependence as the hydrogenic solutions and hence would provide a much better description of the charge density near the origin than Gaussians, multicenter integrals involving Slater type basis functions cannot be evaluated in closed form and hence are computationally expensive to determine. On the other hand, multicenter integrals involving Gaussian type basis functions do have closed form expressions. As a consequence, Gaussian basis sets have come to dominate the recent work in molecular calculations. Even through more than three times as many Gaussian basis functions are required to achieve the same level of accuracy as with Slater type basis functions, the existence of closed form solutions for the multicenter integrals more than compensates for the larger basis set.

From Eq. (123) the problem of calculating the Hartree-Fock molecular orbitals reduces to the problem of finding the expansion coefficients $C_{\mu i}$. By substituting this expansion into the closed-shell restricted spatial Hartree-Fock equation (Eq. (119)) gives,

$$f(1)\sum_\nu C_{\nu i}\phi_\nu(1) = \epsilon_i \sum_\nu C_{\nu i}\phi_\nu(1). \tag{124}$$

By multiplying by $\phi_\mu^*(1)$ and integrating we turn the integro-differential equation into a matrix equation,

$$\sum_\nu C_{\nu i} \int d\mathbf{r}_1 \phi_\mu^*(1)f(1)\phi_\nu(1) = \epsilon_i \sum_\nu C_{\nu i} \int d\mathbf{r}\phi_\mu^*(1)\phi_\nu(1). \tag{125}$$

We will now define two matrices. The first is the *overlap matrix* $\mathbf{S}$ with elements given by,

$$S_{\mu\nu} = \int d\mathbf{r}_1 \phi_\mu^*(1)\phi_\nu(1). \tag{126}$$

$\mathbf{S}$ is a $K \times K$ Hermitian matrix. While the basis functions $\{\phi_\mu\}$ are assumed to be normalized and linearly independent, they are not in general orthogonal. They therefore overlap with a magnitude $0 \leq |S_{\mu\nu}| \leq 1$. The diagonal elements are unity and the off-diagonal elements are less than one in magnitude. If two off-diagonal elements approach unity in magnitude, that is, approach complete

overlap then the two basis functions approach linear dependence. Since the overlap matrix is Hermitian, it can be diagonalized by a unitary transformation as we will later do. The eigenvalues of the overlap matrix can be shown to necessarily be positive numbers[33], hence the overlap matrix is said to be positive-definite. As the functions in the basis set approach linear dependence the eigenvalues of the overlap matrix approach zero.

The second matrix we will define is the *Fock matrix* $\mathbf{F}$, which has elements,

$$F_{\mu\nu} = \int d\mathbf{r}_1 \phi_\mu^*(1) f(1) \phi_\nu(1). \tag{127}$$

$\mathbf{F}$ is also a $K \times K$ Hermitian matrix. The Fock matrix is the matrix representation of the Fock operator with the set of basis functions $\{\phi_\mu\}$.

With the definitions of the overlap and Fock matrices we can now write Eq. (125) as,

$$\sum_\nu F_{\mu\nu} C_{\nu i} = \epsilon_i \sum_\nu S_{\mu\nu} C_{\nu i}, \tag{128}$$

where, $i = 1, 2 \ldots K$. These are the Roothaan equations which can be completely written as a single matrix equation,

$$\mathbf{FC} = \mathbf{SC}\epsilon, \tag{129}$$

where $\mathbf{C}$ is a $K \times K$ matrix of the expansion coefficients $C_{\nu i}$,

$$\mathbf{C} = \begin{pmatrix} C_{11} & C_{12} & \cdots & C_{1K} \\ C_{21} & C_{22} & \cdots & C_{2K} \\ \vdots & \vdots & & \vdots \\ C_{K1} & C_{K2} & \cdots & C_{KK} \end{pmatrix}. \tag{130}$$

The columns in matrix $\mathbf{C}$ describe the molecular orbitals. The elements in column 1 are the expansion coefficients of ψ_1, those in column 2 are the coefficients of ψ_2

etc. . ϵ is a diagonal matrix of the orbital energies ϵ_i,

$$\epsilon = \begin{pmatrix} \epsilon_1 & & & \\ & \epsilon_2 & & \mathbf{0} \\ & & \ddots & \\ \mathbf{0} & & & \\ & & & \epsilon_K \end{pmatrix}. \tag{131}$$

By introducing a basis we have converted the problem into one solving the matrix equation, $\mathbf{FC} = \mathbf{SC}\epsilon$. Before we can describe exactly how this is done we must first discuss a few additional preliminaries.

The charge density

Given an electron described by the spatial wave function $\psi_a(\mathbf{r})$, the probability of finding that electron in a volume element $d\mathbf{r}$ at point $\mathbf{r}$ is $|\psi_a(\mathbf{r})|^2 d\mathbf{r}$. The probability function is $|\psi_a(\mathbf{r})|^2$. If we have a closed shell molecule described by a single determinant wave function with each occupied molecular orbital ψ_a containing two electrons, the total charge density is then,

$$\rho(\mathbf{r}) = 2 \sum_a^{N/2} |\psi_a(\mathbf{r})|^2, \tag{132}$$

where we see that in atomic units, $\rho(\mathbf{r})d\mathbf{r}$ is the probability of finding any electron in $d\mathbf{r}$ at $\mathbf{r}$. In fact, if we integrate the charge density we get the total number of electrons, thus,

$$\int d\mathbf{r}\rho(\mathbf{r}) = 2 \sum_a^{N/2} \int d\mathbf{r}|\psi_a(\mathbf{r})|^2 = 2 \sum_a^{N/2} 1 = N. \tag{133}$$

If we now insert the molecular orbital expansion Eq. (123) into Eq. (132) we find,

$$\begin{aligned} \rho(\mathbf{r}) &= 2 \sum_a^{N/2} \psi_a^*(\mathbf{r})\psi_a(\mathbf{r}) \\ &= 2 \sum_a^{N/2} \sum_\nu C_{\nu a}^* \phi_\nu(\mathbf{r}) \sum_\mu C_{\mu a} \phi_\mu(\mathbf{r}) \end{aligned}$$

$$= \sum_{\mu\nu} \left[2 \sum_a^{N/2} C_{\mu a} C_{\nu a}^* \right] \phi_\mu(\mathbf{r}) \phi_\nu(\mathbf{r})$$

$$= \sum_{\mu\nu} P_{\mu\nu} \phi_\mu(\mathbf{r}) \phi_\nu^*(\mathbf{r}), \tag{134}$$

where we have defined the *density matrix* $P_{\mu\nu}$,

$$P_{\mu\nu} = 2 \sum_a^{N/2} C_{\mu a} C_{\nu a}^*. \tag{135}$$

Given the basis functions $\{\phi_\mu\}$, the density matrix $\mathbf{P}$ specifies the charge density $\rho(\mathbf{r})$. Since the expansion coefficients $\mathbf{C}$ and the density matrix are directly related one could characterize the results of Hartree-Fock calculations by either $P_{\mu\nu}$ or $C_{\mu i}$.

The use of the density matrix gives an intuitive feel as to how the Hartree-Fock procedure operates. We first make a guess of the density matrix $\mathbf{P}$ (that is, we guess the charge density $\rho(\mathbf{r})$). We then use the charge density to calculate the effective one-electron potential $v^{HF}(\mathbf{r})$. We thus have the Fock operator. We then solve the spatial Hartree-Fock equations for the molecular orbitals $\{\psi_i\}$. We then use these molecular orbitals to calculate a new density matrix and thus new Hartree-Fock potential. We repeat this procedure until the Hartree-Fock potential field no longer changes at which point the procedure has converged. This, in general terms, is the self-consistent field (SCF) method. To understand the details as to how these calculations are actually performed we need an explicit expression for the Fock matrix $\mathbf{F}$.

Expression for the closed-shell restricted Fock matrix

From the definition of the closed-shell restricted Fock operator from Eq. (120) and the Fock matrix from Eq. (127) and given a set of known basis functions $\{\phi_\mu\}$ we have,

$$\begin{aligned}
F_{\mu\nu} &= \int d\mathbf{r}_1 \phi_\mu^*(1) f(1) \phi_\nu(1) \\
&= \int d\mathbf{r}_1 \phi_\mu^*(1) h(1) \phi_\nu(1) + \sum_a^{N/2} \int d\mathbf{r}_1 \phi_\mu^*(1) [2J_a(1) - K_a(1)] \phi_\nu(1)
\end{aligned}$$

$$= H_{\mu\nu}^{core} + \sum_{a}^{N/2} 2(\mu\nu|aa) - (\mu a|a\nu) \tag{136}$$

where $(\mu\nu)$ index *basis functions* and a indexes *molecular orbitals* which are linear combinations of basis functions. In the final expression we have defined the core-Hamiltonian matrix,

$$H_{\mu\nu}^{core} = \int d\mathbf{r}_1 \phi_{\mu}^{*}(1) h(1) \phi_{\nu}(1). \tag{137}$$

where,

$$h(1) = -\frac{1}{2}\nabla_1^2 - \sum_{A} \frac{Z_A}{|\mathbf{r}_1 - \mathbf{R}_A|}. \tag{138}$$

We have also introduced a slightly modified notation for the two-electron integrals to indicate that now the integration is over spatial orbitals instead of spin orbitals, otherwise the notation is the same. For instance, as far the placement of $ijkl$ is concerned, $(ij|kl) = [ij|kl]$ except that,

$$(ij|kl) = \int d\mathbf{r}_1 d\mathbf{r}_2 \psi_i^{*}(\mathbf{r}_1)\psi_j(\mathbf{r}_1) r_{12}^{-1} \psi_k^{*}(\mathbf{r}_2)\psi_l(\mathbf{r}_2), \tag{139}$$

is over the spatial orbitals. Another point is that, as far as the notation is concerned, there is no distinction between integrations over molecular orbitals or basis functions. In general one must draw upon the context of the derivation and associated discussion to ascertain the difference. For instance, in the last expression in Eq. (136),

$$(\mu\nu|aa) = \int d\mathbf{r}_1 d\mathbf{r}_2 \phi_{\mu}^{*}(\mathbf{r}_1)\phi_{\nu}(\mathbf{r}_1) r_{12}^{-1} \psi_a^{*}(\mathbf{r}_2)\psi_a(\mathbf{r}_2), \tag{140}$$

so the integration involves the *basis functions* ϕ_{μ} and ϕ_{ν} and the *molecular orbital* ψ_a.

To calculate the elements of the core-Hamiltonian matrix we must calculate the kinetic energy and nuclear attraction matrices, $\mathbf{T}$ and $\mathbf{V}^{nucl}$ respectively, where,

$$T_{\mu\nu} = \int d\mathbf{r}_1 \phi_{\mu}^{*}(1) \left[-\frac{1}{2}\nabla_1^2 \right] \phi_{\nu}(1), \tag{141}$$

$$V_{\mu\nu}^{nucl} = \int d\mathbf{r}_1 \phi_{\mu}^{*}(1) \left[-\sum_{A} \frac{Z_A}{|\mathbf{r}_1 - \mathbf{R}_A|} \right] \phi_{\nu}(1), \tag{142}$$

so that,

$$H_{\mu\nu}^{core} = T_{\mu\nu} + V_{\mu\nu}^{nucl}. \tag{143}$$

For the particular basis set $\{\phi_\mu\}$ the integrals of $\mathbf{T}$ and $\mathbf{V}^{nucl}$ must be calculated and the core-Hamiltonian matrix formed. Unlike the full Fock matrix, the core-Hamiltonian matrix need only be evaluated once and remains constant throughout the iterative process.

Returning to the full Fock matrix and substituting the linear expansion Eq. (123) for the molecular orbitals,

$$\begin{aligned}
F_{\mu\nu} &= H_{\mu\nu}^{core} + \sum_a^{N/2} \sum_{\lambda\sigma} C_{\lambda a} C_{\sigma a}^* [2(\mu\nu|\sigma\lambda) - (\mu\lambda|\sigma\nu)] \\
&= H_{\mu\nu}^{core} + \sum_{\lambda\sigma} P_{\lambda\sigma} \left[(\mu\nu|\sigma\lambda) - \frac{1}{2}(\mu\lambda|\sigma\nu) \right] \\
&= H_{\mu\nu}^{core} + G_{\mu\nu},
\end{aligned} \tag{144}$$

where $G_{\mu\nu}$ is the two-electron part of the Fock matrix. We see therefore that the Fock matrix contains a one-electron part $\mathbf{H}^{core}$ which, for a given basis set, remains constant and a two-electron part $\mathbf{G}$ which depends on the density matrix $\mathbf{P}$ and a set of two-electron integrals,

$$(\mu\nu|\lambda\sigma) = \int d\mathbf{r}_1 d\mathbf{r}_2 \phi_\mu^*(1)\phi_\nu(1) r_{12}^{-1} \phi_\lambda^*(2)\phi_\sigma(2). \tag{145}$$

It is the two-electron part of the Fock matrix that changes during the course of the solution iterations. Because of the large number of the two-electron integrals $(\mu\nu|\lambda\sigma)$ their evaluation and manipulation is the major difficulty in the Hartree-Fock calculation. For example, if the basis functions are real and if we use the symmetry of the two-electron integrals $((\mu\nu|\lambda\sigma) = (\nu\mu|\lambda\sigma) = (\lambda\sigma|\mu\nu)$ etc.), then for a basis set size $K = 100$ there are 12,753,775 unique two-electron integrals[33].

The Fock matrix depends on the density matrix or equivalently, on the expansion coefficients,

$$\mathbf{F} = \mathbf{F}(\mathbf{P}) \quad \text{or} \quad \mathbf{F} = \mathbf{F}(\mathbf{C}). \tag{146}$$

The Roothaan equations are therefore nonlinear,

$$\mathbf{F(C)C} = \mathbf{SC}\epsilon. \tag{147}$$

If we had an orthonormal basis set then $\mathbf{S}$ would be the unit matrix and we would have the standard matrix eigenvalue problem at each iteration,

$$\mathbf{FC} = \mathbf{C}\epsilon, \tag{148}$$

where we would find the eigenvectors $\mathbf{C}$ and eigenvalues ϵ by diagonalizing $\mathbf{F}$. Since in general the basis is nonorthogonal, we first need to orthogonalize the basis.

Orthogonalization of the basis: The transformed Roothaan equations

In molecular calculations the basis functions are normalized but they are not orthogonal. This gives rise to the overlap matrix. In order to convert the Roothaan equations into the form of the usual matrix eigenvalue problem we need to consider orthogonalizing the basis.

Given a set of functions $\{\phi_\mu\}$ that are not orthogonal then,

$$\int d\mathbf{r}\phi_\mu^*(\mathbf{r})\phi_\nu(\mathbf{r}) = S_{\mu\nu} \tag{149}$$

and we will always be able to find a transformation matrix $\mathbf{X}$ (not unitary) so that we may express a transformed set of functions $\{\phi_\mu'\}$ as,

$$\phi_\mu' = \sum_\nu X_{\nu\mu}\phi_\nu, \tag{150}$$

where $\mu = 1, 2, \ldots K$, that do form an orthonormal set,

$$\int d\mathbf{r}\phi_\mu'^*(\mathbf{r})\phi_\nu'(\mathbf{r}) = \delta_{\mu\nu}. \tag{151}$$

We can determine the properties of $\mathbf{X}$ by the following,

$$\int d\mathbf{r}\phi_\mu'^*(\mathbf{r})\phi_\nu'(\mathbf{r}) = \int d\mathbf{r} \left[\sum_\lambda X_{\lambda\mu}^*\phi_\lambda^*(\mathbf{r})\right] \left[\sum_\sigma X_{\sigma\nu}\phi_\sigma(\mathbf{r})\right]$$

$$= \sum_\lambda \sum_\sigma X^*_{\lambda\mu} \int d\mathbf{r} \phi^*_\lambda(\mathbf{r}) \phi_\sigma(\mathbf{r}) X_{\sigma\nu}$$

$$= \sum_\lambda \sum_\sigma X^*_{\lambda\mu} S_{\lambda\sigma} X_{\sigma\nu} = \delta_{\mu\nu}. \qquad (152)$$

The last expression in the equation can be written in matrix notation as,

$$\mathbf{X}^\dagger \mathbf{S} \mathbf{X} = \mathbf{1} \qquad (153)$$

Equation (153) expresses the relation that $\mathbf{X}$ must satisfy for the transformed basis functions to be orthonormal. Now since $\mathbf{S}$ is Hermitian, it can be diagonalized by a unitary matrix $\mathbf{U}$,

$$\mathbf{U}^\dagger \mathbf{S} \mathbf{U} = \mathbf{s}, \qquad (154)$$

where $\mathbf{s}$ is a diagonal matrix of the eigenvalues of $\mathbf{S}$.

One of the more common methods used for the orthogonalization of a set of functions is the method of symmetric orthogonalization*. This method uses the inverse square root of $\mathbf{S}$ for $\mathbf{X}$, that is,

$$\mathbf{X} = \mathbf{S}^{-1/2} = \mathbf{U} \mathbf{s}^{-1/2} \mathbf{U}^\dagger. \qquad (155)$$

Equation (155) shows that we form $\mathbf{S}^{-1/2}$ by diagonalizing $\mathbf{S}$ to form $\mathbf{s}$ and then taking the inverse square root of each of the eigenvalues to form the diagonal matrix $\mathbf{s}^{-1/2}$ and then "undiagonalizing" to finally give $\mathbf{S}^{-1/2}$. With this choice of $\mathbf{X}$ we verify that it satisfies Eq. (153) thus,

$$\mathbf{S}^{-1/2} \mathbf{S} \mathbf{S}^{-1/2} = \mathbf{S}^{-1/2} \mathbf{S}^{1/2} = \mathbf{S}^0 = \mathbf{1}. \qquad (156)$$

Since the eigenvalues of $\mathbf{S}$ are all positive[33] we have no difficulty taking square roots. However, if the basis set contains some linear dependence then some of the eigenvalues of $\mathbf{S}$ will approach zero, then by Eq. (155) we will have some elements divided by quantities that are nearly zero. Thus symmetric orthogonalization will lead to problems in numerical precision for basis sets with near linear dependence.

---

*other methods such as the Schmidt or canonical orthogonalization are also in common use

With $\mathbf{X}$ determined by symmetric orthogonaliztion (or Schmidt or canonical methods) we consider a new coefficient matrix $\mathbf{C}'$ related to the old coefficient matrix $\mathbf{C}$ by,

$$\mathbf{C} = \mathbf{X}\mathbf{C}'. \tag{157}$$

We assume that $\mathbf{X}$ will have an inverse. This will be true if we have eliminated any linear dependencies. If we substitute into the Roothaan equations we get,

$$\mathbf{F}\mathbf{X}\mathbf{C}' = \mathbf{S}\mathbf{X}\mathbf{C}'\epsilon. \tag{158}$$

Multiplying by $\mathbf{X}^\dagger$ on the left gives,

$$(\mathbf{X}^\dagger\mathbf{F}\mathbf{X})\mathbf{C}' = (\mathbf{X}^\dagger\mathbf{S}\mathbf{X})\mathbf{C}'\epsilon. \tag{159}$$

Next we define a new matrix $\mathbf{F}'$ by,

$$\mathbf{F}' = \mathbf{X}^\dagger\mathbf{F}\mathbf{X}, \tag{160}$$

and then use Eq. (153) to produce,

$$\mathbf{F}'\mathbf{C}' = \mathbf{C}'\epsilon. \tag{161}$$

Equation (161) is the transformed Roothaan equation. They are also known as the canonical Roothaan equations[33]. This matrix equation can be solved for $\mathbf{C}'$ and ϵ by diagonalizing $\mathbf{F}'$. Given $\mathbf{C}'$ we can find $\mathbf{C}$ by Eq. (157). In principle it is even unnecessary to transform back to the unprimed equations since the primed matrix equations represent the Fock matrix and expansion coefficients in the orthogonalized basis,

$$\psi_i = \sum_{\mu=1}^{K} C'_{\mu i}\phi'_{\mu} \qquad i = 1, 2\ldots, K \tag{162}$$

$$F'_{\mu\nu} = \int d\mathbf{r}_1 \phi'^*_{\mu}(1) f(1) \phi'_{\nu}(1) \tag{163}$$

The SCF Procedure

With the background reviewed in the previous sections we are now in position to present in more or less detail the SCF procedure. The actual computational procedure for obtaining restricted closed-shell Hartree-Fock wave functions, i. e. wave functions $|\Psi_0\rangle$, is as follows[33]:

1. Specify the molecular geometry $\{\mathbf{R}_A\}$, the atomic numbers $\{Z_A\}$, the number of electrons N, a basis set $\{\phi_\mu\}$ and the total spin.

2. Calculate the molecular integrals necessary to determine, $S_{\mu\nu}$(Eq. (126)), $H_{\mu\nu}^{core}$ (Eq. (143)), and $(\mu\nu|\lambda\sigma)$ (Eq. (145)).

3. Diagonalize the overlap matrix $\mathbf{S}$ and obtain the transformation matrix $\mathbf{X}$ using Eq. (155).

4. Obtain a guess of the density matrix $\mathbf{P}$. One common method is to diagonalize $\mathbf{H}^{core}$ and use the core molecular orbitals to construct a starting density matrix.

5. Calculate $\mathbf{G}$ from the density matrix $\mathbf{P}$ and the two-electron integrals $(\mu\nu|\lambda\sigma)$ using Eq. (144).

6. Add $\mathbf{G}$ to the core-Hamiltonian to form the Fock matrix $\mathbf{F} = \mathbf{H}^{core} + \mathbf{G}$.

7. Calculate the transformed Fock matrix $\mathbf{F}' = \mathbf{X}^\dagger \mathbf{F} \mathbf{X}$.

8. Diagonalize $\mathbf{F}'$ to obtain $\mathbf{C}'$ and ϵ.

9. Calculate $\mathbf{C} = \mathbf{X}\mathbf{C}'$.

10. Form a new density matrix $\mathbf{P}$ from $\mathbf{C}$ using Eq. (135).

11. Determine if the procedure has converged by determining whether the new density matrix of step (10) is the same as the previous density matrix to within a specified criterion. If the procedure has not converged then return to step (5) with the new density matrix.

12. If the procedure has converged use the solution represented by **C** or **P** to calculate expectation values and other quantities of interest.

<div align="center">Configuration Interaction</div>

As already mentioned, in Hartree-Fock theory the motion of electrons with opposite spins are not correlated. This is a consequence of the single Slater determinant form of the variational wave function and as a result even for an infinite basis set the ground state Hartree-Fock energy will always lie above the exact nonrelativistic Born-Oppenheimer ground state energy by the amount of energy involved in this missing correlation. One important method used to obtain this missing correlation energy is the method of configuration interaction (CI). While CI is a well known method and has been described in detail elsewhere[32,33], it will be useful to summarize the essential features.

For a basis set consisting of K basis functions the Hartree-Fock procedure will produce $2K$ molecular spin orbitals. For N electrons, the ground state Hartree-Fock wave function will be a single Slater determinant comprised of the N lowest energy spin orbitals. Representing this ground state wave function as[33],

$$|\Psi_0\rangle = |\chi_1\chi_2\cdots\chi_a\chi_b\cdots\chi_N\rangle, \tag{164}$$

where it is understood that the remaining $2K - N$ spin orbitals are unoccupied. It is clear that the determinant given by Eq. (164) is but one of many N electron determinants that could be formed from the $2K$ spin orbitals. For instance, one could form a singly excited determinant by promoting an electron from the occupied spin orbital χ_a into the previously unoccupied virtual spin orbital χ_r producing the wave function,

$$|\Psi_a^r\rangle = |\chi_1\chi_2\cdots\chi_r\chi_b\cdots\chi_N\rangle, \tag{165}$$

where the notation $|\Psi_a^r\rangle$ designates that the spin orbital χ_a in the ground state Hartree-Fock wave function has been replaced by the virtual spin orbital χ_r. A doubly excited determinant could be produced by exciting electrons from χ_a and

χ_b to χ_r and χ_s thus,

$$|\Psi_{ab}^{rs}\rangle = |\chi_1\chi_2\cdots\chi_r\chi_s\cdots\chi_N\rangle. \qquad (166)$$

In fact the total number of determinants that could be produced in this way is $(2K)!/[N!(2K-N)!]$. While the excited determinants do not in themselves represent the excited states of the system, they do form N-electron basis functions in which the exact N-electron states may be expanded. If $|\Phi\rangle$ is the exact wave function of the system for a given basis, then the CI expansion would be[33],

$$|\Phi\rangle = c_0|\Psi_0\rangle + \sum_{ra} c_a^r|\Psi_a^r\rangle + \sum_{\substack{a<b \\ r<s}} c_{ab}^{rs}|\Psi_{ab}^{rs}\rangle + \sum_{\substack{a<b<c \\ r<s<t}} c_{abc}^{rst}|\Psi_{abc}^{rst}\rangle + \cdots. \qquad (167)$$

Diagonalizing the CI matrix $\langle\Psi_i|\mathbf{H}|\Psi_j\rangle$, where $\{|\Psi_i\rangle\} = \{|\Psi_0\rangle, |\Psi_a^r\rangle, |\Psi_{ab}^{rs}\rangle, \ldots\}$, gives not only the lowest possible upper bound to the ground state energy but also the lowest possible upper bounds to the excited states of the same spin and spatial symmetry for the given basis set. This is known as the Hylleraas–Undheim theorem[36]. While the CI approach is systematic, the number of determinants required to represent all excitations becomes extremely large for even small systems. For most practical calculations the CI expansion Eq. (167) is commonly truncated to include only up to at most triple excitations.

A variation on this theme is the method of multiconfigurational SCF (MC-SCF). This method is a combination of CI and SCF. It is in fact SCF with a multideterminantal wave function obtained from a full CI expansion within a selected manifold of molecular spin orbitals known as the active space[32]. When the truncated CI expansion is constructed out of all possible configurations within the specified active space, the method is known as complete active space SCF (CASSCF). For MCSCF calculations presented in this thesis all possible configurations within the active space will be included in the CI expansion. With this understood, we will used MCSCF synonymously with CASSCF. Thus the MCSCF is a truncated CI expansion in which both the expansion coefficients and the orbitals are optimized[37]. The added advantage is that the orbitals may be optimized for an excited root and thereby, with the proper choice of the active space, one

may obtain accurate excited state energies of the same spin multiplicity. For this reason MCSCF is a powerful computational tool for the calculation of a system's multiplet structure and the correlation with observed optical spectra.

CHAPTER IV

CLUSTER EMBEDDING

Introduction

The main difference between molecular and crystal defect quantum chemical calculations rests in the treatment of the external field effects. Most molecular calculations deal with collections of atoms that when isolated maintain a stable geometry. That is, in a vacuum the forces on the atoms in a molecule are determined solely on the basis of their interaction with the other atoms and in the stable geometry these forces are exactly balanced in the ground state. Furthermore, it is typical for molecular calculations that all the atoms are treated at the same level of quantum chemical theory. This means that the forces, geometry, and electronic structure for the entire system is determined from a quantum mechanical solution to the Schrödinger equation at the same level of theory. The treatment of defects in solids in this fashion is clearly impossible. The ideal method would be to construct a defect (such as a Mn substitutional impurity or an F-center or both in CaF_2) in an otherwise perfect infinite crystal and then solve the system quantum mechanically. While in principle this is possible, in practice this is computationally impossible. An alternative approach, is to define two regions: the *quantum cluster*, and an *external charge distribution*. The quantum cluster consists of the actual defect itself and it's nearest neighbors (typically around at most 10 to 15 atoms), to be treated quantum mechanically. The external charge distribution is designed in such a way so as to have the same symmetry as the crystal, and produce an electrostatic field within the region of the quantum cluster that approximates the field produced by an infinite crystal. The interactions within the charge producing the external field contributes to the overall energy of the system and are treated

classically. In this way the external charge distribution stabilizes the cluster so that in the ground state the net forces on the atoms within the quantum cluster are zero[*]. In this chapter will be described a method for stabilizing an impurity cluster by the variation of the external charge distribution. It should be noted that no variational principle exists with regard to this external distribution so that one could not, for instance, vary the parameters describing it so as to minimize the total energy.

It should be noted that what follows is an original approach published here for the first time. The method to be described in detail consists of the following stages.

- Construct a "non-defect" cluster. This cluster is the quantum cluster without the particular defect and is therefore a small piece of the perfect crystal that is to be treated quantum mechanically. Its geometry is chosen to be that of the perfect crystal.

- Construct around this cluster a point ion field consisting of representative point charges for the atoms in the perfect crystal. These external point charges are assigned the valence charges of the ions in the crystal (for instance, +2 for Ca and -1 for F in CaF_2) and arranged in the host lattice structure. The size of this external arrangement is chosen so that the electrostatic forces produced by this arrangement best balance the forces on the atoms within the isolated non-defect cluster.

- Perform an SCF calculation for the quantum cluster and external point ion arrangement and determine the new forces on the cluster atoms. Replace the point ions with "point Gaussians" with effective charges and vary the Gaussian exponents and effective charges on the external ions so as to balance these new forces.

---

[*]in principle one could zero the forces in an excited state using the method of MCSCF

- Perform another SCF calculation to obtain the new forces on the quantum cluster atoms and then vary the effective charges and Gaussian exponents to balance these new forces. Continue the SCF force calculations and external charge variation until convergence.

- Construct the defect within the quantum cluster by replacing one of the cluster atoms with the impurity atom or by removing one of the cluster atoms to form a vacancy or both.

- With the external field unchanged, geometry optimize the defective quantum cluster.

To illustrate this method we will consider the formation of the F-center defect in CaF_2. First we will start with the non-defective cluster shown in Fig. 10. This figure shows the $(Ca_4F_7)^{+1}$ S=0 cluster that will be treated quantum mechanically and serves to define the coordinate system. The atoms are arranged at the experimental Ca–F distance of 2.731 Å[18]. The F-center defect is constructed from this cluster by the removal of the central F atom to form a vacancy and the addition of one electron. Before proceeding it will be necessary to the develop the mathematical framework of the method.

<div align="center">Mathematical Development</div>

We begin the mathematical development by considering an external charge density $\rho_{ext}(\mathbf{r})$ which produces an external electrostatic potential $V_{ext}(\mathbf{r})$. From classical electrostatics, the external potential is given by,

$$V_{ext}(\mathbf{r}) = \int \frac{\rho_{ext}(\mathbf{r}')}{|\mathbf{r} - \mathbf{r}'|} d\mathbf{r}'. \tag{168}$$

If we assume that the external charge density is given as an arrangement of point Gaussians, then,

$$\rho_{ext}(\mathbf{r}) = \sum_{i=1}^{N} q_i \left(\frac{\alpha_i}{\pi} \right)^{3/2} e^{-\alpha_i |\mathbf{r} - \mathbf{R}_i^{ex}|^2}, \tag{169}$$
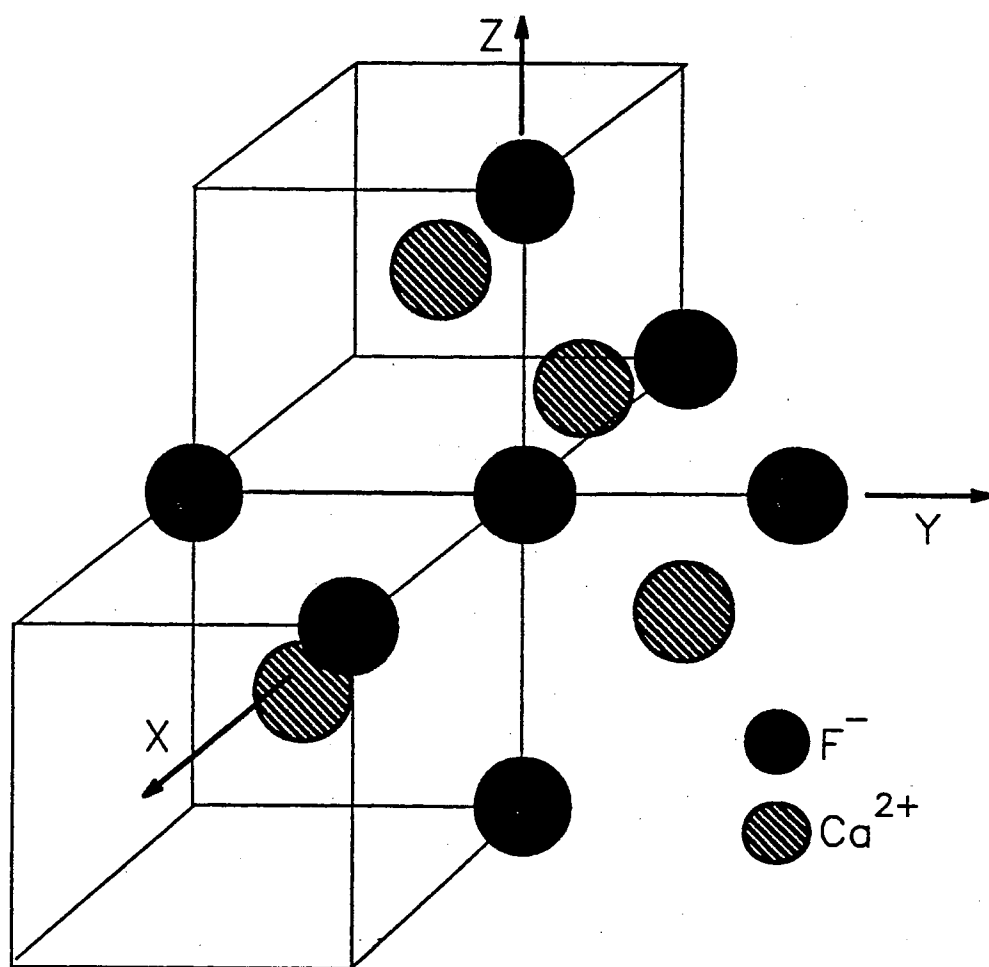
Figure 10. The non-defective cluster $(Ca_4F_7)^{+1}$ S=0 cluster used for the formation of the F-center defect in CaF_2. The Ca-F distance is 2.731 Å[18]. The F-center defect is constructed from this cluster by the removal of the central F atom to form a vacancy and the addition of one electron.

where, N is the number of external lattice sites, $\mathbf{R}_i^{ex}$ locates the external lattice sites, q_i is the total charge associated with lattice point i, and α_i is the Gaussian exponent associated with lattice point i. The next step is to substitute Eq. (169) into Eq. (168) and perform the integration. This integration is carried out in detail in Appendix B, with the result that the external potential can now be written,

$$V_{ext}(\mathbf{r}) = \sum_{i=1}^{N} q_i \frac{\mathrm{erf}[\sqrt{\alpha_i}|\mathbf{R}_i^{ex} - \mathbf{r}|]}{|\mathbf{R}_i^{ex} - \mathbf{r}|}, \tag{170}$$

where $\mathrm{erf}(x)$ is the error function and is defined,

$$\mathrm{erf}(x) = \frac{2}{\sqrt{\pi}} \int_0^x e^{-u^2} du. \tag{171}$$

The quantum cluster electronic charge density, $\rho_{clus}(\mathbf{r})$ is obtained from an SCF calculation and is given by,

$$\rho_{clus}(\mathbf{r}) = \sum_{\nu=1}^{K} \sum_{\mu=1}^{K} P_{\nu\mu} \phi_\nu(\mathbf{r}) \phi_\mu(\mathbf{r}), \tag{172}$$

where, K is the number of basis functions, $P_{\nu\mu}$ is the density matrix and $\phi_\nu(\mathbf{r})$ and $\phi_\mu(\mathbf{r})$ are the primitive Gaussians of type ν and μ centered on cluster sites R_ν and R_μ. The internal quantum cluster potential, $V_{clus}(\mathbf{r})$ is then,

$$V_{clus}(\mathbf{r}) = \int \frac{\rho_{clus}(\mathbf{r}')}{|\mathbf{r} - \mathbf{r}'|} d\mathbf{r}' = \sum_{\nu=1}^{K} \sum_{\mu=1}^{K} P_{\nu\mu} \int \frac{\phi_\nu(\mathbf{r}')\phi_\mu(\mathbf{r}')}{|\mathbf{r} - \mathbf{r}'|} d\mathbf{r}', \tag{173}$$

and the potential due to the atomic nuclei in the cluster is,

$$V_{core}(\mathbf{r}) = \sum_{i=1}^{M} \frac{Z_i}{|\mathbf{r} - \mathbf{R}_i|}, \tag{174}$$

where M is the number of nuclei in the cluster and Z_i is the nuclear charge on cluster atom i at site $\mathbf{R}_i$. The total potential $V(\mathbf{r})$ is then written,

$$V(\mathbf{r}) = V_{clus}(\mathbf{r}) + V_{core}(\mathbf{r}) + V_{ext}(\mathbf{r}), \tag{175}$$

and the total electrostatic field $\mathbf{E}(\mathbf{r})$ as,

$$\mathbf{E}(\mathbf{r}) = -\nabla V_{clus}(\mathbf{r}) - \nabla V_{core}(\mathbf{r}) - \nabla V_{ext}(\mathbf{r}). \tag{176}$$

Using the identity,

$$-\nabla\left(\frac{1}{|\mathbf{r} - \mathbf{r}'|}\right) = \frac{\mathbf{r} - \mathbf{r}'}{|\mathbf{r} - \mathbf{r}'|^3}, \tag{177}$$

we have,

$$
\begin{aligned}
\mathbf{E}(\mathbf{r}) &= \sum_{\nu=1}^{K}\sum_{\mu=1}^{K} P_{\nu\mu} \int \frac{\phi_\nu(\mathbf{r}')\phi_\mu(\mathbf{r}')}{|\mathbf{r} - \mathbf{r}'|^3}(\mathbf{r} - \mathbf{r}')d\mathbf{r}' \\
&+ \sum_{i=1}^{M} Z_i \frac{\mathbf{r} - \mathbf{R}_i}{|\mathbf{r} - \mathbf{R}_i|^3} - \sum_{i=1}^{N} q_i \nabla \frac{\mathrm{erf}[\sqrt{\alpha_i}|\mathbf{R}_i^{ex} - \mathbf{r}|]}{|\mathbf{R}_i^{ex} - \mathbf{r}|}.
\end{aligned} \tag{178}
$$

The first two terms in Eq. (178) contain information concerning the cluster only, therefore, define these first two terms to be $\mathbf{E}_{clus}(\mathbf{r})$, the total field due to the quantum mechanical electronic charge density and the nuclear charges. Next we evaluate Eq. (178) at one of the quantum cluster nuclear sites, say $\mathbf{R}_j$, we then have,

$$\mathbf{E}(\mathbf{R}_j) = \mathbf{E}_{clus}(\mathbf{R}_j) - \sum_{i=1}^{N} q_i \nabla \left.\frac{\mathrm{erf}[\sqrt{\alpha_i}|\mathbf{R}_i^{ex} - \mathbf{r}|]}{|\mathbf{R}_i^{ex} - \mathbf{r}|}\right|_{\mathbf{r}=\mathbf{R}_j}, \tag{179}$$

where it is understood that the nuclear core at $\mathbf{R}_j$ has been excluded from the sum over cores in $\mathbf{E}_{clus}(\mathbf{R}_j)$. Next we observe that if the total electric field is evaluated at one of the cluster sites as in Eq. (179) and if the origin is placed on the central atom as in Fig. 10 then, by symmetry, the total electric field vector must at most have only a radial component. That is $\mathbf{E}(\mathbf{R}_j) = (\text{const.})\hat{\mathbf{r}}$. Therefore, the $\hat{\theta}$ and $\hat{\phi}$ components of the ∇ operator must vanish by symmetry when evaluated at $\mathbf{R}_j$. We then may write,

$$\nabla|_{\mathbf{r}=\mathbf{R}_j} = \left.\frac{\partial}{\partial r}\right|_{\mathbf{r}=\mathbf{R}_j} \hat{\mathbf{r}}. \tag{180}$$

With this simplification, we have,

$$
\begin{aligned}
\nabla \left.\frac{\mathrm{erf}[\sqrt{\alpha_i}|\mathbf{R}_i^{ex} - \mathbf{r}|]}{|\mathbf{R}_i^{ex} - \mathbf{r}|}\right|_{\mathbf{r}=\mathbf{R}_j} &= \left(\frac{R_j - \frac{\mathbf{R}_j \cdot \mathbf{R}_i^{ex}}{R_j}}{|\mathbf{R}_i^{ex} - \mathbf{R}_j|^2}\right) \\
&\times \left(2\sqrt{\tfrac{\alpha_i}{\pi}}\exp[-\alpha_i|\mathbf{R}_i^{ex} - \mathbf{R}_j|^2] - \frac{\mathrm{erf}[\sqrt{\alpha_i}|\mathbf{R}_i^{ex} - \mathbf{R}_j|]}{|\mathbf{R}_i^{ex} - \mathbf{R}_j|}\right) \hat{\mathbf{r}} \equiv \mathbf{I}_i(\mathbf{R}_j).
\end{aligned} \tag{181}
$$

Equation (179) then becomes,

$$\mathbf{E}(\mathbf{R}_j) = \mathbf{E}_{clus}(\mathbf{R}_j) - \sum_{i=1}^{N} q_i \mathbf{I}_i(\mathbf{R}_j). \tag{182}$$

At this point it will be useful to specialize the derivation to the specific system of CaF_2. For CaF_2 we will have two different types of external point Gaussians characterized by the different charges and Gaussian exponents (q_F, α_F) and (q_{Ca}, α_{Ca}). From Eq. (182) the total electric field is then given by,

$$\mathbf{E}(\mathbf{R}_j) = \mathbf{E}_{clus}(\mathbf{R}_j) - q_F \sum_{i=1}^{N_F} \mathbf{I}_i^F(\mathbf{R}_j) - q_{Ca} \sum_{i=1}^{N_{Ca}} \mathbf{I}_i^{Ca}(\mathbf{R}_j), \tag{183}$$

where, N_F and N_{Ca} are the number of F-type and Ca-type external point Gaussians respectively. $\mathbf{I}_i^F(\mathbf{R}_j)$ is given by Eq. (181) with $\mathbf{R}_i^{ex}$ replaced by $\mathbf{R}_i^F$ and α_i replaced by α_F and similarly for $\mathbf{I}_i^{Ca}(\mathbf{R}_j)$, $\mathbf{R}_i^{ex}$ is replaced by $\mathbf{R}_i^{Ca}$ and α_i by α_{Ca}.

If we define the following vector functions,

$$\mathbf{K}_F(\mathbf{R}_j) = \sum_{i=1}^{N_F} \mathbf{I}_i^F(\mathbf{R}_j) \quad \text{and} \quad \mathbf{K}_{Ca}(\mathbf{R}_j) = \sum_{i=1}^{N_{Ca}} \mathbf{I}_i^{Ca}(\mathbf{R}_j), \tag{184}$$

and the following scalar functions,

$$\begin{aligned}
J_F(\mathbf{R}_j) &= \sum_{i=1}^{N_F} \frac{\mathrm{erf}[\sqrt{\alpha_F}|\mathbf{R}_i^F - \mathbf{R}_j|]}{|\mathbf{R}_i^F - \mathbf{R}_j|}, \\
J_{Ca}(\mathbf{R}_j) &= \sum_{i=1}^{N_{Ca}} \frac{\mathrm{erf}[\sqrt{\alpha_{Ca}}|\mathbf{R}_i^{Ca} - \mathbf{R}_j|]}{|\mathbf{R}_i^{Ca} - \mathbf{R}_j|},
\end{aligned} \tag{185}$$

we may simplify the notation. With these definitions, the total electrostatic field is now given by,

$$\mathbf{E}(\mathbf{R}_j) = \mathbf{E}_{clus}(\mathbf{R}_j) - q_F \mathbf{K}_F(\mathbf{R}_j) - q_{Ca} \mathbf{K}_{Ca}(\mathbf{R}_j). \tag{186}$$

To stabilize the quantum cluster we must determine the forces on the cluster nuclei due to the electronic charge density and the other nuclei within the cluster, and the external distribution of charge. From Eq. (186) we see that the total force

on a nucleus with nuclear charge Z_j at site $\mathbf{R}_j$ in the quantum cluster is given by the expression,

$$\mathbf{F}(\mathbf{R}_j) = \mathbf{F}_{clus}(\mathbf{R}_j) - Z_j q_F \mathbf{K}_F(\mathbf{R}_j) - Z_j q_{Ca} \mathbf{K}_{Ca}(\mathbf{R}_j), \qquad (187)$$

where $\mathbf{F}_{clus}(\mathbf{R}_j)$ is the force on the nucleus at site j within the quantum cluster due to the cluster electronic charge density and the other nuclei within the cluster. The terms involving the $\mathbf{K}(\mathbf{R}_j)$ functions represent the force on the nucleus at site j due to the external charge distribution.

When the cluster is completely stabilized, the total force, $\mathbf{F}(\mathbf{R}_j) = 0$. Also, since $\mathbf{F}_{clus}(\mathbf{R}_j)$, $\mathbf{K}_F(\mathbf{R}_j)$, and $\mathbf{K}_{Ca}(\mathbf{R}_j)$ only have components along the $\hat{\mathbf{r}}$-direction, we can write Eq. (187) for the stable cluster as a scalar equation, thus,

$$F_{clus}(\mathbf{R}_j) = Z_j q_F K_F(\mathbf{R}_j) + Z_j q_{Ca} K_{Ca}(\mathbf{R}_j), \qquad (188)$$

where it is understood that positive(negative) forces mean that the vector is directed outward(inward) along the $\hat{\mathbf{r}}$-direction. Referring to Eq. (170) and the $J(\mathbf{R}_j)$ functions in Eq. (185) we see that the electrostatic potential due to the external arrangement of F-type and Ca-type point Gaussians is,

$$V_{ext}(\mathbf{R}_j) = q_F J_F(\mathbf{R}_j) + q_{Ca} J_{Ca}(\mathbf{R}_j). \qquad (189)$$

This completes the formal mathematical development, we will now consider the application of the point Gaussian method to the F-center in CaF_2.

The Point Gaussian Method Applied to the $(Ca_4F_7)^{+1}$ S=0 cluster

Choosing the external lattice size

Equations (188) and (189) form the mathematical basis for the point Gaussian method. In the next section we will apply it to the F-center defect in CaF_2. The first step, however, is to stabilize the non-defect cluster shown in Fig. 10 and then form the F-center by the removal of the central F atom, the addition of an

electron and a geometry relaxation. From Fig. 10 we see that we have three symmetry distinct sites: (1) the central F^{-1} site at $\mathbf{R}_{F0}$, (2) an outer F^{-1} site at $\mathbf{R}_F$, and (3) a Ca^{+2} site at $\mathbf{R}_{Ca}$. As a consequence, it is only necessary to evaluate Eqs. (188) and (189) at these sites and then by symmetry they are automatically satisfied at the other sites reachable by a symmetry operation.

The first step in the point Gaussian procedure is to perform an SCF calculation for the ground state of the quantum cluster in a vacuum. This calculation produces $F_{clus}(\mathbf{R}_F)$ and $F_{clus}(\mathbf{R}_{Ca})$. Note that $F_{clus}(\mathbf{R}_{F0}) = 0$ by symmetry. Then using the effective charges on the cluster nuclei obtained from a Mulliken population analysis[33], the forces on the nuclei due to an arrangement of -1 and +2 external point ions is calculated as a function of the external point ion distribution radius. The -1 and +2 point ions are arranged outside the quantum cluster in the perfect CaF_2 lattice structure. The sum of the forces due to the cluster and due to the external point ion distribution form the net force on a cluster site. A χ^2 error between the net forces on the two symmetry distinct Ca and F sites and zero is then plotted versus the external point ion distribution radius. The χ^2 is defined,

$$\chi^2 = \left[F_{clus}^{vacuum}(\mathbf{R}_F) + F_{ext}(\mathbf{R}_F, R_{ext}^{pi}) \right]^2 + \left[F_{clus}^{vacuum}(\mathbf{R}_{Ca}) + F_{ext}(\mathbf{R}_{Ca}, R_{ext}^{pi}) \right]^2,$$
$$(190)$$

where, for instance, $F_{ext}(\mathbf{R}_F, R_{ext}^{pi})$ is the force on the cluster site $\mathbf{R}_F$ due to the external arrangement of point ions with a radius of R_{ext}^{pi}. The optimum external point ion distribution radius is then determined by that radius that produces the smallest χ^2 as shown in Fig. 11. From this figure we see that minima occur at two points, $R_{ext}^{pi} = 11.542$ Bohr and $R_{ext}^{pi} = 21.282$ Bohr. Based on this observation, we will choose the size of the external arrangement to be 21.282 Bohr. Excluding the quantum cluster atoms this includes 298 F^{-1} and 148 Ca^{+2} point ions.

The force equations

With the size of external distribution chosen using the point ion model, the point ions are replaced by point Gaussians and then Eqs. (188) and (189) are
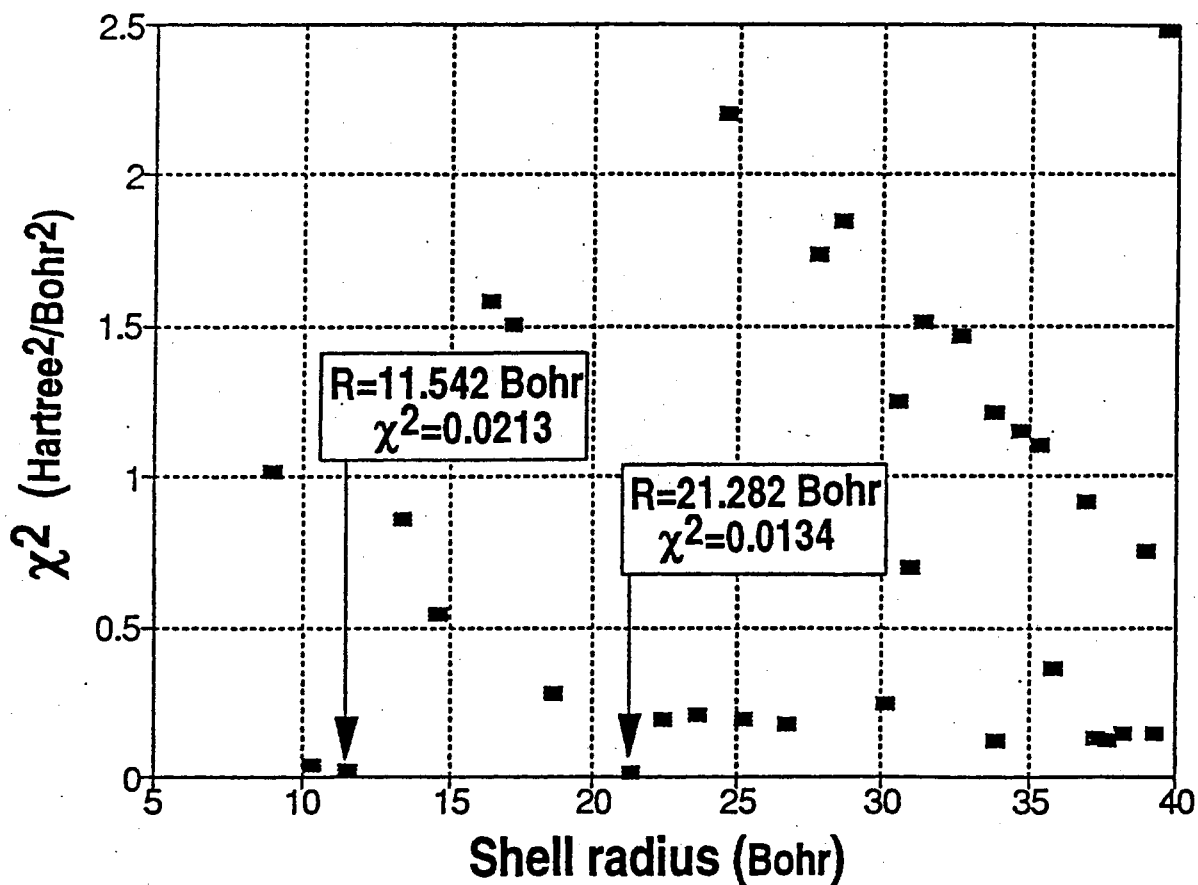
Figure 11. χ^2 error between the net forces on the symmetry distinct cluster sites, $\mathbf{R}_F$ and $\mathbf{R}_{Ca}$ and zero. The χ^2 is plotted as a function of external lattice size. We see that the smallest χ^2 occurs for $R_{ext}^{pi} = 21.282$ Bohr. This radius includes 298 F^{-1} and 148 Ca^{+2} external point ions.

solved for the $q_F, \alpha_F, q_{Ca}, \alpha_{Ca}$ parameters. From the literature, the Madelung potential at a F-site is known to be 10.73 v[18]. After subtracting the contribution to the Madelung potential due to the quantum cluster ions, the *cluster subtracted* Madelung potential is -0.1292 Hartrees. This is the value that the external charge distribution must produce at the central F-site so as to represent an infinite lattice. With V_0 taken to be this value, we find that the parameters are found by solving,

$$Z_F q_F K_{FF} + Z_F q_{Ca} K_{CaF} = F_F, \tag{191}$$

$$Z_{Ca} q_F K_{FCa} + Z_{Ca} q_{Ca} K_{CaCa} = F_{Ca}, \tag{192}$$

$$q_F J_{F0} + q_{Ca} J_{Ca0} = V_0, \tag{193}$$

where, $K_{FF} = K_F(\mathbf{R}_F)$, $K_{CaF} = K_{Ca}(\mathbf{R}_F)$, $K_{FCa} = K_F(\mathbf{R}_{Ca})$, $K_{CaCa} = K_{Ca}(\mathbf{R}_{Ca})$, $J_{F0} = J_F(\mathbf{R}_0)$, and $J_{Ca0} = J_{Ca}(\mathbf{R}_0)$. Also we have written F_F for $F_{clus}(\mathbf{R}_F)$ and F_{Ca} for $F_{clus}(\mathbf{R}_{Ca})$. We note that we cannot write a force equation for the central F ion since by symmetry the net force on this ion is always zero and therefore would not represent an independent condition. Observe that one must solve three equations (Eqs. (191)-(193)) for four unknowns ($q_F, \alpha_F, q_{Ca}, \alpha_{Ca}$). This leaves one parameter undetermined. To resolve this we may impose a neutrality condition namely, $q_{Ca} = -2q_F$. It should be noted that the above equations are linear in the q_F and q_{Ca} parameters while, the equations are highly non-linear in α_F and α_{Ca}. Therefore, from a computational point of view it is more convenient to use Eqs. (191) and (192) to eliminate the q_F and q_{Ca} parameters resulting in an expression that gives α_{Ca} as a function of α_F. Then, numerically, α_F is scanned and α_{Ca}, q_F and q_{Ca} are calculated and the solution that best gives the neutrality condition is chosen. This method avoids having to solve the very complicated equations that result when all the parameters except α_F or α_{Ca} are eliminated.

Following the above method we first solve Eqs. (191) and (192) for q_F and q_{Ca}, thus,

$$q_F = \frac{1}{A}[Z_{Ca} K_{CaCa} F_F - Z_F K_{CaF} F_{Ca}], \tag{194}$$

$$q_{Ca} = \frac{1}{A}[-Z_{Ca}K_{FCa}F_F + Z_F K_{FF}F_{Ca}], \tag{195}$$

where, $A = Z_{Ca}K_{CaCa}Z_F K_{FF} - Z_F K_{CaF}Z_{Ca}K_{FCa}$. Next, these expressions for q_F and q_{Ca} are substituted into Eq. (193) to give,

$$\begin{aligned} Z_{Ca}K_{CaCa}F_F J_{F0} \quad &- \quad Z_F K_{CaF}F_{Ca}J_{F0} + Z_F K_{FF}F_{Ca}J_{Ca0} - Z_{Ca}K_{FCa}F_F J_{Ca0} \\ &= \quad Z_{Ca}K_{CaCa}Z_F K_{FF}V_0 - Z_F K_{CaF}Z_{Ca}K_{FCa}V_0, \tag{196} \end{aligned}$$

which contains only the α_F and α_{Ca} parameters. The next step is to scan over the parameter α_F, use Eq. (196) to calculate α_{Ca} then calculate q_F and q_{Ca} using Eqs. (194) and (195). The solution chosen is the one that best satisfies $q_{Ca} = -2q_F$.

Methodology and results

Stabilizing the nondefective cluster at the experimentally determined geometry requires an iterative procedure. The reason for this is that the altering of the external field changes the quantum cluster electronic charge density which in turn changes the cluster forces. If the external charge density is being adjusted so as to produce forces on the cluster atoms that exactly balance the internal cluster forces, then after each alteration of the external field a corresponding change in the cluster electronic charge density and cluster forces occurs. The method applied in this work is that first the cluster forces are calculated quantum mechanically at the Hartree-Fock level of theory for an isolated cluster* however, in general, correlated methods may be used such as MP2 or CI. With an external lattice of F-type and Ca-type point Gaussians chosen in the fashion described in the previous section, the Gaussian exponents and effective charges are then determined by the solution of Eq. (196). These parameters produce an external field that exactly balances the cluster forces. The cluster forces are then re-calculated in the presence of the new external field. Because of the change in the electronic charge density due to the newly introduced field, new cluster forces are obtained. With these new cluster forces, Eq. (196) is then solved again to produce new parameters and hence a new

---

*that is, the quantum cluster in vacuum

external field that would exactly balance the new cluster forces. The cluster forces are then calculated again. This process is continued until the calculated cluster forces match to within a specified tolerance the opposite of the external field forces of the previous iteration. At this point, the iterative process has converged.

Table VII shows a series of calculations on the $(Ca_4F_7)^{+1}$ S=0 cluster shown in Fig. 10. Columns 2 and 3 show the cluster forces on a F and Ca site due to the electronic charge density and the other nuclei within the quantum cluster in the presence of the external electrostatic field produced by the external charge density specified by the parameters in columns 4 to 7. However, the cluster forces in columns 2 and 3 do not include contributions due to the external field directly, rather, the external field affects the cluster electronic charge density which in turn changes the cluster forces. In this table the cluster forces are calculated quantum mechanically at the Hartree-Fock level of theory. Columns 4 to 7 show the parameters obtained from solving Eq. (196) using the cluster forces for the previous iteration. For instance, the parameters in the iteration 1 row were obtained using the cluster forces from iteration 0. Columns 8 and 9 show the forces on the cluster sites due to the external charge distribution only. Columns 10 and 11 show the net forces on the cluster sites. This is nothing more than the sum of the cluster and external forces.

We see from the results of Table VII the iterative scheme converges rather quickly with convergance achieved by the 5th iteration. The charges on the F-type and Ca-type point Gaussians do not vary significantly from the ionic charges in CaF_2. The average radius of the point Gaussians, however, is about half that of the ionic radii of F and Ca in CaF_2. The last row labeled CISD gives the cluster and net forces on the sites from a configuration interaction calculation using all single and double substitutions of the Hartree-Fock wave function. In all 62 molecular orbitals were used in the CISD calculation so that this calculation was quite expensive computationally. We see that the incorporation of electron correlation does introduce significant changes in the net forces. However, even with correlation the net force on the cluster F-sites is still less by over an order of

magnitude from the isolated cluster forces. For the Ca-sites the net force is less by over three orders of magnitude from the isolated case. We show these results for comparison only since the use of CISD is too computationally expensive with the available machines to use in the iterative scheme.

The Formation and Relaxation of the F-center

With the $(Ca_4F_7)^{+1}$ $S=0$ cluster stabilized by method described in the previous section, the defect cluster can now be formed. Using the parameters from iteration 5 in Table VII for the external field, the central ion is removed from and an electron is added to the quantum cluster thereby forming the $(Ca_4F_6Vac)^{+1}$ $S=1/2$ F-center cluster. The elimination of the central F ion will unbalance the forces on the outer Ca and F ions hence the positions of the outer Ca and F ions must be adjusted to the new equilibrium positions. Table VIII shows a series of SCF force calculations for the F-center cluster. Iteration 0 shows the forces in the isolated F-center cluster. Iterations 1 to 5 incorporate the external field produced by the parameters of iteration 5 in Table VII. Columns 6 and 7 show the external field forces in the outer F and Ca sites. It should be noted that these change as a result of the movement of the F and Ca cluster ions and are not the consequence of any change in the parameters used to generate the field since these remain constant

TABLE VII.

SUMMARY OF THE RESULTS FOR THE POINT GAUSSIAN METHOD APPLIED TO THE $(Ca_4F_7)^{+1}$ $S=0$ CLUSTER

Iter.	$F_{clus}(R_j)\hat{r}$ (au)		New Parameters (au)				$F_{ext}(R_j)\hat{r}$ (au)		$F_{net}(R_j)\hat{r}$ (au)	
	F-site	Ca-site	q_F	α_F	q_{Ca}	α_{Ca}	F-site	Ca-site	F-site	Ca-site
0	-0.0857	-0.2435		–isolated cluster–			0.0000	0.0000	-0.0857	-0.2435
1	-0.0010	-0.0902	-0.710	0.030	1.432	0.018	0.0857	0.2435	0.0847	0.1533
2	-0.0096	-0.1037	-1.067	0.025	2.142	0.020	0.0010	0.0902	-0.0086	-0.0136
3	-0.0088	-0.1024	-1.028	0.025	2.065	0.020	0.0096	0.1037	0.0008	0.0013
4	-0.0089	-0.1026	-1.032	0.025	2.073	0.020	0.0088	0.1024	-0.0001	-0.0001
5	-0.0089	-0.1026	-1.032	0.025	2.072	0.020	0.0089	0.1026	0.0000	0.0000
CISD	-0.0048	-0.1024		–same as above–				–same as above–	0.0041	0.0002

throughout the relaxation. From iteration 1 we see that even with the incorporation of the external field there still exists net inward forces in the outer F and Ca cluster ions. After several inward adjustments of the Ca-Vac and F-Vac distances we are able to obtain an order of magnitude decrease in the net forces on these ions. The final geometry, shown as iteration 5, required a 1.2% inward relaxation for the F ions and a 3.3% inward relaxation for the Ca ions. This is the relaxed geometry used for subsequent calculations on the Mn-perturbed F-center in the following chapter.

TABLE VIII.

SUMMARY OF THE RESULTS FOR THE RELAXATION OF THE F-CENTER CLUSTER

| Iter. | Vac-Ion Distance (Å) | | $F_{clus}(\mathbf{R}_j)\hat{\mathbf{r}}$ (au) | | $F_{ext}(\mathbf{R}_j)\hat{\mathbf{r}}$ (au) | | $F_{net}(\mathbf{R}_j)\hat{\mathbf{r}}$ (au) | |
	Vac-F	Vac-Ca	F-site	Ca-site	F-site	Ca-site	F-site	Ca-site
0	2.7315	2.3655	-0.0918	-0.2707	0.0000	0.0000	-0.0918	-0.2707
1	2.7315	2.3655	-0.0209	-0.1208	0.0089	0.1026	-0.0120	-0.0182
2	2.7315	2.1304	-0.0346	-0.0439	0.0089	0.0930	-0.0257	0.0491
3	2.7315	2.3019	-0.0239	-0.1066	0.0089	0.1001	-0.0150	-0.0066
4	2.7000	2.3019	-0.0157	-0.1100	0.0092	0.1001	-0.0065	-0.0099
5	2.7000	2.2863	-0.0164	-0.1060	0.0092	0.0994	-0.0071	-0.0066

CHAPTER V

CALCULATIONS

Introduction

The main work for this thesis concentrated on electronic structure calculations for two clusters: $(MnF_8)^{-6}$, $(MnCa_3F_6Vac)^{+1}$. Each of these clusters will be discussed in more detail in following sections. These clusters relate to the modeling of Mn defects in irradiated and unirradiated CaF_2:Mn. The $(MnF_8)^{-6}$ cluster will serve to represent an isolated Mn^{2+} substitutional impurity in an otherwise perfect unirradiated CaF_2 lattice. Since the optical spectra of CaF_2:Mn is known[10], the calculation of the excited states of this cluster will serve as a benchmark for the MCSCF technique. By the comparison of the experimental and theoretical results, we will be able to judge the errors likely to be prevalent when we move to the larger Mn-perturbed F-center cluster. The smaller $(MnF_8)^{-6}$ cluster also represents a good starting point as far as choosing a basis set is concerned. Once a basis set is chosen and optimized for this cluster, it could then be transferred almost without change to the larger $(MnCa_3F_6Vac)^{+1}$ cluster.

Programs and Computer Systems

The main analytical tool used in this work is the *Gaussian 92*[19] quantum chemical program package. *Gaussian 92* is a connected system of programs for performing semiempirical and *ab initio* molecular orbital calculations. Originally developed at Carnegie-Mellon University in 1970 to perform simple Hartree-Fock SCF calculations, *Gaussian* has been continuously upgraded so that today this system of programs is capable of performing several of the advanced calculations

involving the various extensions of Hartree-Fock such as large scale configuration interaction, many-body perturbation theory to second and fourth order, and complete active space multiconfigurational SCF. To name a few of its capabilities, *Gaussian 92* can perform geometry optimization to either minima or saddle points, compute force constants, follow reaction paths, perform population analysis, harmonic vibrational analysis, calculate electrostatic potentials, multipole moments and polarizabilities. Of particular interest to this work, *Gaussian 92* can perform force and excited state calculations using the MCSCF technique in the presence of an external arrangement of either point charges or point Gaussians. Both of these capabilities are crucial for work on defects in solids since the cluster must first be stabilized in an electrostatic field that models an external infinite crystal and excited state calculations are required so that transition energies can be computed for comparison with optical spectra. Presently *Gaussian 92* is available for machines that use the VMS, UNIX, UniCOS and IBM MVS operating systems.

The computing facilities presently available for computational solid state research include a VAX/VMS 3100/3900 VAXcluster, the university VAX/VMS 6340 and the IBM 3090-200s vector facility. The present configuration utilizes the 3900 MicroVAX as a front-end to the larger VAX6340 and IBM3090 machines. The 3900 MicroVAX is also used to perform the smaller calculations such as basis set optimization, geometry variation, and force calculations at the Hartree-Fock level of theory. In this way most of the preliminary work is accomplished before the larger CI and MCSCF calculations are performed on either the VAX6340 or IBM3090.

Methodology

In this section we will discuss the practical problems and methods involved in performing electronic structure calculations using the method of Hartree-Fock. We will also discuss the overall calculation sequence from setting up the cluster to performing and CI and MCSCF calculations.

The essential feature of Hartree-Fock theory is the search for the ground state. Once the ground state is accurately determined, extensions of Hartree-Fock theory such as CI or MCSCF may then be employed by which one may arrive at better ground state wave functions or calculate the electronic excited states. Given a system with the locations of the nuclei specified and the number electrons and the total spin known, the Hartree-Fock process starts from an initial guess of the density matrix* and through an iterative process arrives at the best single determinantal wave function for the description of the ground state for the given spin. In theory the method of Hartree-Fock as outlined in Chapter III will work, in practice it often will not converge to the ground state on the first attempt. For cluster calculations convergence problems may arise from basically three areas: (1) the chemical instability of the cluster, (2) the basis set, and (3) the initial guess.

The chemical instability of the cluster stems from the fact that most often the cluster chosen to represent the defect does not correspond to a stable molecule in free space. In fact, if the cluster ions where allowed to move they would at best rearrange themselves into a lower energy geometry that would not represent the known defect structure or at worst simply dissociate. The method for stabilizing the cluster discussed in Chapter IV helps alleviate this problem as far as the forces on the ions are concerned. However, since the part of the crystal that is treated quantum mechanically is quite small while a much larger portion is treated classically one expects to experience distortions in the wave function (and hence density) near the boundary between the quantum cluster and the external charge distribution. This distortion in the wave function, which we call the cluster size effect, arises from the discontinuity associated with the abrupt termination of the cluster or the abrupt transition from the quantum treatment of charge to the classical. One consequence of the cluster size effect may be that the cluster either in isolation or in the presence of an external field may not be able to contain the charge so that the Hartree-Fock procedure may not converge to a negative energy.

---

*arrived at usually by diagonalizing the core Hamiltonian matrix

Convergence problems relating to the initial guess and basis set are closely related. An initial guess obtained by diagonalizing the core Hamiltonian produces a certain density. In general, this starting density may be significantly different from the final SCF converged density. As a consequence, the SCF procedure may not converge to the ground state for a given basis. This problem may be helped somewhat by either expanding the basis set or by improving the initial guess. In practice, expanding the basis set may not be practical and at any rate the question as to exactly how the basis set should be modified is sometimes unclear. For some cases the addition of diffuse functions can resolve this problem. The addition of diffuse functions means that the basis set is no longer minimal, that is, the number of basis functions of a given symmetry is larger than the number of electrons occupying states with that symmetry. However, as we will see this may lead to charge exit under basis set optimizations when the external field is included. Another way to overcome convergence problems is to alter the initial guess. This may require a series of reduced convergence calculations. The molecular orbitals are then examined and the necessary alterations are made. Below we will discuss a systematic procedure we have developed for doing this.

With the cluster geometry, choosing the number of electrons and the total spin is the first step toward choosing a basis. The choice of the variational basis set is perhaps the most important consideration when attempting to perform accurate SCF calculations. One attempts to choose a basis that, while limited enough in size for practical calculations is also flexible enough so as not to unduly bias the results. For the case of the CaF_2 clusters, particular attention must be paid to the Mn $3d$ orbitals which are the ones primarily responsible for the observed transitions.

The standard basis functions used for atomic calculations of the F^- ion and the Ca and Mn atoms from Huzinaga $et.$ $al.$ [38] provide a good starting point. Starting with numerical solutions of the Hartree-Fock equations for atoms, Huzinaga $et.$ $al.$ then carried out a series of fits with s, p and d-type Gaussian functions to the numerical atomic solutions. The Gaussian basis functions are a product of a radial Gaussian and a real spherical harmonic of either the s, p or d-type.

These are called the *primitive Gaussian* basis functions. For a nucleus centered at $\mathbf{R} = X\hat{\mathbf{x}} + Y\hat{\mathbf{y}} + Z\hat{\mathbf{z}}$, the normalized real primitive Gaussian basis functions of s, p and d-type symmetry are:

$$g_{s,\mathbf{R}}(\mathbf{r}) = 4\left(\frac{\alpha^3}{32\pi^3}\right)^{1/4} e^{-\alpha|\mathbf{r}-\mathbf{R}|^2} \tag{197}$$

$$g_{p,\mathbf{R}}(\mathbf{r}) = 8\left(\frac{\alpha^5}{32\pi^3}\right)^{1/4} \left\{ \begin{array}{c} (x-X) \\ (y-Y) \\ (z-Z) \end{array} \right\} e^{-\alpha|\mathbf{r}-\mathbf{R}|^2}$$

$$g_{d,\mathbf{R}}(\mathbf{r}) = 16\left(\frac{\alpha^7}{32\pi^3}\right)^{1/4} \left\{ \begin{array}{c} \frac{1}{2\sqrt{3}}[2(z-Z)^2 - (x-X)^2 - (y-Y)^2] \\ \frac{1}{2}[(x-X)^2 - (y-Y)^2] \\ (x-X)(z-Z) \\ (y-Y)(z-Z) \\ (x-X)(y-Y) \end{array} \right\} e^{-\alpha|\mathbf{r}-\mathbf{R}|^2}$$

The atomic basis functions then consist of a linear combination (contraction) of the primitive Gaussians of the same symmetry. For instance, an s-type atomic basis function consists of a linear combination of s-type primitive Gaussians. The degree of contraction (the number of primitive Gaussians in the linear combination) typically varies from just one to as many as six. By using linear combinations of the atomic basis functions, Huzinaga *et. al.* [38] fitted the numerical atomic Hartree-Fock solutions for a large number of atoms and tabulated the results. These tables then provide the starting basis functions for beginning the molecular calculations. Because these tables produced basis functions adequate for atomic calculations, they must be augmented by the addition of more diffuse s, p and d Gaussian atomic basis functions for molecular calculations. In total, nine atomic basis functions were used for fluorine, 13 for calcium and 23 for manganese. Since the molecular orbitals are then represented as linear combinations of atomic basis functions when the Roothaan equations are solved, this technique is best referred to as the linear combination of atomic basis functions method and not, as in usual parlance, as the linear combination of atomic orbitals method.

With the basis set chosen, one may begin the SCF calculations. For the calculations in this thesis the initial guess is determined by diagonalizing the core Hamiltonian matrix. As already stated above, this method of generating an initial guess generally produces a density that is significantly removed from the density of the Hartree-Fock ground state. Furthermore, since the basis set is finite, the SCF procedure generally will not converge to the ground state in the first attempt. The method used to overcome this problem is to perform a series of SCF calculations each time diagonalizing the CI singles matrix. This process gives the singles configuration interaction (CIS) energy spectrum and the leading coefficients for the singles CI expansion. From the energy spectrum one may determine the approximate energy of those states with the same spin lying below the SCF converged result. From the leading coefficients in the CIS expansion one may determine which alterations need to be made to the guess for the next SCF-CIS calculation. This is continued until CIS does not produce an energy below the present SCF converged result. Of course, the ground state for some spin multiplicities are multideterminantal (such as $^4T_{1g}$), in this case CIS will always give a lower energy. For this case CIS will produce a lower energy eigenvalue, however, the CIS expansion will contain several determinants with similar expansion coefficients indicating that the wave function is best described as a linear combination of determinants. At this point it is unlikely that further alterations will lead to a lowering of the Hartree-Fock energy. It is at this point that one has obtained the best Hartree-Fock ground state in a single determinantal form for the given basis. It should be noted that during this process that it may be necessary to relax the convergence criteria temporarily so that one may obtain the partially converged molecular orbitals.

Once the ground state has been found for the given basis, the next step is to optimize the basis set. To understand how this process works, Eq. (198) below shows the form of an s-type atomic basis function $\phi_\mu(r)$,

$$\phi_\mu(r) = \sum_{i=1}^{N} d_{i\mu} e^{-\alpha_{i\mu} f^2 r^2}, \tag{198}$$

where N is the number of primitive Gaussians composing the atomic basis function called the *degree of contraction*. The coefficients $d_{i\mu}$ are the *contraction coefficients*[*]. The quantities $\alpha_{i\mu}$ are the Gaussian exponents and f is the *scale factor*. Note that in the contraction sum, $d_{i\mu}$ and $\alpha_{i\mu}$ vary for each primitive Gaussian. The scale factor, however, is the same for all the primitive Gaussians. Thus changing the scale factor f scales the entire atomic basis function ϕ_μ. Optimizing the basis set then involves varying the scale factors to minimize the energy. For practical reasons, this variation is performed at the Hartree-Fock level of theory and only the basis functions representing the valence electrons are changed. Furthermore, has been found that this variation works best for the cluster in isolation. Attempting to vary the valence basis functions in the presence of an external charge distribution tends to make the diffuse basis functions so extended that a significant amount of charge accumulates in the region of the nearest neighbor point Gaussians. The charge has then, in effect, exited from the quantum cluster.

The next step is the introduction of the external charge distribution and the building in of correlation with singles and doubles CI (CISD) and complete active space multiconfigurational SCF (MCSCF). If it can be shown that the presence of an external field does not significantly affect the relative the spacing of excited state energy levels as in the case with the $(MnF_8)^{-6}$ cluster then the external field can be dispensed with. On the other hand, for systems where electrons are not bound tightly to a nuclear core as in the case of the F-center $(Ca_4F_6Vac)^{+1}$ or the Mn perturbed F-center $(Mn_4F_6Vac)^{+1}$ clusters where the vacancy electron is quite diffuse, then the external field must be carefully constructed. The details as to how the non-defective cluster is stabilized, the defect formed and the cluster atoms relaxed has already been discussed in Chapter IV.

The final step is utilization of the MCSCF method for the systematic calculation of the electronic excited states. Since the application of this technique is

---

[*]the primitive Gaussian normalization factor is absorbed into the contraction coefficients and the contraction coefficients are chosen such that the entire atomic basis function is normalized

quite specialized to the particular system in question, a detailed discussion of its application will be made when the clusters themselves are discussed.

$$\text{The } (MnF_8)^{-6} \text{ Cluster}$$

Cluster geometry and external field

Mn^{2+} ions enter the CaF_2 lattice substitutionally and are surrounded by eight F^- ions arranged in O_h symmetry. To model the isolated Mn impurity, we construct a cluster consisting of a central Mn^{2+} ion and the nearest neighbor F^- ions as shown in Fig. 12. With the Mn^{2+} ion at the origin the F^- ions are located at $(\pm\frac{a}{2}, \pm\frac{a}{2}, \pm\frac{a}{2})$, where a is the F-F distance. Recent experimental evidence in the form of x-ray absorption near-edge structure (XANES)[39] indicate a first shell at 2.20 Å. This yields a value of 2.54 Å for a and represents about a 7% *inward* relaxation from the perfect CaF_2 lattice constant of 2.73 Å[18]. It has been pointed out that in many cases the modeling of crystal defects by isolated cluster calculations can lead to inaccurate results[40]. While this may certainly be true for defect complexes where the electronic charge density is delocalized in, for instance, an *F*-center, or for materials exhibiting a large degree of covalent bonding, one expects this problem to be less severe for point impurities in ionic crystals. This assertion is born out by the success the method of ligand fields has had in its application to the transition metals in the alkali halides and alkali earth fluorides. Nevertheless, in every case it must be demonstrated to what degree the external field affects the calculated transitions.

To a first approximation, an external arrangement of point ions must produce the Madelung potentials within the cluster. For a finite external arrangement, however, this requires a judicial choice of where the external cut-off radius should be. The Madelung potentials for CaF_2 available in the literature[18] are $\phi_F^\infty = 10.73$ v for a F site and $\phi_{Ca}^\infty = -19.95$ v for a Ca site. The ∞ superscript is used to indicate the potentials for the infinite lattice. A finite external arrangement of point ions must be chosen such that it produces the cluster-subtracted Madelung
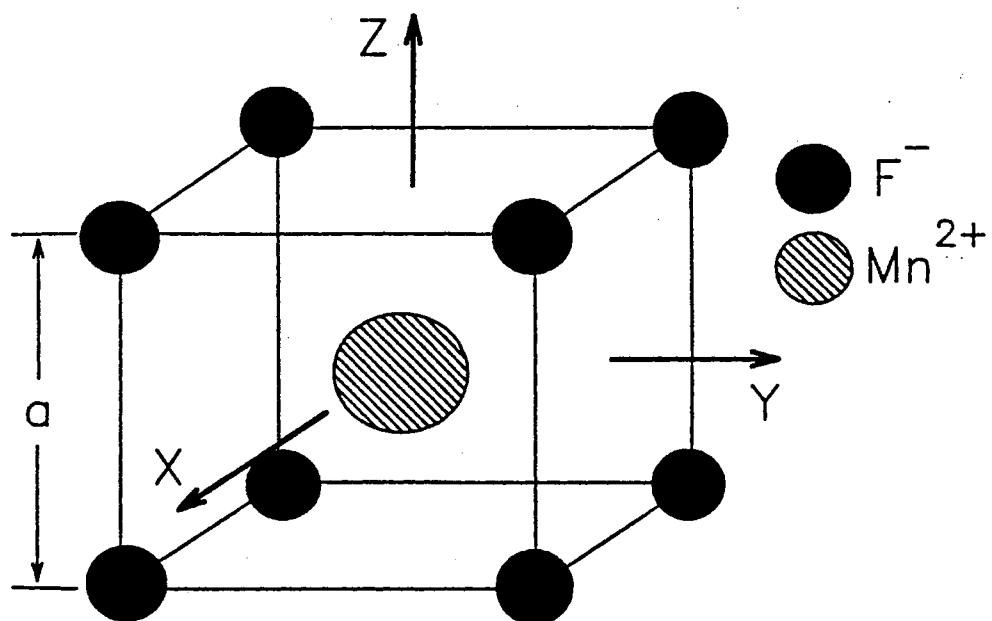
Figure 12. Diagram of the $(MnF_8)^{6-}$ cluster used to model the isolated Mn impurity in CaF_2.

potentials at the Mn and F sites within the quantum cluster. Accounting for the electrostatic contributions to the Madelung potential due to the cluster ions the cluster-subtracted Madelung potentials are, $\phi_F^{\infty\prime} = 1.051$ Hartrees and $\phi_{Mn}^{\infty\prime} = 1.056$ Hartrees. The external lattice size therefore will be chosen such that its potential reproduces the difference, $\phi_{Mn}^{\infty\prime} - \phi_F^{\infty\prime} = 0.005$ Hartrees.

For these calculations, the external field was produced by arranging outside the quantum cluster -1 and +2 point charges representing the F^{-1} and Ca^{+2} ions respectively. These external ions were situated so as to conform to the structure of a perfect CaF_2 lattice. Figure 13 shows the potential difference $\phi_{Mn}'(R) - \phi_F'(R)$ as a function of the radius of the external arrangement of point ions from the central Mn ion. This figure shows that as the size of the external arrangement increases, the potential difference begins to converge as one would expect. As the size is further increased, one would expect the potential difference produced from the finite arrangement to approach the value for the infinite lattice, namely 0.005 Hartrees. The goal of modeling the infinite lattice with a finite arrangement of point ions can be achieved by selecting the size of this finite arrangement so that the potential difference produced by it most closely matches the value for the infinite lattice. Figure 13 shows that this is accomplished with an external point ion radius of 20.65 Bohr consisting of 412 point ions. This arrangement produced the desired potential difference of 0.005 Hartrees.

Calculations

The Mn defect cluster shown in Fig. 12 has an overall charge of -6. Each F^- has closed $2p$ shells and the Mn^{2+} has a $3d^5$ configuration outside closed shells. The ground state is $^6A_{1g}$ arising from the $t_{2g}^3 e_g^2$ configuration. The first excited state is $^4T_{1g}$ from the $t_{2g}^2 e_g^3$ configuration. The $^6A_{1g}$ ground state Hartree-Fock wave function was obtained through the SCF-CIS procedure discussed in the previous sections with the SCF technique being the unrestricted Hartree-Fock (UHF) method. The basis set scale factors where then optimized. The first excited state, $^4T_{1g}$, was then calculated from the S=5/2 ground state by flipping a spin.
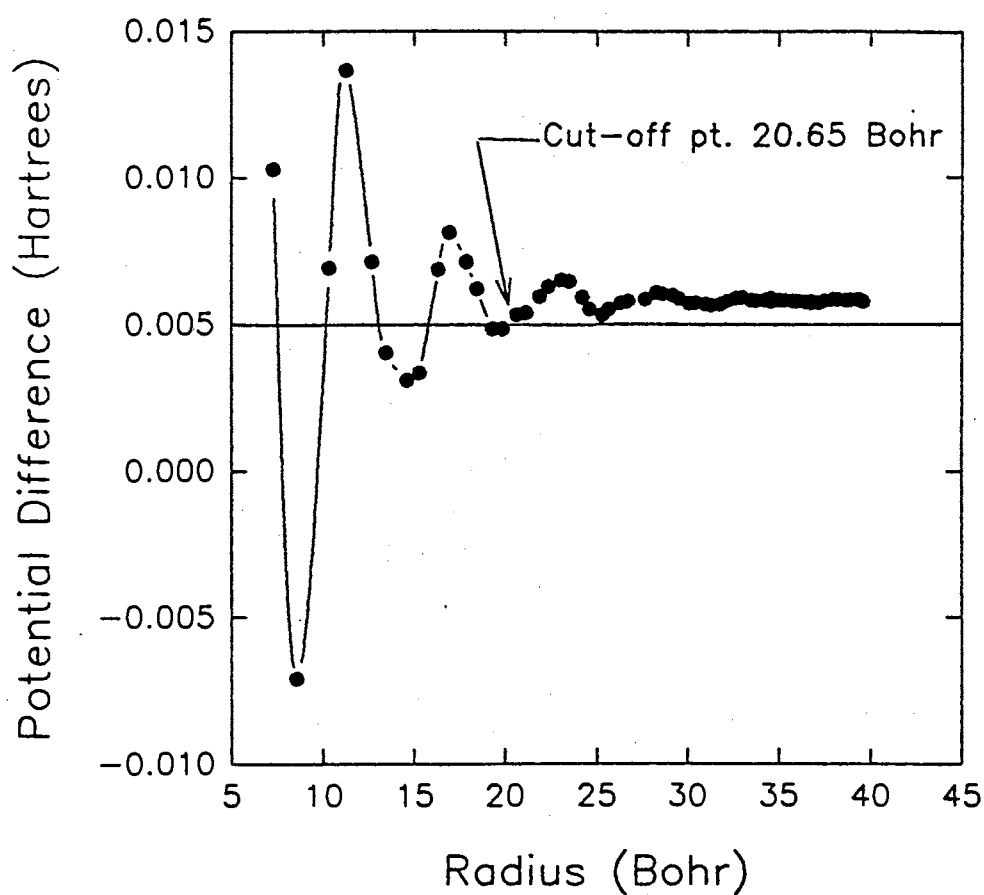
Figure 13. The electrostatic potential difference between the central Mn-site and a F-site, $\phi'_{Mn}(R) - \phi'_F(R)$, as a function of the radius of the external point ion arrangement, R, from the central Mn ion. As shown in the figure the arrangement actually used for SCF calculations consisted of those external point ions less than 20.65 Bohr from the central Mn-site.

The UHF wave functions for both the ground $^6A_{1g}$ and first excited state, $^4T_{1g}$, were then improved upon by utilizing the correlated methods of MP2, MP4, CISD and MCSCF. The results are given in the next section.

In particular, the MCSCF method was used to calculate the excited state energies within the spin 3/2 manifold of states. The choice of the proper active space for MCSCF is of utmost importance. For these calculations, the active space was chosen so that all orbitals in the active space correspond to the N-electron problem. This was done in the following fashion. The method of MCSCF as implemented by *Gaussian 92*[19] is a spin-restricted procedure. Therefore a restricted open-shell Hartree-Fock (ROHF) calculation of the ground state is first performed. This state is spin 5/2 with all five $3d$ electrons spin aligned. Choosing the active space to be these five spin-restricted $3d$ molecular orbitals (MO) and flipping one spin so as to produce the spin 3/2 first excited state, the active space now consists of five electrons and five MO's except that now one MO is doubly occupied and one MO is empty. Since the empty MO was obtained from the spin 5/2 calculation, it still corresponds to the N-electron problem and is therefore, strictly speaking not a virtual MO. The complete active space expansion produces 24 distinguishable determinants with which to represent the spin 3/2 states. The results of the MCSCF calculations are presented in the next section.

Results

In Table IX we present a summary of the ground state to first excited state transition energies obtained experimentally and from the various quantum chemical methods. One point to note is that at the UHF level of theory, the calculated transition energy both with and without the external field differ by only 0.05 eV. As we will point out later, this difference is slightly higher than the resolution obtainable in these calculations from the MCSCF technique for the excited states. We may conclude, therefore, that as far as the transition energies are concerned, the effect of the external field is quite small. This observation is consistent with studies of Mn centers in other hosts such as ZnS by Richardsen *et. al.* [41]. As

further evidence, Fig. 14 shows the percent change in the electron density about the quantum cluster arising due to the effect of the external field. The percent change is calculated by $[(\rho_{ext}(\mathbf{r}) - \rho(\mathbf{r}))/\rho_{ext}(\mathbf{r})] \times 100$, where $\rho_{ext}(\mathbf{r})$ is the electronic charge density in the presence of the external field. Figure 14(a) shows the percent change in the F plane of the cluster and Fig. 14(b) shows the same in the Ca plane. The location of the Mn ion and a F ion are indicated in the figures. Figure 14(a) also includes the presence of a +2 external point ion. In Fig. 14(b) the indicated location of the F ion is actually the location of its projection onto the Ca plane. Both figures show that within the confines of the quantum cluster, the percent change in the electron charge density arising from the introduction of the external point ion field is no more than approximately 1%. Since the excited states are due to d-to-d transitions and since the d-orbitals are rather localized about the Mn ion, one expects the presence of the external field to have little effect. Therefore, having introduced an external field and finding its effects to be negligible for transition energies, we may now proceed without the external field for further calculations.

The remaining results in Table IX were calculated without an external field. While the CISD method yields the best transition energy, it is still 0.59 eV above

TABLE IX.

VALUES OF THE TRANSITION ENERGY
FROM THE GROUND STATE $^{6}A_{1g}$
TO THE FIRST EXCITED
STATE $^{4}T_{1g}$

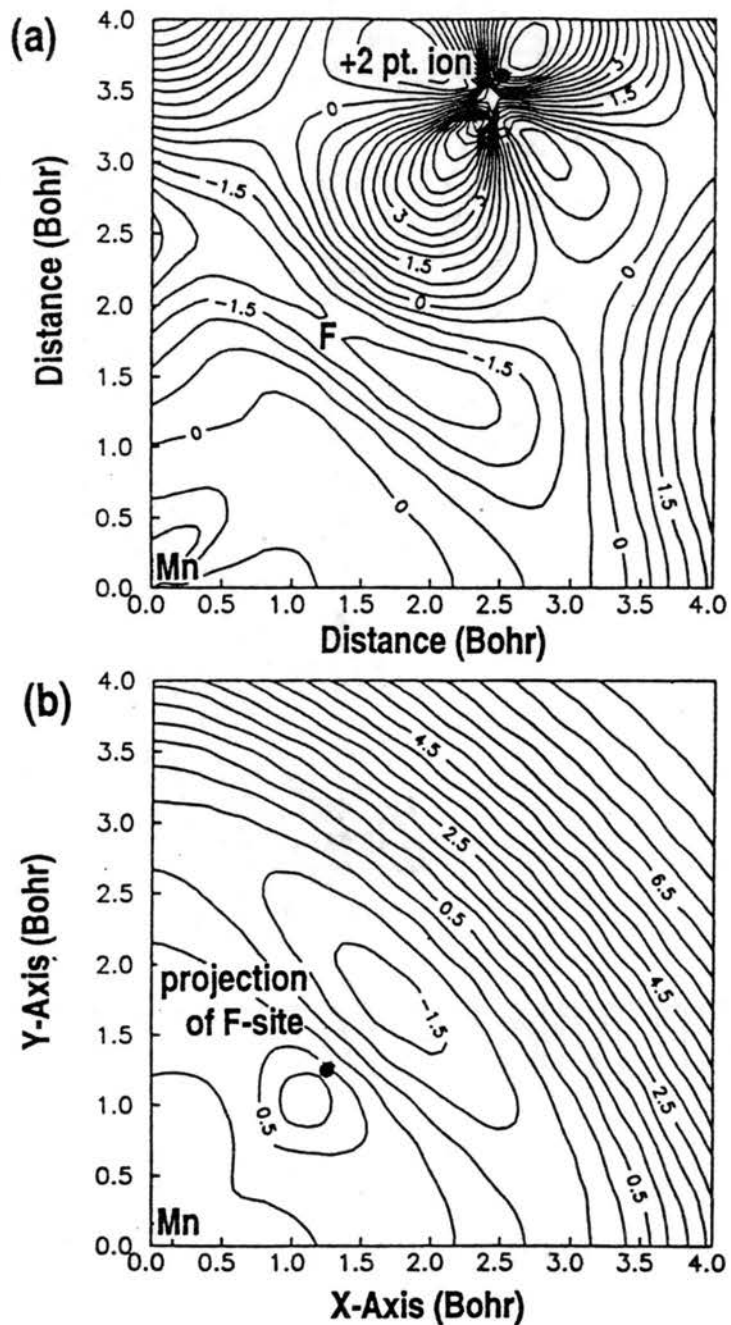| Method	$^{6}A_{1g} \rightarrow {}^{4}T_{1g}$ (eV)
Experimental	2.81
UHF (with ext. field)	3.71
UHF	3.76
MP2	3.53
MP4	3.49
CISD	3.40
MCSCF	3.52

Figure 14. The percent change in the electronic charge density in (a) the F-plane and (b) the Ca-plane of the quantum cluster. Both figures show that within the confines of the quantum cluster the percent change in the electronic charge density arising from the introduction of the external point ion field is no more than approximately 1%.

the experimental value. An error of this magnitude for d-to-d transitions in Mn-related defects is quite common. Richardsen *et. al.* for instance, report a UHF error of 1.6 eV for the ground to first excited state transition for Mn defects in ZnS which they associate primarily with intra-atomic correlation effects[41]. For the Mn in CaF_2, we see that the UHF error is 0.95 eV. Thus, the CISD method has accounted for approximately 0.36 eV of the missing correlation energy with the present basis. Since the main part of the correlation effects are accounted for at the MP4 and CISD level of theory for sufficently large basis sets[33], the likely explanation is that the 0.59 eV CISD error is mostly basis set related. A final observation from Table IX is that the MCSCF technique is at the same as MP2 as far as correlation is concerned.

In Fig. 8 we show the optical absorption data by McKeever *et. al.* [10]. Their experimental values are presented in Table X as column four. The assigned term designations were made by them based on a ligand field analysis from fitting to the $3d^5$ Tanabe-Sugano diagram for an ion in the presence of a point ion field of O_h (six-coordinated) symmetry. This resulted in a Dq value of 420 cm^{-1} for the

TABLE X.

SUMMARY OF THE TRANSITION ENERGIES FROM THE
GROUND STATE $^6A_{1g}$ ROHF ENERGY
OBTAINED BY MCSCF

State	Energy (eV)	After rigid shift of -0.647 eV	Experimental (eV)
$^4T_{1g}(^4G)$	3.54 ± 0.02	2.89 ± 0.02	2.81
$^4T_{2g}(^4G)$	3.75 ± 0.01	3.10 ± 0.01	3.10
$^4E_g(^4G)\ [^4A_{1g}]^*$	3.78 ± 0.01	3.13 ± 0.01	3.14
$^4A_{1g}(^4G)\ [^4E_g]^*$	3.81	3.16	3.16
$^4T_{2g}(^4D)$	4.59 ± 0.01	3.94 ± 0.01	3.70
$^4E_g(^4D)$	4.64 ± 0.03	3.99 ± 0.03	3.87
$^4T_{1g}(^4P)$	4.72 ± 0.03	4.07 ± 0.03	4.20
$^4A_{2g}(^4F)$	6.25	5.60	5.17
$^4T_{1g}(^4F)$	6.39 ± 0.03	5.74 ± 0.03	5.17
$^4T_{2g}(^4F)$	6.49 ± 0.02	5.84 ± 0.02	5.30

*assignments made by McKeever *et. al.* [10].

crystal field splitting parameter[10]. As discussed in Chapter II, we have reworked the Tanabe-Sugano diagram for a $3d^5$ eight-coordinated O_h system and presented the results as Fig. 9. The dashed line shows the Dq value that gives the best fit to the new diagram using the experimental data of column four of Table X. This results in a new Dq value of 570 cm^{-1}.

Table X shows the results of MCSCF calculations. The second column gives the transition energies from the ground state calculated at the ROHF level of theory to the excited states calculated at the MCSCF level of theory. The error values given indicate the spread in energy of the partners to the irreducible representations of the O_h group indicated in column one. The energy given in column two is taken as the average energy of these partners. From Fig. 8 we observe that experimentally some energies are known better than others. Since the peak designated $^4A_{1g}(^4G)$ is the sharpest and hence provides the most precise experimental energy, the calculated values are rigidly shifted by -0.647 eV to match the experimental $^4A_{1g}(^4G)$ level. These results are given in column three. Figure 15 shows graphically the calculated values of column three and experimental values of column four.

Discussion

There are essentially two ways to obtain the electronic excited states of defects involving transition metal ions in crystals. One is the method of ligand fields developed in a series of papers by Tanabe and Sugano[22] and Orgel[23]. Later several books and review articles appeared in the literature most notably by Tanabe and Sugano[20] and Schläfer and Gliemann[24]. These researchers discussed the splitting in the free ion terms of $3d$ ions for ligand fields with various symmetries. Essentially the ligand field approach centers around treating the d electrons of a central ion through a screened interaction with the otherwise closed shells. The d electrons then interact via perturbation theory with a point ion external field produced by the nearest neighbor ions (or "ligands"). This interaction results in
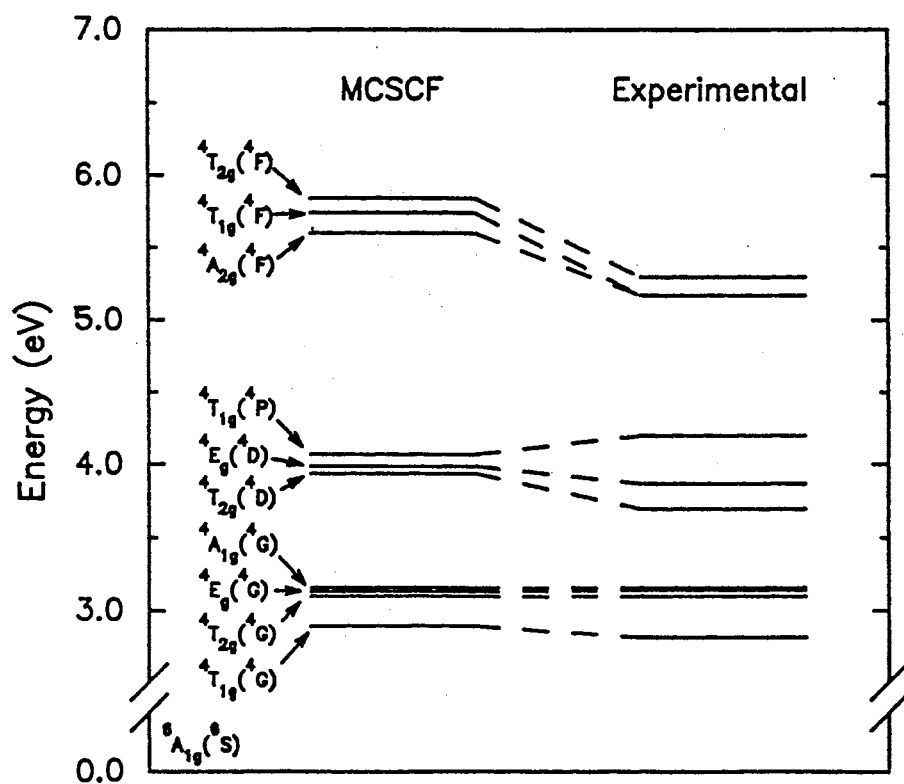
Figure 15. Graphical representation of the MCSCF results presented in Table X
for the $(MnF_8)^{6-}$ cluster after the -0.647 eV rigid shift. The exper-
imental results are from McKeever *et. al.* [10].

a splitting of the free ion terms into multiplets identified by the irreducible representations of the symmetry group of the cluster (in this case O_h). This method has enjoyed considerable success when applied to ionic crystals, however, its limitation is manifest when one begins to consider more complicated systems, such as an impurity ion adjacent to an F-center in CaF_2. For instance, if a Mn^{2+} ion enters substitutionally for Ca^{2+} and is adjacent to a vacancy in which an electron is trapped. The -1 charge of the electron in the vacancy behaves in the ligand field point ion approximation exactly as another F^- ion surrounding the Mn impurity. Therefore, ligand field theory would treat this system in the same way as it would treat the Mn impurity surrounded by the eight nearest neighbor F^- ions in CaF_2.

Clearly then, for these more complicated systems a more general quantum chemical method must be employed. Since large scale CI calculations are impractical for systems of this size, the only practical alternative is the complete active space multiconfigurational SCF method. It is then the intent of this work to demonstrate that the MCSCF technique produces reliable transition energies that are in good agreement with experiment. The active space chosen to calculate the excited states for the $[MnF_8]^{-6}$ cluster within the spin 3/2 manifold of states consists of the Mn d-like molecular orbitals. In all, this produced 24 configurations. The MCSCF technique then starts with the ROHF orbitals, diagonalizes the CI matrix consisting of the 24 configurations and produces the CI expansion coefficients and eigenvalues. Then, with the wave function represented by this truncated CI expansion, the orbitals are then varied so as to minimize the desired eigenvalue. With the new orbitals, the CI matrix is diagonalized again and the process is repeated until the desired eigenvalue converges. Since at every step of the way the CI eigenvalues are rigorous upper bounds to the excited state energy[36], by choosing to optimize the orbitals for one of the excited CI eigenvalues, one obtains the best possible excited state energy for the given active space.

Table X shows the results of successively incrementing the optimized eigenvalue for each MCSCF calculation. Figure 15 shows the same results graphically. With regard to these results there two important points. First, it was found that

the MCSCF method does a much better job predicting the *relative* spacing of the energy levels within a given spin manifold. Column 2 in Table X gives the energies of the spin 3/2 states with respect to the spin 5/2 ground state. By comparing these values with the experimental results in this table, we see that they depart from the experimental values by on the average of about 1eV. By performing a rigid shift of -0.647 eV to match the experimental $^4A_{1g}(^4G)$ level the agreement as shown in Fig. 15 is much better. The main reason for this, we believe, is that within an MCSCF approach, the $^6A_{1g}(^6S)$ level can only be treated at the ROHF level of theory. Since this level is spin 5/2 with all five spins aligned, constructing the active space from the Mn d-like molecular orbitals produces only one possible configuration. This means that if the spin 3/2 and spin 5/2 levels are to be treated at the same level of theory (as they must for purposes of comparison) the $^6A_{1g}(^6S)$ is represented by a single determinantal wave function while the quartet levels are represented by a multideterminantal wave function consisting of 24 determinants. Since the $^6A_{1g}(^6S)$ state has all five spins aligned and since in Hartree-Fock theory electrons with parallel spins are correlated, the single determinantal wave function for the $^6A_{1g}(^6S)$ state includes more of the exchange correlation energy than does the 24 determinantal wave function of the spin 3/2 states. This, however, is only part of the story, in fact, this effect accounts for only approximately 0.12 eV of the 0.647 eV rigid shift. From Table IX we show the $^6A_{1g} \rightarrow {}^4T_{1g}$ transition energies for the different levels of theory. We observe that the best calculated value is obtained from a large configuration interaction calculation involving all non-core single and double substitutions (CISD). The CISD calculations therefore include essentially all the correlation energy obtainable from the basis set employed in this study. The CISD result is 0.12 eV below the MCSCF result but is still approximately 0.59 eV above the experimental result. Based on the fact that CISD is a highly correlated method, we believe then that 0.59 eV of the 0.647 eV rigid shift is primarily associated with the basis set. That is, if the basis set were enlarged then the CISD could account for more of the missing 0.59 eV correlation energy.

The second point is that as one moves up in energy the calculated results begin to depart further and further from the experimental values. As one tries to calculate excited states with higher and higher energies the finite size of the active space becomes more and more relevant. This is because the higher roots, while rigorous upper bounds, are also orthogonal to the lower roots as determined using the same basis as that obtained by the MCSCF procedure for the optimized root. This, therefore, introduces an additional error into the result that increases as higher roots are optimized. The solution that could be consistently applied to all the states would be to increase the size of the active space to include some F s- and p-like molecular orbitals and the virtual Mn $3d$ MOs and then re-calculate the states. However, we found that increasing the active space for this system would be computationally unfeasible.

Another point concerns degeneracies and term assignments. As one moves up in energy with successive MCSCF calculations, one observes the clustering of the levels into the two- and three-fold degeneracies of the various ^4E_g, $^4T_{1g}$ and $^4T_{2g}$ terms. Because of the finite basis set and the fact that the O_h symmetry of the Mn impurity must be relaxed in the MCSCF calculations, these degeneracies will be broken. The errors shown in Table X indicate this spread in energy. Based upon the results of ligand field theory and the groupings of the levels calculated by the MCSCF technique, we where able to make the term assignments in column 1 of Table X.

According to ligand field theory, we see from Fig. 9 that the $^4E_g(^4G)$ and $^4A_{1g}(^4G)$ terms remain degenerate under variations in the crystal field splitting parameter Dq. Experimentally, of course one will observe a small separation in these terms. From Fig. 8 we observe that McKeever $et.$ $al.$ [10] assigns $^4A_{1g}(^4G)$ to be the lower energy of these two terms. From the grouping of the MCSCF energy levels, however, we find that $^4E_g(^4G)$ is the lower in energy of the two terms. Consequently, based on our MCSCF calculations we reverse the term assignments of these two levels relative to the published assignments[10]. As one moves beyond ligand field theory the $^4A_{1g}(^4G)$ and $^4E_g(^4G)$ terms will split. For instance, Ng

and Newman[42] examine a spin-correlated crystal field model designed to include covalency effects. They found that this model places the ^4E_g level below the ^4A_g level. In addition, Ferguson, Krausz, and Guggenheim[43], using magnetic circular dichroism measurements found that in $KMgF_3$:Mn^{2+}, the ^4E_g level lies approximately 90 cm^{-1} below the ^4A_g level. Thus MCSCF predicts the proper ordering of these levels.

The $(MnCa_3F_6Vac)^{+1}$ Cluster

Cluster geometry, basis set and external field

The Mn-perturbed F-center has been proposed as a model for the defect largely responsible for the absorption spectrum from CaF_2:Mn (3%) following irradiation[10]. While the model envisioned by McKeever $et.$ $al.$ [10] consists of an F-center perturbed by two Mn ions as shown in Fig. 1, we believe that a double Mn-perturbed F-center cluster may not be necessary to explain the observed absorption spectra. There are essentially two reasons for this. First, optical spectra on Mn^{2+} in MnF_2 by Finlayson $et.$ $al.$ [44], in $KMnF_3$ and $KMgF_3$:Mn by Sibley $et.$ $al.$ [45] and in $NaMnF_3$ by Srivastava $et.$ $al.$ [46] show, to within a scaling factor, very similar Mn absorption structure. Therefore, since Mn absorption appears to be largely independent of the host and thus of the nature of the immediate surroundings of the Mn ion, this implies that the Mn related absorption would not change radically if the immediate surroundings consisted of another Mn ion. Second, given the photon density involved in absorption measurements, it is statistically unlikely that two adjacent Mn atoms would be simultaneously excited. Note that we are not claiming that double Mn F-centers don't exist (in fact they probably do exist at 3% concentration), we are merely asserting that within this cluster only one Mn ion is excited at a time and that the presence of the other Mn ion serves to provide only a perturbation to the system. From this reasoning, we believe that the general features of Mn absorption in irradiatied CaF_2:Mn can be explained in terms of a single Mn F-center cluster.

The analysis of the $(MnCa_3F_6Vac)^{+1}$ cluster started with an analysis of the non-defective cluster shown in Fig. 10. As described in Chapter IV and shown in Table VII, the non-defective cluster is stabilized in the presence of an external field of point Gaussians. The F-center is then created by the removal of the central F^- ion and the addition of an electron to the system. The cluster is then relaxed as shown in Table VIII to stabilize the geometry. Next, one of the nearest-neighbor Ca^{2+} ions is replaced by a Mn^{2+} to form the Mn-perturbed F-center. Figure 16 shows the final geometry used for the following calculations. It is to be noted that upon introducing a Mn in place of one of the Ca ions the cluster was not relaxed further, therefore, in Fig. 16 the vacancy-F distance is 2.70 Å and the vacancy-Mn(Ca) distance is 2.29 Å. In addition, the external point Gaussian arrangement was maintained to be that which stabilized the non-defective cluster utilizing the parameters at the bottom of Table VII.

The basis set for this cluster is the same as for the non-defect cluster for the F^- and Ca^{2+} ions in Chapter IV. The basis set for the Mn^{2+} ion was taken from the $(MnF_8)^{-6}$ cluster. To model an electron in the vacancy requires the placement of basis functions in a region of space for which no nuclear core exists. Within the *Gaussian 92*[19] set of programs this is accomplished by the use of a "ghost atom" at the origin. A ghost atom is merely a nuclear site with zero charge about which basis functions may be located. Ghost atoms may be located anywhere and have seen use in the description of covalency for molecular calculations where their placement between atoms allows for the placement of basis functions centered between the bonding atoms. This in turn allows for the possibility of charge build-up between the atoms and the formation of a covalent bond. They are also useful for the calculation electrostatic quantities at locations other than at the nuclear sites within the quantum cluster. For our purpose, the ghost atom and associated basis functions will be used to model the electronic charge distribution within the vacancy.

Figure 17 shows the atomic basis functions used for the vacancy. The atomic basis functions were chosen to physically occupy most of the vacancy region with
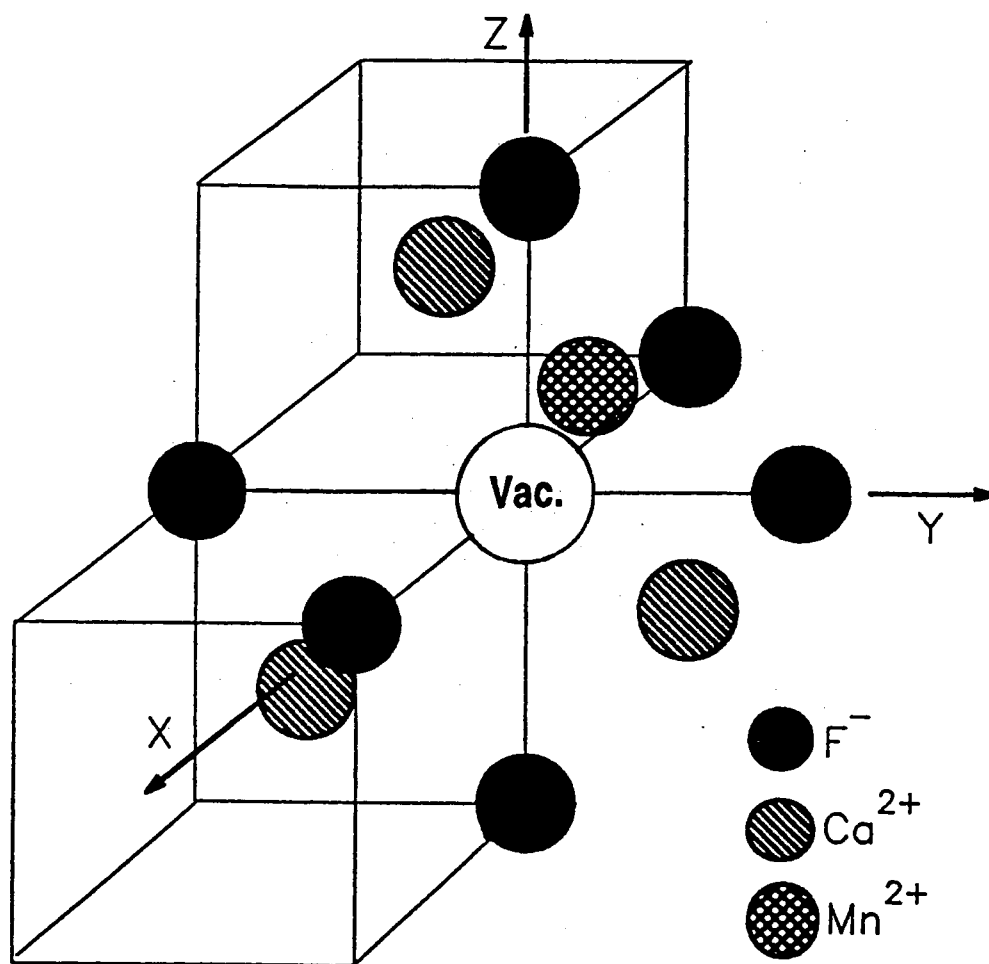
Figure 16.   Cluster geometry representing the Mn-perturbed F-center, $(MnCa_3F_6Vac)^{+1}$. The vacancy-F distance is 2.70 Åand the vacancy-Mn(Ca) distance is 2.29 Å. Surrounding this cluster is an arrangement of point Gaussians utilizing the parameters at the bottom of Table VII.

four s-type and two p-type uncontracted Gaussian functions centered at the origin. All the vacancy atomic basis functions have a scaling factor of one and the Gaussian exponents are shown in the figure.

Calculations

The Mn-perturbed F-center defect shown in Fig. 16 has an overall charge of $+1$. Each F^- has closed $2p$ shells and each Ca^{2+} has closed $3p$ shells. The Mn^{2+} has a $3d^5$ configuration outside closed shells and, in addition, there is a single electron which in the lowest energy configuration resides in an s-like state within the vacancy.

There are two spin configurations we must consider. One configuration consists of the five Mn $3d^5$ electrons spin aligned. With the vacancy electron parallel to these electrons, the total spin is 6/2. Only the ground state of 6/2 spin will be important in these calculations. The reason for this is that to construct a state with 6/2 spin other than the ground state would require transferring an electron from a nearby Ca^{2+} ion or the excitation of the F-center. The excited Ca electron would pair with either the vacancy electron or with one of the Mn $3d$ electrons. The remaining unpaired electron on one of the Ca^{2+} ions would give it a net spin of 1/2 but the total spin of the entire cluster would still be 6/2. Since excited states of spin 6/2 involving the Ca ions necessarily requires a charge transfer, the energies of these states would be well above the energy range required to explain the observed spectra.

The next spin configuration is spin 4/2. The ground state of this spin consists of all five Mn $3d^5$ electrons spin aligned with the vacancy electron anti-parallel to these. This configuration produces the ground state of this spin since each electron occupies a different spatial orbital and hence the Coulomb repulsion is minimized. There will exist a whole manifold of states of spin 4/2. These states will consist of linear combinations of determinants representing different occupancies of the five d-like and vacancy molecular orbitals. For instance, an excited state may consist of doubly occupying the lowest d-like MO, leaving the highest d-like MO empty
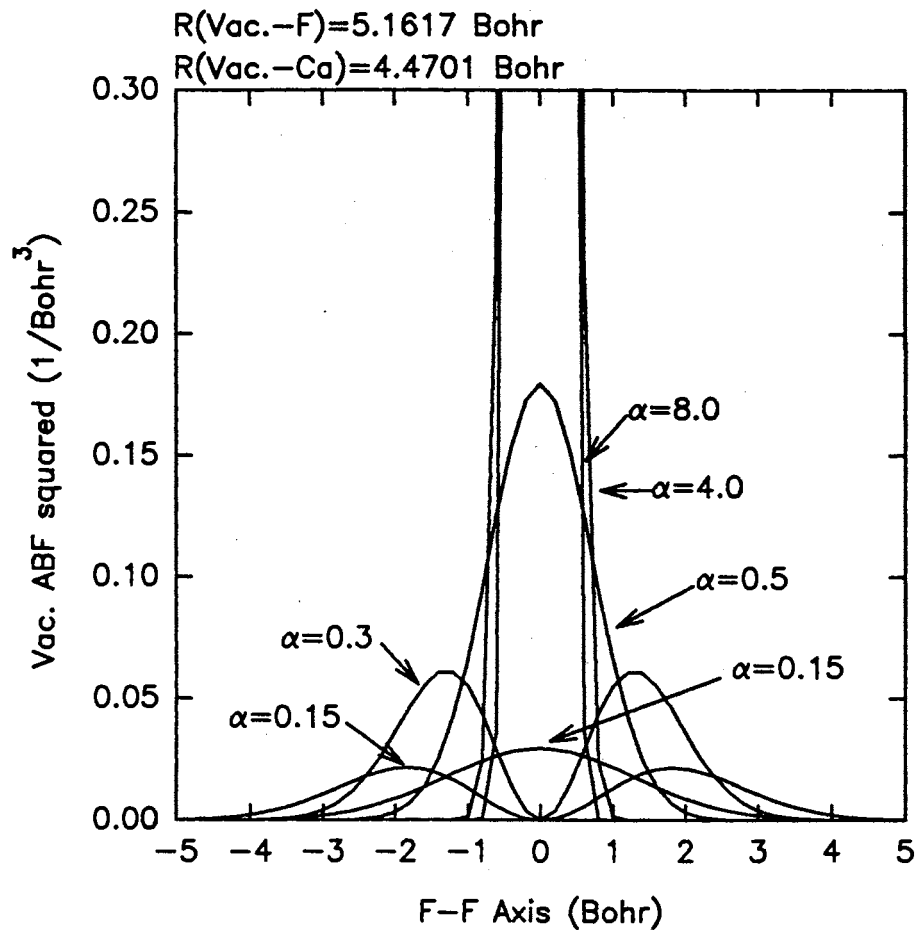
Figure 17. Plot of the atomic basis functions used to model the charge distribution within the vacancy. The vacancy region consists of four s-type and two p-type uncontracted Gaussian functions centered at the origin.

and aligning the spin in the vacancy with the majority spin thus producing an overall 4/2 spin state. The reason this configuration would be higher in energy is that since a d MO is doubly occupied, the Coulomb repulsion would be greater. Thus, the excited configurations are produced by doubly occupying the different d-like and vacancy MOs while keeping an overall spin 4/2. The states themselves will consist of linear combinations of these different configurations. It is possible to identify three types of excited configurations within the spin 4/2 manifold.

The lowest energy excited configurations consist of s and p admixture within the vacancy. From Fig. 17 we see that the region within the vacancy is spanned by s- and p-type atomic basis functions. In the ground state the vacancy electron will be represented primarily by an s-type MO and be anti-parallel to the Mn $3d^5$ electrons. A configuration with slightly higher energy would consist of a promotion of the vacancy electron without change of spin into a state where the Mn $3d^5$ electrons are essentially unchanged and the vacancy electron is described by a MO with a definite p-like character. Since this transition is localized within the vacancy, it will be known as the *F-center transition*. A transition of this sort was postulated by McKeever *et. al.* [10] to be responsible for the low energy 540 nm absorption peak observed in irradiated CaF_2:Mn.

The next type of excited configurations consist of the various double occupancies of the Mn $3d$ molecular orbitals. With one of the $3d$ MOs doubly occupied, the spin of the vacancy electron would have to be aligned with the majority spin so that the overall spin is 4/2. These configurations will be collectively referred to as the *d-to-d transitions.*

The final type and most energetic of the spin 4/2 configurations consist of an electron transfer either out of the vacancy to form a $3d^6$ configuration or an electron transfer into the vacancy to form a $3d^4$ Vac^2 configuration. The energy required to transfer an electron either into or out of the vacancy is expected to be such that absorption peaks arising from this process are not likely to occur in the visible region as measured by McKeever *et. al.* [10]. These are referred to as *charge transfer transitions* and will generally not be considered in this analysis.

The method of MCSCF will provide the mechanism by which states constructed from the excited configurations within the spin 4/2 manifold may be calculated. By choosing the active space to consist of the five d-like MOs and vacancy MO, the MCSCF method then is to construct the trial wave function from all possible configurations of spin 4/2 within this space. The orbitals and expansion coefficients within this truncated CI expansion are then varied within an SCF iterative procedure to minimize either the lowest root or any desired higher root.

The calculation sequence proceeds in much the same way as in the $(MnF_8)^{6+}$ cluster. UHF calculations are performed for the spin 6/2 and 4/2 ground states. These are improved further by the incorporation of electron correlation at the MP2 level of theory. CISD calculations were found to be computationally unfeasible for this cluster given the available computer resources. To form the active space for the MCSCF calculations, ROHF results were first obtained for the spin 6/2 ground state. In this way all six orbitals are singly occupied. The spin in the vacancy is flipped to form the spin 4/2 ground state and the active space is chosen to consist of these six molecular orbitals. The truncated CI expansion is then formed from distributing the six electrons over these six orbitals. As stated earlier this method of choosing the active space insures that all the molecular orbitals in the active space correspond to an N electron problem. Repeated MCSCF calculations each time incrementing the root to be optimized produces the energy spectrum. It must be pointed out that this particular choice of the active space–five d-like MOs and one s-like vacancy MO–means that only d-to-d transitions can be calculated. To calculate F-center transitions one must include in the active space a p-like vacancy MO. The results of the MCSCF calculations for both active spaces as well as the UHF, MP2 and ROHF results are presented in the next section.

Results

The calculations began with UHF results obtained for the ground states of 6/2 and 4/2 spin. At the UHF level of theory it was found that the 6/2 ground state lies 0.11 eV *above* the 4/2 ground state. To test this unexpected ordering

of levels, MP2 calculations were performed to see if this ordering holds up when correlation is brought in. The MP2 results for the spin 6/2 and 4/2 ground states show the 6/2 state lies 0.17 eV above the 4/2 state. Thus the MP2 calculations show the same ordering with a slight increase in the separation when correlation is included. This particular ordering of the ground states (i. e. spin 4/2 below spin 6/2), will be important in the description of the irradiated CaF_2:Mn absorption spectra.

After a spin 6/2 ROHF calculation to set up the active space, a series of MCSCF calculations were performed within the 4/2 spin manifold. Table XI shows the transition energies from the spin 4/2 ground state to the excited states of the same spin calculated by the method of MCSCF. All of these excited states are due to d-to-d transitions. Also, since the same basis set is being used in this analysis as was used for the Mn ion within the $(MnF_8)^{6+}$ cluster, we may use the same correction factor of -0.647 eV. Column three shows the results of this rigid shift and column four shows these energies in terms of wavelength. In Fig. 18 we show the observed absorption spectrum by McKeever *et. al.* [10] of CaF_2:Mn(3%) recorded at 77K after irradiation at room temperature. The calculated levels in column three of Table XI are indicated by the lines in the figure.

Unlike the isolated Mn impurity one cannot identify the spectra peaks or energy levels by irreducible representations of the O_h group. In fact, the symmetry of the Mn-perturbed F-center cluster is C_{3v} which consists of the A_1, A_2 and E irreducible representations. One should therefore observe at most 2-fold degeneracies in the calculated MCSCF energy spectrum. While *Gaussian 92* has routines that can determine the symmetry of a given state once it is calculated, these routines are unable to determine the symmetry of a state in the presence of ghost atoms. As a consequence, group theory will play only a limited role in the analysis of this cluster.
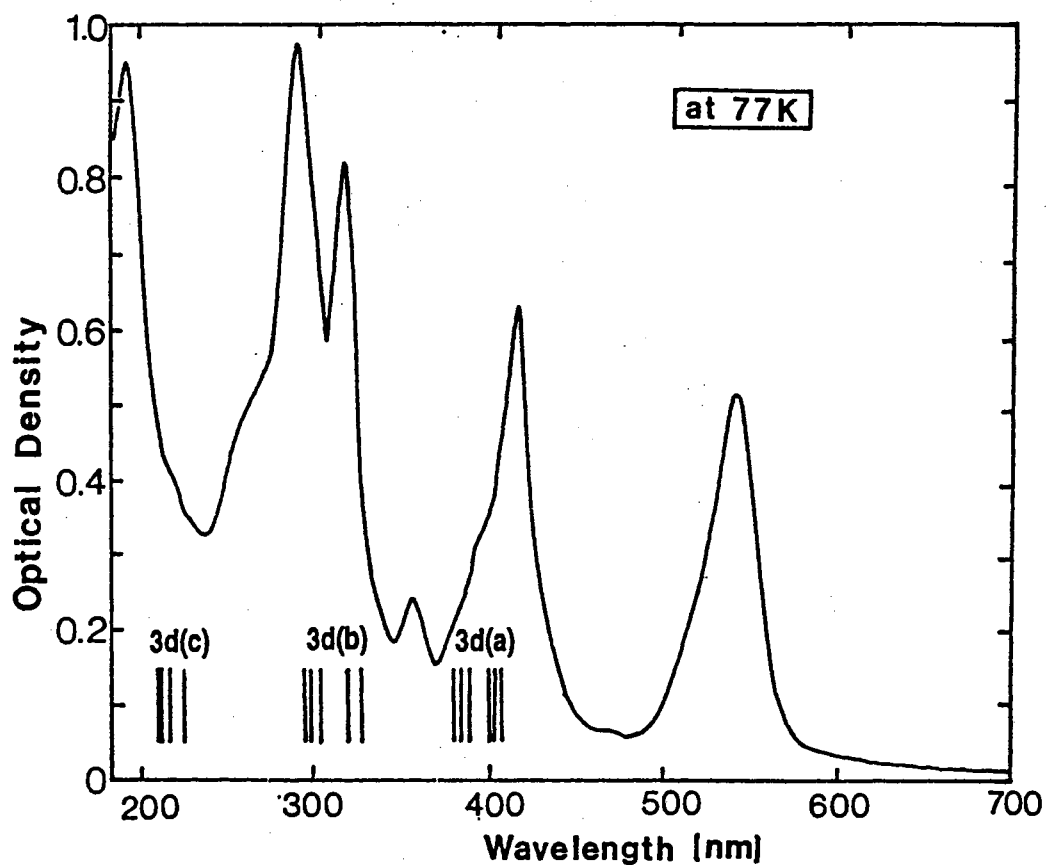
Figure 18. Optical absorption of CaF_2:Mn (3%) recorded at 77 K following 367-Gy gamma irradiation at room temperature. The lines indicate the calculated d-to-d transitions for the Mn-perturbed F-center cluster. (McKeever et. al. [10])

Discussion

In this final section we return to the original problem posed in the introduction of this thesis. We wish to explain, as far as possible, the optical absorption spectra of CaF_2:Mn following irradiation at room temperature. It should be noted that the spectrum presented in Fig. 18 cannot be obtained when the sample is irradiated at 77 K[10]. Instead McKeever et. al. observe this spectrum only after irradiation at room temperature. Based on this observation they conclude that defect migration and clustering is a necessary condition to form the defect complex or complexes responsible for the observed absorption structure in Fig. 18. A second observation is that relative to the spectrum for unirradiated samples (Fig. 8), the spectrum for irradiated samples (Fig. 18) is not only completely different in peak shapes and locations but also enhanced by over two-orders of magnitude. A final important observation of McKeever et. al. [10] involves the appearance of a peak at approximately 540 nm in Fig. 18 and its thermal quenching behavior. By measuring the absorption spectra after irradiation at room temperature at various temperatures from 77 K to above room temperature they observed the transformation from the spectrum in Fig. 18 to the spectrum in Fig. 8. This transformation, however, is not continuous but occurs abruptly at approximately 250 °C. The important point is that the 540 nm peak quenches at the same temperature as the other higher energy peaks. This indicates that the 540 nm and the other peaks are all due to the same defect. In addition, this decay step is related to the production of TL with an emission at 495 nm[10]. Since this is the same wavelength observed in photoluminescence studies before irradiation and has already been confirmed to be due to the first excited state to ground state transition in Mn^{2+}[11], the 540 nm peak cannot be due to Mn^{2+} absorption. Since the 540 nm peak and the other higher energy peaks are due to the same defect, this would imply that these other peaks could not be due to Mn^{2+} absorption either[10].

To reconcile these observations, McKeever et. al. suggest a model consisting of Mn-vacancy centers. In this model they propose that the 540 nm absorption

peak may be due to transitions within the Mn-perturbed vacancy while the other higher energy peaks are more closely related to the vacancy-perturbed Mn, that is, vacancy-perturbed Mn d-to-d transitions. Actually they propose a complex consisting of a vacancy perturbed by two Mn^{2+} ions as shown in Fig. 1, however, in this thesis we will try to explain the experimental observations based on the simpler single Mn^{2+} vacancy model shown in Fig. 16.

We begin our explanation by referring to the diagram in Fig. 19. and the data and levels presented in Fig. 18. The MCSCF calculation for the d-to-d transitions uses a 35 configurational wave function*. The calculated energy levels seem to fall into three groups which are labeled 3d(a), 3d(b) and 3d(c) in Figs. 18 and 19. The locations of groups 3d(a) and 3d(b) correspond to the absorption peak groups around 400 nm and 300 nm indicating that these peaks are in large part due to d-to-d transitions. The group 3d(c) does not seem to line up with a clear peak structure. Since the higher levels calculated from MCSCF tend to have greater errors than the lower levels and since this error will always be too high we suspect that the 3d(c) levels may be responsible for the "hump" at around 260 nm (see for example Fig. 15 for the $(MnF_8)^{6+}$ cluster). The 3d(c) group certainly should not be responsible for the peak at 200 nm since all MCSCF results correspond to upper bounds.

In Fig. 19 we show graphically the levels from Table XI. The levels are with respect to the spin 4/2 ground state of configuration $(3d\alpha)^5(s\beta)^1$ where $(s\beta)^1$ indicates that the electron in the vacancy has β spin (spin down) and occupies an s-like MO. Next comes the ground state of 6/2 spin. Following this comes the d-to-d transitions 3d(a), 3d(b) and 3d(c). These levels correspond to the various excitations within the Mn 3d manifold with configurations of the form $(3d\alpha)^4(3d\beta)^1(s\alpha)^1$ with an overall spin 4/2. The fact that the ground state was found to be spin 4/2 is important in explaining the large increase in the absorption spectrum after irradiation. Not only are the transitions now parity allowed because

---

*this is the number of ways of arranging six electrons over six orbitals such that the total spin is 4/2

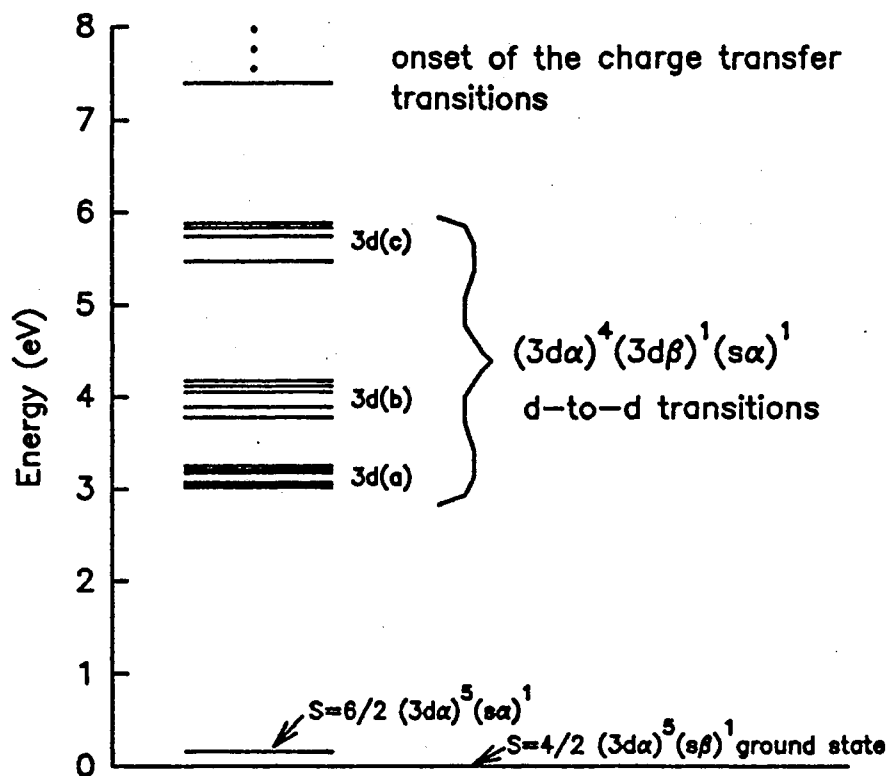Figure 19. Energy diagram showing the results of MCSCF calculations for the
(MnCa$_3$F$_6$Vac)$^{+1}$ cluster. The levels are with respect to the spin 4/2
ground state of configuration $(3d\alpha)^5(s\beta)^1$. Choosing the active space
to consist of five Mn d-like and one vacancy s-like molecular orbitals,
the d-to-d excited states are represented by a 35 configurational wave
function.

of the reduced symmetry of the cluster, but the transitions into the excited d states are now spin allowed as well. Following the d-to-d transitions comes the beginning of the charge transfer transitions representing configurations of the type $(3d\alpha)^4(s\alpha)^1(s\beta)^1$ or $(3d\alpha)^5(3d\beta)^1$.

As shown in Fig. 18, transitions within the Mn $3d$ manifold does not explain the presence of the peak at 540 nm. We suggest that this peak is due to either transitions from the spin 4/2 ground state to a state dominated by a configuration of the type $(3d\alpha)^5(p\beta)^1$ or by transitions from the spin 6/2 ground state to a state dominated by a configuration of the type $(3d\alpha)^5(p\alpha)^1$. In either case, the MCSCF active space would have to be enlarged to include vacancy p-like MOs. Since the active space presently in use includes only the Mn $3d$ and a vacancy s-like MO, the present MCSCF calculations do not yield results for the F-center transitions.

It must be remembered that the MCSCF states are multiconfigurational and hence one cannot, in general, associate an energy level with a single configuration. However, when certain energy levels are dominated by one or few configurations, then one can talk about a certain configuration giving rise to a particular transition. To explain the separations between the 3d(a), 3d(b) and 3d(c) groups of levels we refer to the diagram represented as Fig. 20. Since the molecular orbitals are the eigenfunctions of the Fock operator, and since the Fock operator has the same symmetry as the Hamiltonian, the eigenfunctions of the Fock operator must form a basis for the various irreducible representations of the symmetry group. In going from the full rotation group to C_{3v} the d orbitals break up into e, a_1, and e in order of increasing energy. p orbitals break up into a_1 and e and s orbitals transform as a_1.

In Fig. 20 we show the dominate configurations representing the various states as determined by MCSCF calculations. The spin 4/2 ground state is shown as having two α electrons in the lower e MO, one α electron in the middle a_1 MO, two α electrons in the highest e MO, and one β electron in the a_1 MO within the vacancy. The next state is dominated by the configuration which is the same as for the spin 4/2 except now the electron in the vacancy a_1 MO has α spin. Next
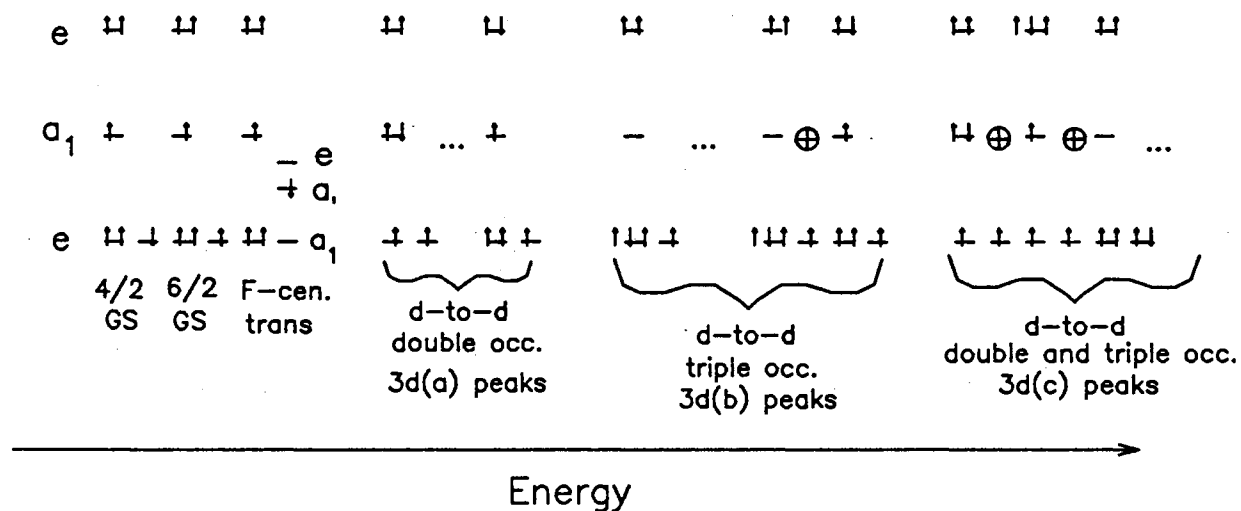
Figure 20. Diagram showing the dominate configurations representing the various states as determined by MCSCF calculations for the $(MnCa_3F_6Vac)^{+1}$ cluster. Indicated are the dominate configurations for the 4/2 ground state, the 6/2 ground state and the proposed excited F-center state. Also shown are the dominate configurations of the starting and ending states of the 3d(a) group, the 3d(b) group and the starting state of the 3d(c) group.

we show the F-center transition which as the same arrangement among the e, a_1 and e MO on the Mn but the electron in the vacancy has now been promoted into the upper a_1 MO in the vacancy.

The first group of d-to-d transitions, 3d(a), are found from the MCSCF calculations to be dominated by double occupancies of the Mn molecular orbitals. In Fig. 20 we show the dominate configuration of the first 3d(a) excited state. All the various permutations of double occupancy are not shown except the last. After a gap in energy the first dominate configuration starting the 3d(b) group is shown. The transitions within the 3d(b) group correspond to mostly triple occupancies with some small admixture of double occupancies. We see some of this mixing in the last 3d(b) level. After another gap the mixing between double and triple occupancies becomes quite strong. This starts the 3d(c) group of states. In the diagram we see the first state of the 3d(c) group is a mixture of single and double occupancies and even some charge transfer configurations. From the calculations we find that the single and double mixing is almost equal in the 3d(c) group. The charge transfer mixing is quite small initially but near the high energy end of this group the charge transfer configuration takes on more and more dominance.

Based on the evidence from these calculations, we find that with the exception of the peak at 540 nm, most of the other peaks can be explained in terms of d-to-d transitions taking place on the Mn ion perturbed by an adjacent vacancy. Thus, the group of peaks near 400 nm and 300 nm can be explained in this way. The small peak at approximately 360 nm is probably not a d-to-d transition. The transition responsible for this peak is unknown. The large peaks starting at approximately 200 nm may be due to the onset of the charge transfer transitions. As far as the origin for the peak at 540 nm, McKeever $et.$ $al.$ [10] are probably correct in saying that it may be due to transitions within the F-center perturbed by the adjacent Mn. The only question remaining is whether it is from the spin 4/2 or spin 6/2 ground state. This question is discussed further in the next chapter.

TABLE XI.

MCSCF TRANSITION ENERGIES FROM THE
S=4/2 GROUND STATE

MCSCF root	Energy (eV)	After rigid shift of -0.647 eV	Wavelenght (nm)
2	3.667	3.021	408
3	3.706	3.059	403
4	3.728	3.081	400
5	3.823	3.176	388
6	3.858	3.212	384
7	3.904	3.257	379
8	4.424	3.778	327
9	4.544	3.897	317
10	4.703	4.056	304
11	4.767	4.120	299
12	4.822	4.175	296
13	6.122	5.475	225
14	6.389	5.742	215
15	6.482	5.835	211
16	8.052	7.405	166

CHAPTER VI

SUMMARY AND CONCLUSIONS

Discussion

The work reported in this thesis is the theoretical/computational component of an overall research effort to understand the optical properties of CaF_2:Mn when subjected to irradiation. In particular, this effort sought to explain the optical absorption spectra in terms of Mn-related defect structures which arise as a result of irradiation. The experimental component of this project made good headway with the measurement of Mn absorption in unirradiated CaF_2 and its analysis within a ligand field theory framework[10]. Also McKeever *et. al.* [10] from the measurement of optical absorption after irradiation was able to propose a model for a defect consisting of an *F*-center adjacent to one or more Mn ions. Since ligand field theory does not lend itself well to the analysis of structures of this symmetry, more advanced quantum chemical methods in the form of molecular orbital calculations were needed to either verify or reject this model. This thesis reports on the results of molecular orbital calculations on Mn-related defect clusters within the Hartree-Fock formalism and its extensions such as configuration interaction, many-body perturbation theory and multiconfigurational self-consistent field.

To model the absorption spectrum before irradiation, calculations were performed on the $(MnF_8)^{6-}$ cluster which was chosen to represent the isolated Mn substitutional impurity in an otherwise perfect crystal. The symmetry of this cluster is eight-coordinated O_h designated $O_h^{(8)}$ to distinguish it from six-coordinated O_h designated $O_h^{(6)}$. Previous ligand field analysis was performed on the basis of $O_h^{(6)}$ symmetry. Therefore, one aspect of this project was to re-work the ligand field analysis for the proper $O_h^{(8)}$ symmetry. The result of this analysis showed a

narrowing of the multiplet terms in energy with respect to the $O_h^{(6)}$ result. As a consequence, the crystal field parameter Dq increased from 420 cm^{-1} to 570 cm^{-1}. Since the energy levels of $O_h^{(8)}$ Mn in CaF$_2$ are well known[10], this cluster also provided a good test cluster for the MCSCF technique. After embedding the (MnF$_8$)$^{-6}$ in an external point ion field designed to reproduce the Madelung potentials within the quantum cluster, a series of MCSCF calculations were performed. The results showed that good agreement with experiment could be obtained only after a rigid shift of the levels by -0.647 eV. While some of this shift could be accounted for by the inclusion of electron correlation energy most of it was attributable to the finite basis set size. Because the same basis set was carried over for use in the Mn-perturbed F-center cluster, this correction value for d-to-d transitions was used to analyze d-to-d transitions in that cluster as well.

Unlike the (MnF$_8$)$^{6-}$ cluster, it was found that the external field played more important role in the Mn-perturbed F-center cluster (MnCa$_3$F$_6$Vac)$^{1+}$. Because of this, a method for embedding the cluster in an external arrangement of charge had to be developed. The method presented in this thesis involves starting from the "non-defective" cluster (Ca$_4$F$_7$)$^{1+}$ then arranging outside this cluster charge represented by Gaussians located at the external lattice sites ("point Gaussians"). Through a series of SCF calculations the charge and Gaussian exponents of the external distribution were varied so as to minimize the forces on the atoms in the quantum cluster. With this done, the F-center defect was created by the removal of the central Ca and the addition of an electron. Without adjusting the external field, the defect cluster was then relaxed. Finally the Mn-perturbed F-center defect cluster is created by the replacement of one of the Ca ions with Mn.

With the cluster embedded in the external field, UHF and MCSCF calculations were performed on the Mn-perturbed F-center cluster (MnCa$_3$F$_6$Vac)$^{1+}$. The results showed that the ground state of the system is spin 4/2 with the lowest spin 6/2 state 0.17 eV above this. The results also show that the excited states of 4/2 spin corresponding to d-to-d transitions can account for the optical absorption

peaks near 400 nm and 300 nm. Transitions involving the removal of an electron from the d-like MOs on the Mn to doubly occupy the vacancy site may be responsible for peak groups starting at approximately 200 nm.

The origin of the peak at approximately 540 nm is still somewhat unresolved. McKeever $et.$ $al.$ [10] proposed that this may be due to transitions within the F-center. In the model presented here, that could correspond to transitions from the spin 4/2 ground state $(3d\alpha)^5(s\beta)^1$ to the excited spin 4/2 state $(3d\alpha)^5(p\beta)^1$. Alternatively, it could correspond to transitions from spin 6/2 ground state $(3d\alpha)^5(s\alpha)^1$ to the excited spin 6/2 state $(3d\alpha)^5(p\alpha)^1$. The alternative–that this peak has nothing to do with Mn–appears to have been ruled out by the experimental work of McKeever $et.$ $al.$ [10]. They observed large variations in this peak under variations in Mn dopant concentration. Also, they observe this peak to quench at the same temperature as the other higher energy Mn-related peaks. Finally, another possibility is that this peak is due to an excited state that is unique to the F-center perturbed by two Mn ions. One argument against the double Mn F-center cluster being significantly different than the single Mn F-center cluster is that since the peaks identified in this thesis are due mainly to d-to-d transitions on a single Mn, the energy required to excite simultaneously both Mn ions to perform d-to-d transitions would be statistically unlikely. A likely scenario is that even in the double Mn cluster only one Mn is excited at a time. Thus, the levels calculated for this thesis would only be perturbed by the presence of the additional Mn. Since the double Mn F-center cluster is not considered in this thesis, this last possibility has yet to be investigated.

Future Work

Future work in this area should center around identifying the origin of the 540 nm peak in the optical absorption spectrum of CaF_2:Mn following irradiation at room temperature. While the single Mn-perturbed F-center cluster has been successful in identifying the majority of peak groups in the spectrum, it would be useful to see if the double Mn-perturbed F-center produces states that also agree

with this spectrum. More importantly, it would be useful to see if this cluster is responsible for the 540 nm peak. Also, there is a peak of unknown origin at approximately 360 nm. This too might be explained in terms of the double Mn cluster.

Another avenue for future work could involve using the point Gaussian method developed for this thesis to obtain the proper relaxed geometry of the isolated Mn cluster $(MnF_8)^{6+}$. For the calculations presented in this thesis, the geometry used was obtained experimentally by Barkyoumb and Mansour[39]. Their results show that when the larger Mn ion replaces the smaller Ca ion the cluster relaxes *inward*. Why or how there is an inward relaxation in this case is still unresolved. Perhaps by the careful modeling of the external field by the point Gaussian method as for *F*-center clusters and by the inclusion of correlation effects into the relaxation calculations, this question could be resolved.

BIBLIOGRAPHY

1. R. J. Ginther and R. D. Kirk, J. Electrochem. Soc. **104**, 365 (1957).

2. J. H. Schulman, F. H. Attix, E. J. West and R. J. Ginther, Rev. Sci. Instrum. **31**, 1263 (1960).

3. J. H. Schulman, *Proceedings of the Symposium on Solid State and Chemcal Radiation and Dosimetry in Medicine and Biology* (IAEA, Vienna, 1967), p. 3.

4. J. H. Schulman, R. J. Ginther, S. G. Gorbics, A. E. Nash, E. J. West and F. H. Attix, Int. J. Appl. Radiat. Isotopes **20**, 523 (1969).

5. A. C. Lucas and B. M. Kapsar, *Health Physics* **27**, 600 (1974).

6. W. Gehlhoff and W. Ulrici, Phys. Status Solidi B **102**, 11 (1980).

7. R. Alcalá, P. J. Alonso, G. Lalinde and A. Carretero, Phys. Status Solidi B: **98**, 315 (1980).

8. P. J. Alonso, V. M. Orera and R. Alcalá, Phys. Status Solidi B: **99**, 585 (1980).

9. D. W. McMasters, B. Jassemnejad and S. W. S. McKeever, J. Phys. D: **20**, 1182 (1987).

10. S. W. S. McKeever, B. Jassemnejad, J. F. Landreth and M. D. Brown, J. Appl. Phys. **60**(3), 1124 (1986).

11. P. J. Alonso and R. Alcalá, J. Lumin. **22**, 321 (1981).

12. J. F. Rhodes, R. J. Abbundi, D. Wayne Cooke, V. K. Mathur and M. D. Brown, Phys. Rev. B: **31**(8), 5393 (1985).

13. S. W. S. McKeever, *Photoluminescence Measurements in CaF_2:Mn*, Naval Surface Warfare Center Reports, Oklahoma State University, Stillwater, April 1985 to June 1987 (unpublished).

14. P. J. Alonso and R. Alcalá, J. Lumin. **21**, 147 (1980).

15. D. Wayne Cook, Evangelos P. Gavathas and M. D. Brown, J. Appl. Phys. **54**(2), 1165 (1983).

16. B. Jassemnejad, R. J. Abbundi, M. D. Brown and S. W. S. McKeever, Phys. Status Solidi A: **108**, 753 (1988).

17. S. W. S. McKeever, *Optical Dichroism in Calcium Fluoride Doped with Manganese*, Naval Surface Weapons Center Reports, Oklahoma State University, Stillwater, January 1988 (unpublished).

18. W. Hayes, ed. , *Crystals with the Fluorite Structure* (Oxford University, Oxford, 1974).

19. M. J. Frisch, G. W. Trucks, M. Head-Gordon, P. M. W. Gill, M. W. Wong, J. B. Foresman, B. G. Johnson, H. B. Schlegel, M. A. Robb, E. S. Replogle, R. Gomperts, J. L. Andres, K. Raghavachari, J. S. Binkley, C. Gonzalez, R. L. Martin, D. J. Fox, D. J. Defrees, J. Baker, J. J. P. Stewart, and J. A. Pople, GAUSSIAN 92 (Gaussian Inc. Pittsburgh PA, 1992).

20. S. Sugano, Y. Tanabe and H. Kamimura, *Multiplets of Transition-Metal Ions in Crystals* (Academic Press, New York, 1970).

21. J. W. Stout, J. Chem. Phys. **31**(3), 709 (1959).

22. Y. Tanabe and S. Sugano, J. Phys. Soc. Japan **9**, 753 (1954); **9**, 766 (1954); **11**, 864 (1956).

23. L. E. Orgel, J. Chem. Phys. **23**(6), 1004 (1955); **23**(10), 1819 (1955); **23**(10), 1824 (1955).

24. H. L. Schläfer and G. Gliemann, *Basic Principles of Ligand Field Theory* (Wiley, New York, 1969).

25. R. K. Bagai and A. V. R. Warrier, Phys. Status Solidi B **73**, K123 (1976).

26. M. T. Barriuso and M. Moreno, Chem. Phys. Let. **112**(2), 165 (1984).

27. F. A. Cotton, *Chemical Applications of Group Theory* (Wiley, New York, 1990).

28. M. Tinkham, *Group Theory and Quantum Mechanics* (McGraw-Hill, New York, 1964).

29. H. Eyring, J. Walter and G. Kimball, *Quantum Chemistry* (Wiley, New York, 1961).

30. E. U. Condon and G. H. Shortley, *The Theory of Atomic Spectra* (Cambridge, New York, 1953).

31. S. Wolfram, *Mathematica: A System for Doing Mathematics by Computer* (Addison-Wesley, New York, 1991).

32. K. P. Lawley, Ed. , *Advances in Chemical Physics* (Wiley, New York, 1987), Vol. 67.

33. A. Szabo and N. S. Ostlund, *Modern Quantum Chemistry* (McGraw-Hill, New York, 1989).

34. A. C. Hurley, *Introduction to the Electron Theory of Small Molecules* (Academic Press, New York, 1976).

35. C. C. J. Roothaan, Rev. Mod. Phys. **23**, 69 (1951).

36. E. A. Hylleraas and B. Undheim, Ann. Physik **65**, 759 (1930); J. K. L. MacDonald, Phys. Rev. **43**, 830 (1933).

37. A. C. Wahl and G. Das, *Methods of Electronic Structure Theory*, H. F. Schaefer III Ed. (Plenum, New York, 1977) p. 51.

38. S. Huzinaga, J. Andzelm, M. Klobukowski, E. Radzio-andzelm, Y. Sakai and H. Tatewaki, *Gaussian Basis Sets for Molecular Calculations* (Elsevier, Amsterdam, 1984).

39. J. H. Barkyoumb and A. N. Mansour, Phys. Rev. B: **46**(14), 8768 (1992).

40. R. F. Wood and T. M. Wilson, *Defects in Insulating Solids*, V. M. Tuchkevich and K. K. Shvarts, Eds. (Springer-Verlag, Berlin, 1981), pp. 186-206.

41. J. W. Richardsen and G. J. M. Janssen, Phys. Rev. B **39**(8), 4958 (1989).

42. B. Ng and D. J. Newman, J. Chem. Phys. **84**(6), 3291 (1986).

43. J. Ferguson, E. R. Krausz and H. J. Guggenheim, Mol. Phys. **27**, 577 (1974).

44. D. M. Finlayson, I. S. Robertson, T. Smith and R. W. H. Stevenson, Proc. Phys. Soc. **76**, 355 (1960).

45. W. A. Sibley, S. I. Yun, and W. E. Vehse, J. Phys. C **6**, 1105 (1973).

46. J. P. Srivastava and A. Mehra, J. Chem. Phys. **57**, 1587 (1972).

APPENDICES

APPENDIX A

COULOMB INTERACTION MATRICES FOR THE DOUBLET TERMS

In this appendix we present the Coulomb interaction matrices for the doublet terms arising from the d^5 configuration. As before a common factor of A is subtracted from the diagonal. The quartet and the ground state sextet matrices are given in Table IV. To obtain the complete crystal splitting diagram shown in Fig. 7 for an $O_h^{(8)}$ field, $(4n - 6m)\frac{8}{9}Dq$ for $t_{2g}^n e_g^m$ is added to the diagonals of the following matrices and then they are diagonalized using the $Mathematica^{TM}$[31] program package. These matrices are reproduced from Tanabe and Sugano[20].

$$^2A_2(a^2F, b^2F, {}^2I)$$

$t_2^4({}^1E)e$	$t_2^3({}^2E)e^2({}^1E)$	$t_2^2({}^1E)e^3$
$-23B + 9C$	$-3\sqrt{2}B$	$2B - C$
	$-12B + 8C$	$-3\sqrt{2}B$
		$-23B + 9C$

$$^2A_1(^2S, a^2G, b^2G, {}^2I)$$

$t_2^4({}^1E)e$	$t_2^3({}^2E)e^2({}^1E)$	$t_2^3({}^4A_2)e^2({}^3A_2)$	$t_2^2({}^1E)e^3$
$-3B + 9C$	$3\sqrt{2}B$	0	$-6B - C$
	$-12B + 8C$	$-4\sqrt{3}B$	$3\sqrt{2}B$
		$-19B + 8C$	0
			$-3B + 9C$

$$^2E(a^2D, b^2D, c^2D, a^2G, b^2G, {}^2H, {}^2I)$$

$t_2^4(^1A_1)e$	$t_2^4(^1E)e$	$t_2^3(^2E)e^2(^1A_1)$	$t_2^3(^2E)e^2(^3A_2)$	$t_2^3(^2E)e^2(^1E)$
$-4B+12C$	$-10B$	$6B$	$6\sqrt{3}B$	$6\sqrt{2}B$
	$-13B+9C$	$3B$	$-3\sqrt{3}B$	0
		$-4B+10C$	0	0
			$-16B+8C$	$2\sqrt{6}B$
				$-12B+8C$

$t_2^2(^1E)e^3$	$t_2^2(^1A_1)e^3$
$-2B$	$4B+2C$
$-2B-C$	$-2B$
$-3B$	$-6B$
$-3\sqrt{3}B$	$6\sqrt{3}B$
0	$6\sqrt{2}B$
$-13B+9C$	$-10B$
	$-4B+12C$

$$^2T_1(^2P, a^2F, b^2F, a^2G, b^2G, ^2H, ^2I)$$

$t_2^4(^3T_1)e$	$t_2^4(^1T_2)e$	$t_2^3(^2T_1)e^2(^1A_1)$	$t_2^3(^2T_1)e^2(^1E)$	$t_2^3(^2T_2)e^2(^3A_2)$
$-22B+9C$	$-3B$	$3\sqrt{2}B/2$	$-3\sqrt{2}B/2$	$3\sqrt{2}B/2$
	$-8B+9C$	$-3\sqrt{2}B/2$	$-3\sqrt{2}B/2$	$-15\sqrt{2}B/2$
		$-4B+10C$	0	0
			$-12B+8C$	0
				$-10B+10C$

$t_2^3(^2T_2)e^2(^1E)$	$t_2^2(^1T_2)e^3$	$t_2^2(^3T_1)e^3$
$3\sqrt{6}B/2$	0	$-C$
$-5\sqrt{6}B/2$	$-4B-C$	0
$10\sqrt{3}B$	$3\sqrt{2}B/2$	$-3\sqrt{2}B/2$
0	$-3\sqrt{2}B/2$	$-3\sqrt{2}B/2$
$2\sqrt{3}B$	$15\sqrt{2}B/2$	$-3\sqrt{2}B/2$
$-6B+10C$	$5\sqrt{6}B/2$	$-3\sqrt{6}B/2$
	$-8B+9C$	$-3B$
		$-22B+9C$

$$^2T_2(a^2F, b^2F, a^2G, b^2G, {}^2H, {}^2I, a^2D, b^2D, c^2D)$$

t_2^5	$t_2^4(^3T_1)e$	$t_2^4(^1T_2)e$	$t_2^3(^2T_1)e^2(^3A_2)$	$t_2^3(^2T_1)e^2(^1E)$
$-20B+10C$	$-3\sqrt{6}B$	$-\sqrt{6}B$	0	$-2\sqrt{3}B$
	$-8B+9C$	$3B$	$-\sqrt{6}B/2$	$3\sqrt{2}B/2$
		$-18B+9C$	$-3\sqrt{6}B/2$	$3\sqrt{2}B/2$
			$-16B+8C$	$2\sqrt{3}B$
				$-12B+8C$

$t_2^3(^2T_2)e^2(^1A_1)$	$t_2^3(^2T_2)e^2(^1E)$	$t_2^2(^1T_2)e^3$	$t_2^2(^3T_1)e^3$	t_2e^4
$4B+2C$	$2B$	0	0	0
$-3\sqrt{6}B/2$	$-3\sqrt{6}B/2$	0	$-4B-C$	0
$-5\sqrt{6}B/2$	$5\sqrt{6}B/2$	$-C$	0	0
0	0	$-3\sqrt{6}B/2$	$-\sqrt{6}B/2$	0
$-10\sqrt{3}B$	0	$3\sqrt{2}B/2$	$3\sqrt{2}B/2$	$-2\sqrt{3}B$
$2B+12C$	0	$-5\sqrt{6}B/2$	$-3\sqrt{6}B/2$	$4B+2C$
	$-6B+10C$	$-5\sqrt{6}B/2$	$3\sqrt{6}B/2$	$-2B$
		$-18B+9C$	$3B$	$-\sqrt{6}B$
			$-8B+9C$	$-3\sqrt{6}B$
				$-20B+10C$

APPENDIX B

EVALUATION OF THE GAUSSIAN INTEGRAL

In this appendix we will detail the evaluation of the integral having the form,

$$I(\mathbf{r}) = \int \frac{e^{-\alpha|\mathbf{r}'-\mathbf{R}|^2}}{|\mathbf{r}'-\mathbf{r}|} d\mathbf{r}'. \tag{199}$$

An integral of this form appears in the modeling of the electrostatic properties of charge distributions consisting of an arrangement of Gaussians. The derivation presented here follows along the similar lines as in the evaluation of multicenter integrals with Gaussian basis functions as presented in Szabo and Ostlund[33]. To evaluate the integral in Eq. (199) we will use the method of the Fourier transform. The Fourier transform, $F(\mathbf{k})$, and its inverse, $f(\mathbf{r})$, will be defined by,

$$F(\mathbf{k}) = \int f(\mathbf{r})e^{-i\mathbf{k}\cdot\mathbf{r}} d\mathbf{r}, \tag{200}$$

$$f(\mathbf{r}) = (2\pi)^{-3} \int F(\mathbf{k})e^{i\mathbf{k}\cdot\mathbf{r}} d\mathbf{k}. \tag{201}$$

A useful result for this derivation is the following expression for the delta function,

$$\delta(\mathbf{r}_1 - \mathbf{r}_2) = (2\pi)^{-3} \int e^{i\mathbf{k}\cdot(\mathbf{r}_1-\mathbf{r}_2)} d\mathbf{k}. \tag{202}$$

Table XII gives a short list of Fourier transforms that will be necessary for our purposes. From this table we see that,

$$e^{-\alpha|\mathbf{r}'-\mathbf{R}|^2} = (2\pi)^{-3} \int \left(\frac{\pi}{\alpha}\right)^{3/2} e^{-k^2/4\alpha} e^{i\mathbf{k}\cdot(\mathbf{r}'-\mathbf{R})} d\mathbf{k}, \tag{203}$$

and,

$$\frac{1}{|\mathbf{r}'-\mathbf{r}|} = (2\pi)^{-3} \int \frac{4\pi}{k^2} e^{i\mathbf{k}\cdot(\mathbf{r}'-\mathbf{r})} d\mathbf{k}. \tag{204}$$

132

Substituting Eqs. (203) and (204) into Eq. (199) and rearranging we obtain,

$$I(\mathbf{r}) = \frac{1}{2\pi^2}\left(\frac{\pi}{\alpha}\right)^{3/2}\int e^{-k_1^2/4\alpha}e^{-i\mathbf{k}_1\cdot\mathbf{R}}e^{-i\mathbf{k}_2\cdot\mathbf{r}}\left(\frac{1}{k_2^2}\right)d\mathbf{k}_1d\mathbf{k}_2$$
$$\times \left((2\pi)^{-3}\int e^{-i\mathbf{r}'\cdot(\mathbf{k}_1+\mathbf{k}_2)}d\mathbf{r}'\right) \tag{205}$$

From Eq. (202) we identify the last term in parenthesis as $\delta(\mathbf{k}_1 + \mathbf{k}_2)$. Next we perform the integration over $\mathbf{k}_2$. Because of the delta function we see that $\mathbf{k}_1 = -\mathbf{k}_2$, this leads to the expression,

$$I(\mathbf{r}) = \frac{1}{2\pi^2}\left(\frac{\pi}{\alpha}\right)^{3/2}\int e^{-k_1^2/4\alpha}e^{-i\mathbf{k}_1\cdot\mathbf{R}}e^{i\mathbf{k}_1\cdot\mathbf{r}}\left(\frac{1}{k_1^2}\right)d\mathbf{k}_1. \tag{206}$$

Rename the dummy integration variable $\mathbf{k}_1$ to $\mathbf{k}$ we then have,

$$I(\mathbf{r}) = \frac{1}{2\pi^2}\left(\frac{\pi}{\alpha}\right)^{3/2}\int e^{-k^2/4\alpha}e^{-i\mathbf{k}\cdot(\mathbf{R}-\mathbf{r})}\left(\frac{1}{k^2}\right)d\mathbf{k}. \tag{207}$$

If we arrange the coordinate system in k-space such that the vector $(\mathbf{R} - \mathbf{r})$ lies along the z-axis, then $\mathbf{k}\cdot(\mathbf{R}-\mathbf{r}) = k|\mathbf{R}-\mathbf{r}|\cos\theta$. With $d\mathbf{k} = k^2dk\sin\theta d\theta d\phi$ and after integrating ϕ from 0 to 2π, Eq. (207) becomes,

$$I(\mathbf{r}) = \frac{1}{\pi}\left(\frac{\pi}{\alpha}\right)^{3/2}\int_0^\infty e^{-k^2/4\alpha}dk\int_0^\pi e^{-ik|\mathbf{R}-\mathbf{r}|\cos\theta}\sin\theta d\theta. \tag{208}$$

The integration over θ is straightforward after the substitution of $u = k|\mathbf{R}-\mathbf{r}|\cos\theta$ becoming $\frac{2}{k|\mathbf{R}-\mathbf{r}|}\sin(k|\mathbf{R}-\mathbf{r}|)$. Equation (208) then becomes,

$$I(\mathbf{r}) = \frac{2}{\pi}\left(\frac{\pi}{\alpha}\right)^{3/2}\frac{1}{|\mathbf{R}-\mathbf{r}|}\int_0^\infty e^{-k^2/4\alpha}\left(\frac{1}{k}\right)\sin(k|\mathbf{R}-\mathbf{r}|)dk. \tag{209}$$

TABLE XII.

A SHORT LIST OF USEFUL
FOURIER TRANSFORMS

$f(\mathbf{r})$	$F(\mathbf{k})$
$1/r$	$4\pi/k^2$
$e^{-\alpha r^2}$	$(\pi/\alpha)^{3/2}e^{-k^2/4\alpha}$
$\delta(\mathbf{r})$	1

To evaluate Eq. (209) we must evaluate an integral of the form,

$$J(x) = \int_0^\infty e^{-ak^2} \left(\frac{1}{k}\right) \sin(kx)dk. \tag{210}$$

Then,

$$\frac{dJ(x)}{dx} = \int_0^\infty e^{-ak^2} \cos(kx)dk, \tag{211}$$

but if we note that $\cos(k(-x)) = \cos(kx)$ then we can write,

$$\frac{dJ(x)}{dx} = \frac{1}{2} \int_{-\infty}^\infty e^{-ak^2} \cos(kx)dk. \tag{212}$$

Since $\cos\theta = \text{Re}(e^{i\theta})$ we have,

$$\frac{dJ(x)}{dx} = \frac{1}{2}\text{Re}\left(\int_{-\infty}^\infty e^{-ak^2} e^{ikx}dk\right). \tag{213}$$

After completing the square in the argument of the exponential function, we have,

$$\frac{dJ(x)}{dx} = \frac{1}{2}e^{-x^2/4a}\text{Re}\left(\int_{-\infty}^\infty e^{-\left(\sqrt{a}k - \frac{ix}{2\sqrt{a}}\right)^2} dk\right). \tag{214}$$

After making the substitution $u = \sqrt{a}k - ix/(2\sqrt{a})$ we may write Eq. (214) as,

$$\frac{dJ(x)}{dx} = \frac{1}{2}e^{-x^2/4a}a^{-1/2}\text{Re}\left(\int_{-\infty}^\infty e^{-u^2} du\right) = \frac{1}{2}\sqrt{\frac{\pi}{a}}e^{-x^2/4a}, \tag{215}$$

where, we observe $\text{Re}\left(\int_{-\infty}^\infty e^{-u^2} du\right) = \sqrt{\pi}$. We may then write $J(x)$ as,

$$J(x) = \int_0^x \frac{dJ(x')}{dx'}dx' = \frac{1}{2}\sqrt{\frac{\pi}{a}} \int_0^x e^{-x'^2/4a}dx', \tag{216}$$

where we note that $J(0) = 0$. With the substitution $u = x'/(2\sqrt{a})$, Eq. (216) becomes,

$$J(x) = \sqrt{\pi} \int_0^{x/(2\sqrt{a})} e^{-u^2} du. \tag{217}$$

With the definition of the error function, $\text{erf}(x) = \frac{2}{\sqrt{\pi}}\int_0^x e^{-u^2} du$, we have,

$$J(x) = \frac{\pi}{2}\text{erf}\left(\frac{x}{2\sqrt{a}}\right). \tag{218}$$

We must now use this expression in Eq. (209). This is accomplished by setting $x = |\mathbf{R} - \mathbf{r}|$ and $a = 1/(4\alpha)$ in Eq. (218). With these substitutions, Eq. (209) becomes,

$$I(\mathbf{r}) = \left(\frac{\pi}{\alpha}\right)^{3/2} \frac{1}{|\mathbf{R} - \mathbf{r}|} \text{erf}[\sqrt{\alpha}|\mathbf{R} - \mathbf{r}|]. \tag{219}$$

Thus, we have expressed the Gaussian integral in terms of the error function. $I(\mathbf{r})$ can therefore be easily evaluated since the IBM and VAX FORTRAN compilers have highly efficient built-in $\text{erf}(x)$ functions.

VITA

ANTHONY C. LEWANDOWSKI

Candidate for the Degree of

Doctor of Philosophy

Thesis: *AB INITIO* SELF-CONSISTENT FIELD CALCULATIONS ON Mn-RELATED DEFECTS IN CALCIUM FLUORIDE

Major Field: Physics

Biographical:

Personal Data: Born in Fort Benning Georgia, April 26, 1964, the son of William Howard and Billie Jean Lewandowski. Married to Kyong R. Yi on October 16, 1989.

Education: Graduated from Lawton High School, Lawton, Oklahoma, in May, 1982; received a Bachelor of Science degree from Oklahoma State University in December, 1986 with a major in physics and a minor in mathematics; completed the requirements for the Master of Science degree at Oklahoma State University in December, 1990; completed the requirements for the Doctor of Philosophy degree at Oklahoma State University in December 1993.

Professional Experience: United States Marine Corps Reserve, May, 1982 to May, 1987; Teaching Assistant, Department of Physics, Oklahoma State University, January, 1986 to December, 1986; Graduate Research Assistant, June, 1987 to present. Member of the American Physical Society, and Phi Kappa Phi.